Natland, J.H., Dick H.J.B., Miller, D.J., and Von Herzen, R.P. (Eds.)
Proceedings of the Ocean Drilling Program, Scientific Results Volume 176

10. Primary Silicate Mineral Chemistry of a 1.5-km Section of Very Slow Spreading Lower Ocean Crust: ODP Hole 735B, Southwest Indian Ridge[1]

Henry J.B. Dick,[2] Kazuhito Ozawa,[3] Peter S. Meyer,[2] Yaoling Niu,[4] Paul T. Robinson,[5] Marc Constantin,[6] Rejean Hebert,[6] Jinichiro Maeda,[7] James H. Natland,[8] James Gregory Hirth,[2] and Suzie M. Mackie[4]

ABSTRACT

We present a synthesis of some 20,504 mineral analyses of ~500 Hole 735B gabbros, including 10,236 new analyses conducted for this paper. These are used to construct a mineral stratigraphy for 1.5-km-deep Hole 735B, the only long section of the lower crust drilled in situ in the oceans. At long wavelengths, generally >200 m, there is a good chemical correlation among the principal silicate phases, consistent with the in situ crystallization of three or four distinct olivine gabbro bodies, representing at least two major cycles of intrusion. Initial cooling and crystallization of these bodies must have been fairly rapid to form a crystal mush, followed by subsequent compaction and migration of late iron-titanium–rich liquids into shear zones and fractures through which they were emplaced to higher levels in the lower crust where they crystallized and reacted with the olivine gabbro host rock to form a wide variety of ferrogabbros. At the wave lengths of the individual intrusions, as represented by the several olivine gabbro sequences, there is a general upward trend of iron and sodium enrichment but a poor correlation between the compositions of the major silicate phases. This, together with a wide range in minor incompatible and compatible element concentrations in olivine and pyroxene at a given Mg#, is con-

[1]Dick, H.J.B., Ozawa, K., Meyer, P.S., Niu, Y., Robinson, P.T., Constantin, M., Hebert, R., Maeda, J., Natland, J.H., Hirth, J.G., and Mackie, S.M., 2002. Primary silicate mineral chemistry of a 1.5-km section of very slow spreading lower ocean crust: ODP Hole 735B, Southwest Indian Ridge. *In* Natland, J.H., Dick, H.J.B., Miller, D.J., and Von Herzen, R.P. (Eds.), *Proc. ODP, Sci. Results,* 176, 1–61 [Online]. Available from World Wide Web: <http://www-odp.tamu.edu/publications/176_SR/VOLUME/CHAPTERS/SR176_10.PDF>. [Cited YYYY-MM-DD]
[2]Department of Geology and Geophysics, Woods Hole Oceanographic Institution, Woods Hole MA 02543, USA. Correspondence author: **hdick@whoi.edu**
[3]Geological Institute, Faculty of Science, University of Tokyo, Tokyo 113, Japan.
[4]Department of Earth Sciences, The University of Queensland, Brisbane QLD 4072, Australia.
[5]Institute of Geochemistry, GeoForschungsZentrum, Telegrafenberg, D-14473 Potsdam, Germany.
[6]Département de géologie et de génie géologique, Pavillon Pouliot, Université Laval, Québec G1K 7P4, Canada.
[7]Division of Earth and Planetary Sciences, Graduate School of Science, Hokkaido University, N10 W8 Kita, Sapporo, Hokkaido 060-0810, Japan. [N1]
[8]School of Oceanography, University of Miami, 4600 Rickenbacker Causeway, Miami FL 33149, USA.

Initial receipt: 7 September 2000
Acceptance: 6 June 2002
Web publication: 16 October 2002
Ms 176SR-001

sistent with widespread permeable flow of late melt through these intrusions, in contrast to what has been documented for a 600-m section of reputedly fast-spreading ocean crust in the Oman Ophiolite. This unexpected finding could be related to enhanced compaction and deformation-controlled late-stage melt migration at the scale of intrusion at a slow-spreading ocean ridge, compared to the relatively static environment in the lower crust at fast-spreading ridges.

INTRODUCTION

Hole 735B represents the only deep section of lower crust drilled by the Ocean Drilling Program (ODP). Crystallized beneath the ultra slow spreading Southwest Indian Ridge, where normal ocean crust is believed to be typically only ~4 km thick (Bown and White, 1994; Muller et al., 1999; Muller et al., 1997), it likely represents a major portion of the lower ocean crust at the time of accretion. Thus, it is by default the only type section of lower ocean crust formed at slow-spreading ridges. A detailed understanding of how the Hole 735B gabbros were emplaced, how they crystallized, and how this process reflects the unique tectonically active environment of slow-spreading ridges is critical then to constraining the formation of the lower ocean crust. Whereas an abundance of whole-rock major, trace element, and isotopic data has been collected, these data have inherent problems for interpreting the igneous petrogenesis of plutonic rocks. Whole-rock compositions integrate the influence of mineral mode and mineral chemistry as well as the effects of alteration. Moreover, large changes in lithology and texture can often be produced by petrologically minor events in the crystallization history of a pluton, whereas major events may be marked by only minor changes in these parameters. Events in the crystallization of plutonic rocks such as a major new phase of intrusion or a major fault discontinuity in the section are often revealed only in the cryptic variations of the mineral chemistry. While the effects of modal variations during subsolidus reequilibration have to be considered, mineral chemistry is also the best way to understand melt evolution during crystallization. Mineral zonation also provides the best means of addressing postcumulus processes, late-stage melt migration, and melt-rock reaction, which are now viewed as critical to understanding the formation of plutonic rocks.

The first 500 m of Hole 735B was drilled in 1987 during Leg 118, and the lower 1008 m was drilled 10 yr later during Leg 176. Consequently, two scientific parties, among whom there is only partial overlap, have collected mineral data. These data represent a variety of analytical schemes, facilities, and standards. Moreover, because of periodical space limitations, most of the Leg 118 data have been unavailable to the scientific community. This paper presents a large new systematically collected data set for ~200 samples of the Leg 176 gabbros and also synthesizes most of the data collected to date by the Leg 118 and Leg 176 scientists. The data presented in Tables **T1, T2, T3, T4,** and **T5** (available in both ASCII and Excel format [see **"Supplementary Material"**]) includes 7508 clinopyroxene, 6759 plagioclase, 2955 olivine, 2427 orthopyroxene, and 855 hornblende spot analyses. A preliminary analysis of this data is presented here as well, though with 20,504 analyses, it hardly does justice to the data set. It should also be kept in mind that although this may seem to be a remarkably large data set, there are 952 discrete lithologic intervals in the Hole 735B core described on the

T1. Plagioclase analyses, p. 56.

T2. Clinopyroxene analyses, p. 57.

T3. Olivine analyses, p. 58.

T4. Orthopyroxene analyses, p. 59.

T5. Brown Hornblende analyses, p. 60.

basis of clear textural and mineralogic differences. This breakdown did not generally include intervals of less than ~4 cm, and further subdivision of the core could be made. With the analytical data set estimated to represent ~500 discrete samples, it remains inadequate to describe the core in anywhere near its entirety.

ANALYTICAL METHODS

The data sets reported in Tables T1, T2, T3, T4, and T5, other than those collected by the first author and his colleagues at Massachusetts Institute of Technology (MIT), were collected by investigators using different analytical schemes, techniques, and standards. They describe these in papers in the Leg 118 and Leg 176 volumes (Bloomer et al., 1991; Hebert et al., 1991; Natland et al., 1991; Niu et al., Chap. 8, this volume; Ozawa et al., 1991; Robinson et al., Chap. 9, this volume). The new data collected at the MIT Electron Microprobe Facility used a JEOL JXA-733 Superprobe. The operating conditions included a 15-keV accelerating voltage, 10-nA probe current, 10-µm spot size, and 10- to 40-s per element counting time. Standards used included diopside-jadeite (dj35, synthetic), aluminous orthopyroxene (synthetic), forsterite (synthetic), fayalite (synthetic), marjalotti olivine, Amelia albite, anorthite (synthetic), orthoclase glass (synthetic), Lake County labradorite, spinel (synthetic), hematite (synthetic), rutile (synthetic), uvarovite (synthetic), rhodonite (synthetic), nickel sulfide (synthetic), chromite (synthetic), and Wilberforce apatite. Data reduction was done using the Phi-Rho-Z method.

The reader will note that there is no systematic comparison of interlaboratory bias here. Insofar as these analyses represent the analytical procedures of many different laboratories and were collected over some 11 yr, this is not really possible. Accordingly, the user and reader should take note and not draw too fine a distinction between analyses exhibiting small differences in concentration. Generally, for example, it is safe to assume that differences of few mole percent forsterite between data sets are real but one is on very shaky ground for differences less than that without careful justification.

TABLES OF ANALYSES

Tables T1, T2, T3, T4, and T5 present the compositions of individual analytical points (spots), averages, and standard deviations by individual mineral grain. We have placed all the available data into a standard format, which required transcribing highly variable sets of data submitted in a wide variety of formats. The tables have many fields for different kinds of data, usually far more than are used by any one data set. However, an attempt was made to create a flexible format so that many types of information could be included. As much data as possible is also given in numerical format so that the user can easily sort the data by grain size, location of analysis, depth in the hole, sample number, and the like. Editing of the data in the tables was largely left to the analysts, and the analyses have largely been included as submitted. Analyses falling outside the range of analytical totals of 98.0 to 101.5 or with improbable stoichiometry, however, were usually rejected. We refer to the successive columns here as lettered from A to Z from left to right, though these headings are not actually printed out in the appended ex-

ample pages of these tables (first page of each table only), but are found when the electronic ASCII format is uploaded to Excel format or the Excel tables available in the volume **"Supplementary Material"** are opened. Column A lists a simple serial number from 1 to *N* that can be used to restore the data set back to its original form after various sorting routines by the user.

Sample Identification

Column B gives the thin section number if it is different from the sample number; otherwise, a simple three-letter code is given, usually identical to that assigned by ODP, referencing whose sample was analyzed. Where only a number is given in this column, it refers to one of the shipboard thin sections owned by ODP. These thin sections are available on loan from the ODP Gulf Coast Repository for further study. Column C gives the source of the analysis, often, but not always, the person whose sample it is. Columns D through J give the standard ODP sample code. This includes, sequentially: the leg number, hole number, core number, section number, the top and bottom of the thin-sectioned interval containing the specific rock type listed under column M (Rock type) measured in centimeters from the top of the core section, and, finally, the piece number. A note of caution here: individual thin sections often contain more than one rock type. Thus, the interval listed in columns I and J may give the interval over which the rock type appears in the thin section or more often may give simply the top and bottom of the thin section. Thus, with the exception of the rock name, all the sample identifiers can be the same for two different lithologies in a thin section. Therefore, for these tables, the sample identifier must include the rock name in addition to the original ODP sample code. Column K gives the vertical position of the analyzed grain, measured from the top of the section in which the sample was taken (oriented sections only). Column L gives the vertical position of the analysis measured from the top of the hole in expanded meters, where the length of the cored section is expanded (or compressed) to fill the section cored using the algorithm given in the "Igneous Petrology" section of the "Explanatory Notes" chapter in the Leg 176 *Initial Results* volume (Dick, Natland, Miller, et al., 1999).

Rock Names

Column M gives the rock type, usually a modified version of the name assigned to the sample by the analyst. Rock nomenclature is a problem. Despite an attempt to adhere to the standard International Union for the Geological Sciences (IUGS) nomenclature (le Maitre, 1989; Streckeisen, 1976), particularly on the part of the Leg 176 Scientific Party, the allure of site-specific genetic nomenclature is a siren song evidently impossible to resist. This is particularly the case when the presence or absence of a particular mineral, often in trace amounts, or a specific texture seems to have real genetic meaning at different horizons in the core (e.g., Ozawa et al., 1991). With some 20 different scientists assigning rock names between shore-based investigators and two different shipboard parties, differences in criteria for naming rocks are perhaps unavoidable. We have, however, simplified many rock names in order to make it easier for the reader to sort rocks with similar attributes together, but we have not eliminated analyst-specific names entirely, as this was not possible to do in all cases. Hebert et al. (1991)

drew the dividing line for the use of "oxide" as a prefix at 4% opaques in thin section, whereas the remaining analysts used an estimate of between 1% and 2% oxides for the prefix "disseminated oxide" and >2% opaques for the use of "oxide" as a prefix. We have used visual modes provided by Constantin to rename their samples to fit the Leg 176 conventions, so the rock names in our tables are different than theirs. In the case of the data provided by P. Robinson, H. Dick went through most of his thin sections to check for consistency in the use of igneous terms, as his research objectives were focused on alteration rather than igneous petrology. Thus, there are likely some minor differences in rock names for different samples between this paper and Robinson et al. (**Chap. 9,** this volume). There is, then, a multiplicity of rock names used for the different kinds of gabbroic rock found in the Hole 735B cores, which only in part reflects their often-bewildering diversity. The reader may want to refer back to the individual papers in the Leg 118 *Scientific Results* volume to see the original unmodified rock names and how different analysts use them. We also note that rock names were particularly hard to assign where rocks were significantly altered; thus, many names are tenuous and this can obscure significant genetic meaning of the appearance or disappearance of a given phase when plotting the data. Users are advised when distinctions are important that checking thin sections for outlying points in various plots may reveal that the section has more than one rock type, and mineral data from one rock has been plotted with data from another or that the assigned rock name may be inappropriate.

In general, the term "oxide" refers to ilmenite and titanomagnetite, but often the estimate was based simply on the amount of opaques in the thin section, which lumped in any sulfides present. This is hazardous, particularly for "disseminated oxide gabbros," as sulfides are often present in the gabbros in amounts up to 0.5%–1%. "Olivine" is generally used as a prefix where it constitutes ≥5%. We note, however, that there is a continuous gradation from 0% to >20% modal olivine from "gabbro" to "olivine gabbro" with no obvious break in mode, texture, or mineral chemistry at 5%; thus, the distinction is to a certain degree meaningless for the Hole 735B cores. The prefix "orthopyroxene" is used for rocks containing granular rather than interstitial orthopyroxene in amounts <5%, as the term "gabbronorite" is used for gabbros with >5% orthopyroxene, following IUGS. Intergranular orthopyroxene was generally ignored when assigning rock names, as it is present in small amounts in nearly all rocks and its appearance, as evidenced by its large range in composition, has little specific genetic meaning other than the presence of a small amount of melt trapped in or migrating through the rock toward the end of crystallization. "Troctolite" refers to a rock with <5% clinopyroxene and "anorthositic" to rocks with >80% plagioclase. "Troctolitic" is used as a prefix for olivine gabbros with 5%–15% clinopyroxene. High proportions (>65%) of mafic and leucocratic minerals are noted by the prefixes "mela" and "leuco," though we note that the mineral compositions show no systematic variation with mineral mode in these cases, with complete overlap between specific rock types with and without these prefixes. The prefix "micro" is generally used to describe fine-grained equigranular gabbros crosscutting the coarser-grained olivine gabbros. The Leg 176 Scientific Party specifically restricted this name to rocks with dominant grain size of <1 mm, though the Leg 118 Scientific Party and Dick et al. (1991a) did not generally do this, including somewhat coarser-grained (millimeter to centimeter scale) crosscutting equigranular gabbro bodies in this

designation, as these bodies appear otherwise identical in their occurrence, textural characteristics, and composition range.

The reader is advised that as a consequence of this nomenclature confusion, the troctolites described in Unit 6 (Dick, 1991a) around 404 to 550 meters below seafloor (mbsf) in Hole 735B are quite distinct from the troctolites found lower in the hole. The former are all small meter-scale intrusions with sharp crosscutting contacts with the olivine gabbros that grade from microtroctolite (fine grained) to troctolite (medium to coarse grained) under this classification. They are the most primitive rocks recovered from Hole 735B—apparently having crystallized from a different or at least more primitive parental magma than those giving rise to the olivine gabbros. By contrast, the "troctolites" deeper in the hole simply represent a continuum from gabbro, olivine gabbro, and troctolitic gabbro, representing an increase in the proportion of modal olivine. Otherwise, these latter rocks are texturally and mineralogically identical.

Medium- to coarse-grained leucocratic igneous rocks make up ~1% of the Hole 735B core. They are generally present as crosscutting small veins and are commonly very altered. In many cases, they are hard to distinguish from purely hydrothermal "felsic" veins. Although they range from diorite through tonalite to trondhjemite and include a few granite veins, the specific igneous protolith is often very difficult to identify. Thus, many specific identifications made by the analysts and the shipboard party must be regarded as somewhat suspect. Many readers will be more familiar with these rocks as "plagiogranites," a common field term for white felsic igneous rocks of ambiguous nature, specifically not recommended by IUGS as it overlaps with other long-used valid rock names. Because we would prefer to leave the final identification of most of these to those with some specialization in the field of late igneous leucocratic magmatic veins, we have lumped them in the tables collectively under the name "felsic vein." There is no denying the usefulness of the term plagiogranite in this context when trying to deal with these rocks, but because there is little agreement among ourselves over the term "plagiogranite," we do not use it here.

The complexity of the terminology and diversity of rock names used will undoubtedly intimidate the reader—as it does the authors. Whereas good reasons exist for each name and most turn out to have genetic significance, we often simplify this terminology in this paper. The reader is advised that when we use the plural form we are generally referring to a clan of rocks with petrologic affinity. By gabbros we mean collectively all the gabbroic rocks in the hole, excluding the crosscutting microgabbros. When we refer to olivine gabbros we mean collectively all the oxide-poor olivine-bearing gabbros (gabbro, olivine gabbro, and troctolitic gabbro). Similarly, oxide gabbros, or the term "ferrogabbro," refers to the many varieties of oxide-rich, orthopyroxene-poor olivine-bearing and olivine-free gabbro. Gabbronorites include all the rock types with significant amounts of granular orthopyroxene (gabbronorite, orthopyroxene gabbro, orthopyroxene-olivine gabbro, pigeonitic gabbro, etc.). Specific rock types are generally referred to in the singular. Troctolite and disseminated oxide olivine gabbro are unique in this respect, as they are generally not included in the three general rock clans (olivine gabbros, gabbronorites, and oxide gabbros). Many of the troctolites are distinct from all other rock types in various compositional plots, and the disseminated oxide olivine gabbros appear to be transitional from the olivine gabbro clan to the oxide gabbro clan without having significant orthopyroxene.

Columns N through S give the average Mg# (molar Mg×100/[Mg+Fe*]) and forsterite, anorthite, and orthoclase contents of coexisting olivine, clinopyroxene, orthopyroxene, plagioclase, and brown hornblende in the thin section analyzed, except for the analytical point whose measured values are given. Modal data are given in columns T through AC, where available. Data for the ODP thin sections were collected by Dr. Peter Meyer during Leg 176 and are taken from the Leg 176 *Initial Reports* volume. These data were used to assign rock names to all the ODP thin sections analyzed by H. Dick using the criteria laid out in the Leg 176 *Initial Reports* volume. Modes for the Y. Niu samples were collected by S. Mackie, whereas modes given for the R. Hebert and M. Constantin samples are visual estimates provided by them. Modes for the J. Maeda samples were also estimated by H. Dick. "Other" refers largely to metamorphic replacements of primary minerals, as can be seen where the sum of the major igneous minerals is <100. This presents a problem that the user should be aware of insofar as most of the remaining data represent simple "primary modes" where the replacements are lumped with the amount of relict igneous mineral phase. A quantity of 0.1 has been arbitrarily used wherever an analyst gives a modal estimate of "trace."

Textural Classification

Textural terms are difficult to quantify, as they are often quite subjective, particularly for igneous rocks. However, column AD gives codes corresponding to the deformation microfabrics and intensity of crystal-plastic deformation intensity seen in many thin sections as well as the presence or absence of an igneous lamination. These are based on the guidelines set forth in table T4 in "Structural Geology" in the "Explanatory Notes" chapter of the Leg 176 *Initial Reports* volume. These textural codes were assigned by the structural geology team to all the Leg 176 shipboard thin sections, and we have taken their data from the Leg 176 *Initial Reports* volume. In addition, J. Hirth, who was a member of the Leg 176 structure team, has further described his, W. Bach's, and H. Dick's samples with Dick; and Dick has described the textures of J. Maeda's and most of P. Robinson's samples using the same criteria. In addition, M. Constantin provided unpublished textural data for their samples that permitted H. Dick to estimate the deformation grade, which has been included in the tables.

Textures 1a and 1b refer to a largely undeformed simple igneous texture without and with an igneous lamination, respectively (usually defined by a feldspar-shape fabric). Textures 2, 3, and 4 refer to the intensity of crystal-plastic deformation. Texture 2 represents <30% recrystallized plagioclase with only minor crystal-plastic deformation of pyroxene and relict igneous fabric preserved, whereas texture 3 represents >30% recrystallization of plagioclase with moderate recrystallization of pyroxene and a moderate shape-preferred orientation fabric. Texture 4 represents an extensively recrystallized rock with strongly bimodal grain size distribution with plagioclase, clinopyroxene, and olivine, all extensively recrystallized with bent and kinked porphyroclasts of the original igneous minerals. Textures 5 and 6 refer to the presence of semibrittle and brittle/cataclastic fabrics. The latter can be superimposed on either crystal-plastic or igneous fabrics, and so in some cases there may be two codes given in the CP field.

Detailed information on the analyses are given in columns AE through AI, with "pt" being the analyst's analytical point number,

which may start over with each grain or may represent the sequential point number for an entire analytical run on the microprobe. Where the analyst did not give a point number, we have arbitrarily assigned one. Where the row in the table represents an average or the standard deviation of the average rather than a single analytical point, the number given is the number of analytical points in the average. Column AF gives the grain number, prefixed by a two- or three-letter code for the mineral analyzed. This allows the user to combine and sort data from the different tables. Column AG gives the location of the point analyzed on the grain. C = core, R = rim, and i1, i2, i3, and so on = successive analytical points between the core and the rim numbered sequentially outward (thus, "C, i1, i2, i3, R" represents five sequential analyses from core to rim). B = an isolated point somewhere within a grain. In column AG, neo = neoblast, and ANe and sdNe = averages and standard deviations for neoblast analyses. AC, sdC, AR, and sdR = averages and standard deviations for multiple analyses on cores and rims of grains. Whereas standard deviations are given for all sets of two or more analyses on a single grain, the user is advised that a standard deviation for two points is not very meaningful. Pt = a single analytical point on a grain where no additional spots were analyzed, and thus no average or standard deviation is given for the grain. This is often referred to in the text as a "spot analysis." Columns AH and AI give the rough dimensions of the grain analyzed in millimeters or a simple estimate of the grain size: F = fine grained (<1 mm), M = medium grained (1–5 mm), C = coarse grained (5–30 mm), and P = pegmatoidal (>30 mm). Where only a single letter code is given, it generally is for the average grain size of the rock. When two-letter codes are given, the first code is for the grain analyzed and the second for the average grain size of the rock.

Averaging of Analyses

Average analyses for individual mineral grains and their standard deviations are given in the tables. Different analysts, however, used different analytical schemes with different goals in mind. For the most part, the averages given in the tables represent a single grain. Several analysts, however, notably P. Robinson, K. Ozawa, and P. Meyer, were generally attempting to obtain average compositions for the thin section rather than averages for individual grains. For P. Robinson and P. Meyer, we have recast their data such that averages represent average compositions for individual grains, though this often produces many averages and single-point analyses, whereas for K. Ozawa, there are insufficient data to identify the individual grains analyzed and so all analytical points for a given mineral from a thin section are averaged in the tables. The user seeking average compositions for thin sections may want to recombine and average the data by thin section. A point of caution, however, is advisable here. The Hole 735B core is highly heterogeneous, with nearly a thousand discrete igneous intervals identified in hand specimen by the shipboard scientific parties. Additional subdivision on the centimeter scale is possible (e.g., Natland, **Chap. 11,** this volume), and it should be noted that there are abrupt changes in lithology and mineral chemistry present on the centimeter and millimeter scale. Thin sections commonly cross boundaries between different lithologies, so averaging compositions by thin section may be inappropriate for many samples.

The first author sought to systematically document the extent of chemical zoning present in a thin section. For this purpose, grains were

selected for analysis representing a combination of coarse grain size and the greatest optically apparent zoning, with usually only a single grain analyzed for each rock type. Thus, for plagioclase, a single grain was usually analyzed at six locations, starting at the core and moving sequentially out to the rim. For pyroxene, where exsolution was often present, a 10-µm spot size was used with 10 adjoining spots analyzed in a traverse across the plane of exsolution in an attempt to obtain the primary igneous composition. Wherever the grain size was suitable, a separate traverse was made on the core and the rim of the pyroxene grain. Thus, most of H. Dick's analyses represent pyroxene core and rim compositions, rather than bulk grain composition. The effect of this can be seen in many of the downhole plots presented later in this paper, where the small offset between core and rim compositions makes them plot together as an oval—giving the impression that the plot is blurred. In many cases, however, particularly with orthopyroxene, the grain was interstitial to olivine, plagioclase, and clinopyroxene and only one traverse was made, representing a bulk composition. Users are advised to use column AE to sort out averages representing a satisfactory number of points on a given grain if they are attempting to evaluate the extent of heterogeneity on a grain scale.

RESULTS

Mineral Compositions

Below, we discuss the chemistry of the major silicate phases. Though microgabbros are included in Tables **T1, T2, T3, T4,** and **T5,** we generally describe only variations in the relatively coarse grained gabbros in the plots and discussions. We do this because the plots are already cluttered and variations in the microgabbros mimic those of the gabbros and show no overall coherent stratigraphic variations.

Plagioclase

Although a few grains of true igneous potassium feldspar were found in rare granitic veins, close to 60% of the Hole 735B gabbros are made up of plagioclase. Plagioclase ranges in abundance up to 80% in some troctolites, with most gabbros lying within the range of 50%–65% and extending down to <20% in rare oxide gabbronorite and troctolitic gabbros (Dick, Natland, Miller, et al., 1999). It is present in every rock type examined, typically in near cotectic proportions with clinopyroxene and olivine (Bloomer et al., 1991). It is generally equigranular and relatively coarse grained with a subeuhedral to anhedral shape interlocking with clinopyroxene and olivine or subophitically enclosed by clinopyroxene. Rocks composed of near euhedral plagioclase in a matrix of clinopyroxene and olivine are rare. Figure **F1A** shows single-spot analyses and average feldspar compositions for 1656 feldspar grains plotted in the feldspar ternary (the few analyses of K-feldspar are not included here). With the exception of a few isolated Or-rich analyses, which are likely bad data that passed our preliminary screen, all the compositions define a very tight trend close to the anorthite-albite join far from saturation with respect to orthoclase. Whereas they range from An_{80} to An_{8}, there is a sharp drop in abundance at An_{30}, with most of the remaining feldspars found in felsic veins ranging from diorite through tonalite and trondhjemite. Plagioclase is typically very uniform in composition,

F1. Feldspar ternary for plagioclase grains, p. 32.

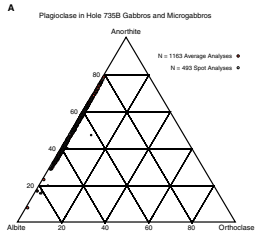

with the average composition close to that of its core and a locally more sodic rim. The average standard deviation for anorthite content for analyses of individual grains (generally four to six points per grain) is only 1.9%. Although both normal and reversed zoning are present, the former is far more common. Locally large core to rim variations exist, with up to 10 mol% anorthite variations common. No systematic pattern has been found downhole for zoning, with large intragranular variations in feldspar compositions locally present downhole (Fig. F1B).

In general, plagioclase is quite fresh, a characteristic of Hole 735B gabbros, where total alteration rarely exceeds a few percent. Examination of the data in Table T1 will show the reader that whereas neoblast compositions in deformed gabbros may be identical to the primocryst compositions in many cases, in others they may be significantly more sodic than relict primocrysts. In part, this is due to reaction with late iron-rich fluids migrating through the gabbros, and in other cases, it is due to reaction with hydrothermal fluids that have locally metasomatized the gabbro. Distinguishing between these two origins is tricky. Examination of the P. Robinson data set, however, taken largely from the most altered gabbros in the hole, shows that secondary or altered primary feldspar is locally quite abundant where alteration is heavy. Since this paper is primarily concerned with igneous petrogenesis, we have attempted to screen out the most obviously altered and secondary feldspar compositions. The primary criterion used is a strongly bimodal feldspar composition distribution with a high-calcium plagioclase population lying close to the cotectic trend for plagioclase-olivine or plagioclase clinopyroxene crystallization and a second population lying between An_0 and An_{30}. Analyses were excluded if this second population lay far from the inferred igneous cotectic trend (with an absence of a second population of coexisting late-magmatic igneous pyroxene and oxides representing obvious late-stage melt infiltration) and in the presence of significant amounts of hydrothermal amphibole, chlorite, or quartz.

As can be seen in Figure F2, there is a good correlation between feldspar composition and rock type, with the most calcic feldspar (up to An_{84}) in troctolites followed successively by olivine gabbros, disseminated oxide-olivine gabbro, gabbronorites, oxide gabbros, and finally the various felsic veins. An impressive feature of Hole 735B compared to layered intrusions is the very large range in feldspar compositions found from the hand-specimen to the outcrop scale. In many layered intrusions, variations of only 4 or 5 mol% anorthite may occur over 1000 m or more. In Hole 735B, it is possible to find nearly the full range of igneous feldspar composition in a single hand-specimen scale (Table T1). This reflects the incredible diversity of rock types at all levels in the Hole 735B section.

There are also significant differences in the feldspar population with depth. A strongly bimodal population is present in the upper 500 m (Bloomer et al., 1991; Dick, 1991a; Natland et al., 1991; Ozawa et al., 1991); a feature that is also observed in the whole-rock chemistry. This bimodal distribution disappears entirely in the lower 1000 m, however, with the distribution becoming strongly skewed to calcic feldspars in the range of An_{50}–An_{65} in the bottom 500 m. It is noteworthy, however, that this does not simply reflect the decrease in abundance of oxide gabbros and gabbronorites, as the composition of feldspar in oxide gabbros and gabbronorites in the bottom 500 m is also more calcic than in the same rock types in the upper 500 m (Fig. F2). The lack of very sodic

F2. Distribution of anorthite values, p. 34.

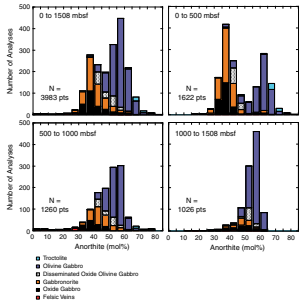

plagioclase compositions (<An_{30}) in the upper 500 m, on the other hand, is not due to an absence of felsic veins, which constitute 1% of the Leg 118 core (Dick, 1991a) but is instead due to sampling bias. Whereas the Leg 118 igneous petrologists largely ignored the felsic veins, the reverse was true for the Leg 176 Scientific Party, where they were extensively (obsessively) sampled.

The anorthite content of average and spot plagioclase analyses of the Hole 735B gabbros is shown plotted against FeO in Figure **F3.** Here again, the strong bimodal distribution of anorthite content is clearly evident. Despite the large scatter in the data, however, there is also a strong overall increase in plagioclase FeO from troctolite to olivine gabbro, followed by a significant decrease in oxide gabbros, with gabbronorites and disseminated oxide olivine gabbro having somewhat intermediate compositions. Again, with considerable scatter of a few outlying points, a second trend of decreasing iron content with decreasing anorthite is evident for the felsic veins, offset to significantly higher iron than the gabbro trend. If this second trend is real, it might suggest that the mechanism of formation of the felsic veins was not simple fractionation of a ferrobasalt melt but could involve other processes such as liquid immiscibility.

F3. FeO* vs. anorthite content, p. 35.

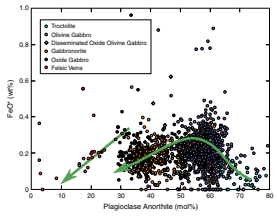

Clinopyroxene

Clinopyroxene is the second most abundant phase in the Hole 735B gabbros, ranging from a few percent in troctolite to close to 60% in a few gabbros, varying inversely with plagioclase abundance. It is generally present in near-cotectic proportions with plagioclase and olivine, however, with the large majority of Hole 735B gabbros having from 15% to 45% (Dick, Natland, Miller, et al., 1999). It is most often present as a coarse granular or subophitic phase with plagioclase and olivine but also commonly forms large oikocrysts, typically several centimeters or more in length, enclosing plagioclase and olivine chadocrysts. In addition it forms small selvages or reaction rims on the margins of plagioclase and olivine grains, where it is easily confused when in low birefringence orientations with relatively birefringent sections of hypersthene present in the same habit.

The major element composition of Hole 735B pyroxene is shown in the quadrilateral in Figure **F4A** along with the composition of enstatite and diopside from Atlantis II Fracture Zone residual mantle peridotites. The clinopyroxene from Hole 735B gabbros is largely augite, with a small but significant gap in composition between them and the field for the peridotites. Overall, given the large number of analyses, there is a fairly tight grouping with fewer than 20 of 861 analyses plotting away from the main cluster. Again, there is a broad trend corresponding to lithology, with the most magnesium and calcic augites present in the troctolites, followed by the olivine gabbros, disseminated oxide olivine gabbro, gabbronorites, and oxide gabbros, all trending overall to lower wollastonite contents. This trend broadly parallels the pyroxene solvus of Lindsley et al. (Fig. **F4B**), consistent with crystallization from a fractionating basalt liquid (Lindsley, 1983; Lindsley and Dixon, 1976). It should be noted that there is much broader overlap between the fields for different rock types than was originally found by K. Ozawa and coworkers in the upper 500 m of Hole 735B. In part, this could be due to somewhat different criteria in assigning rock names between the Leg 118 scientists and those from Leg 176, but we suggest, based on the distribution of plagioclase compositions in Figure **F2,** where oxide gabbros

F4. Pyroxene analyses, p. 36.

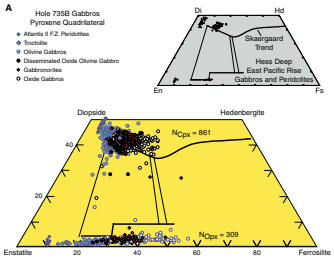

deeper in the hole have more calcic plagioclase on average than those in the upper 500 m, that the greater overlap is largely real and therefore reflects significant differences in petrogenesis of the rocks downhole. The scattered analyses lying intermediate between the main clinopyroxene and orthopyroxene trends could represent bad analyses, but without an opportunity to carefully examine the thin sections from which they were obtained, this would be difficult to prove one way or the other.

A systematic study of zoning in clinopyroxene in the Leg 176 section is shown if Figure **F5,** where core and rim compositions are plotted downhole. No discernible consistent pattern of clinopyroxene zoning, however, can be seen downhole. Clinopyroxene generally shows normal zoning with rims consistently more iron, sodium, and titanium rich than the cores. The extent of zoning is relatively limited for magnesium and iron, rarely amounting to more than 5 mol% of the iron-rich end-member. Reversed zoning is rare, identifiable in only a few oxide and olivine gabbros downhole. An exception is found for titanium, which is frequently lower on the rims of oxide-rich gabbros, even while the latter are more iron rich and sodic. This is easily explained, however, by the appearance of iron-titanium oxides on the liquidus. The latter would cause titanium in the liquid to rapidly drop with additional crystallization after reaching a peak prior to their appearance. Overall, the greatest zoning is seen for titanium, which commonly exceeds a factor of two in concentration from core to rim. This is consistent with the formation of late iron-titanium–rich interstitial liquid during crystallization of the gabbros and its migration by porous flow through the section.

Minor element (Cr, Al, Ti, and Na) concentrations in the Hole 735B gabbro clinopyroxenes define rough differentiation trends correlating with decreasing Mg# (Fig. **F6**). Chrome exhibits a striking strong exponential drop in abundance with decreasing Mg#. This corresponds to the presence of cumulus chrome spinel in the troctolites and the strong preference of chrome for pyroxene relative to melt with the onset of cotectic pyroxene crystallization. Alumina shows a strong linear decrease with decreasing Mg#, whereas sodium, if anything, exhibits a slight enrichment. The most interesting element is titanium, which, with decreasing pyroxene Mg#, first increases sharply, reflecting its preference for the melt during cotectic crystallization of olivine, plagioclase, and pyroxene, then abruptly decreases, reflecting the appearance of iron-titanium oxides on the liquidus with crystallization of the oxide gabbros. What is particularly interesting is that at any particular pyroxene Mg#, there is a factor of two range in typical (not outlier) titanium concentrations. Moreover, magmatic oxides are also found in greater than accessory amounts in gabbros with pyroxene Mg# much greater than 75—the point at which the overall trend suggests oxides first appeared on the liquidus. This latter oxide, the presence of oxide gabbros with relatively high Mg# clinopyroxene, and the dispersion of the titanium contents all argue for extensive postcumulus melt-rock interaction with reequilibration of crystals and trapped melt and precipitation of additional oxides both from trapped melt and from relatively iron-rich melts migrating through the cumulus crystal mass.

Orthopyroxene

Orthopyroxene is ubiquitous as an accessory phase throughout the Hole 735B gabbros, appearing as thin selvages or reaction rims, gener-

F5. Clinopyroxene vs. depth, p. 38.

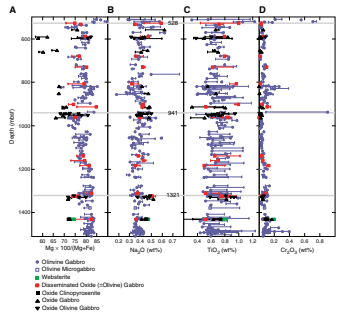

F6. Minor element oxides vs. Mg#, p. 39.

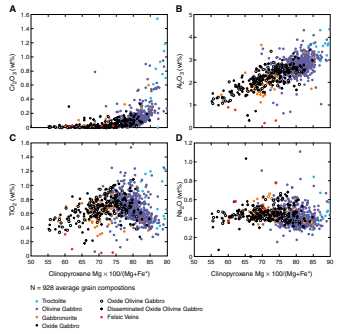

ally between olivine and plagioclase and minor overgrowths on clinopyroxene. It is also present as a relatively coarse grained granular phase in rocks of intermediate composition, including both orthopyroxene-olivine gabbro and gabbronorites of various descriptions. It does not generally persist as a granular, presumably cumulus, crystallization phase to the more extreme iron-rich compositions found for many oxide gabbros. The composition field for orthopyroxene is shown in the pyroxene quadrilateral in Figure F4A. Orthopyroxene defines a very tight trend parallel to the pyroxene saturation surface of Lindsley and co-workers (Lindsley, 1983; Nabelek et al., 1987), with slightly increasing wollastonite content with decreasing enstatite (Mg#) content. This broad range in composition, from En_{86} to En_{43}, was previously noted by Ozawa (Ozawa et al., 1991). What can be seen here, however, is that the trend passes through the infamous Skaergaard trend, where pigeonite is supposed to replace hypersthene as a cumulus phase. In the Skaergaard Intrusion, however, pigeonite is actually present as an intercumulus phase only in the marginal border group (S. Morse, pers. comm., 2001) and this replacement of hypersthene is actually better seen in the Bushveld Complex (G. Cawthorn, pers comm., 2000). Pigeonite is present in the Hole 735B gabbros, where it has been reported by Ozawa et al. (1991), but is largely absent in the lower kilometer of Hole 735B. Because of the difficulty in analysis of this latter phase, which generally shows coarse exsolution, there are only a couple of pigeonite analyses in Table T2. The scarcity of pigeonite in Hole 735B could reflect relatively low pressure crystallization of the Hole 735B gabbros in an ocean ridge environment and differences in melt composition relative to the rare pigeonite-bearing layered intrusions.

Perhaps the most significant aspect of the orthopyroxene distribution in Figure F4A is its very low wollastonite content and the tightness of the trend. The latter can in part be attributed to the steepness of the pyroxene solvus relative to clinopyroxene (see Fig. F4B) but also implies relatively low equilibration temperatures. This is not likely an analytical problem due to exclusion of clinopyroxene lamellae from the analysis, as several investigators specifically used techniques designed to include these. As seen from Figure F4, hypersthenes in Hess Deep gabbronorites have significantly higher wollastonite content yet were analyzed using the same techniques as many of the orthopyroxenes in Table T2 (Natland and Dick, 1996). Thus, the difference in orthopyroxene compositions here reflects a difference in equilibration temperature. The Hess Deep gabbronorites are generally fine-grained rocks, believed to have crystallized from the melt lens below the sheeted dikes at the East Pacific Rise (Natland and Dick, 1996). The lower equilibration temperature of the relatively coarse grained Hole 735B orthopyroxenes could reflect reequilibration during relatively large scale percolation of late-magmatic liquids through the cumulates or relatively slow cooling and massive subsolidus recrystallization. The former possibility is presented by the gabbronorites, which contain coarse granular orthopyroxene, believed to originally represent cumulus grains precipitated during initial crystallization of the gabbro. If rapid cooling occurred in the absence of the widespread percolation and reequilibration with late-magmatic liquids, one would expect that the orthopyroxene compositions would be similar to those in the Hess Deep gabbronorites.

Orthopyroxene shows very similar composition trends for aluminum, sodium, and titanium with Mg# as those previously described for clinopyroxene, so they will not be described in detail here. Unlike cli-

nopyroxene, chrome shows no trend—probably because its concentration is very low and is likely close to the detection limit for most probes.

Olivine

Olivine is typically present in the Hole 735B gabbros as rounded anhedral grains but varies from subhedral to amoeboid and locally may enclose plagioclase crystals in an oikocrystic or poikilitic habit. Its abundance varies from 0 to >50 vol% in a few rare examples, with the large majority of olivine-bearing gabbros having <20 vol% olivine, with 5% to 10% representing the most typical values. There is only a rough correlation of volume percent modal clinopyroxene with olivine abundance, which generally decreases with increasing clinopyroxene (Dick, Natland, Miller, et al., 1999).

Olivine composition shows a large continuous range in the Hole 735B gabbros ranging from $<Fo_{30}$ to Fo_{84}. Overall, there is a fair relationship with rock type, with the most magnesian olivine present in the troctolite microintrusions above 550 mbsf and becoming successively less magnesian from troctolitic gabbro, to olivine-gabbro, disseminated oxide olivine gabbro, gabbronorite, oxide gabbro, and, finally, oxide olivine gabbro. Overall, it is again noteworthy that there is more overlap among these fields for the entire Hole 735B section than was found higher in the hole for the Leg 118 section (e.g., Ozawa et al., 1991). Whereas nickel concentration is highly variable and there is no correlation with forsterite content, the limiting value of nickel decreases sharply with fayalite, consistent with the strong preference of nickel for olivine and its rapid depletion in the melt with fractional crystallization (Fig. F7). The broad range of nickel concentration, ranging down to the detection limit at all forsterite values, suggests that the concentration of nickel in olivine has been strongly affected by postcumulus processes and reequilibration with late melt compositions.

F7. NiO vs. forsterite, p. 40.

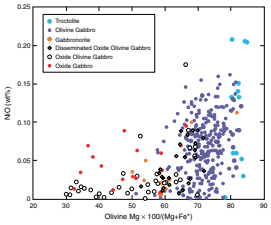

Brown Hornblende

Brown hornblende is nearly ubiquitous in the Hole 735B gabbros but only rarely exceeds trace amounts (<1%). It is commonly present as an intergranular selvage between olivine, pyroxene, and plagioclase with much the same growth habit as orthopyroxene. It appears to have a particular affinity to oxides and is commonly found intergrown with or enclosing ilmenite and titanomagnetite. It also reaches its greatest abundance in the oxide-rich gabbros, where it may be present in more than trace amounts (1%–5%). The olivine gabbros, with a single exception, generally have significantly <1% brown hornblende, usually present in only trace amounts. Based on textural criteria, most of the brown hornblende appears to be igneous. However, there is clear petrographic evidence that it can grade into metamorphic amphibole, with dark reddish brown hornblende locally grading into ragged green amphibole. Brown hornblende exhibits only weak compositional patterns with a tendency toward lower aluminum, calcium, titanium, and chromium and somewhat higher potassium with decreasing Mg# (Fig. F8). There is also considerable downward scatter from the main cluster of aluminous titaniferrous amphibole compositions (10%–13% Al_2O_3 and 2%–4% TiO_2), likely due to the inclusion of metamorphic amphibole compositions in the database.

F8. Oxides vs. Mg#, p. 41.

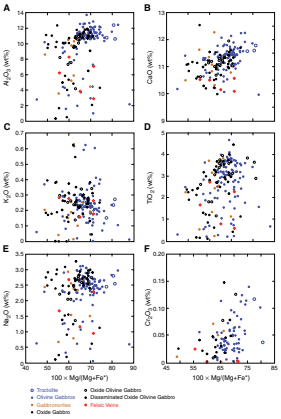

Mineral Covariations

Plagioclase-Ferromagnesian Silicates

Shown in Figure F9 are plots of plagioclase anorthite content vs. Mg# (100 × Mg/[Mg+Fe]) of olivine, orthopyroxene, clinopyroxene, and brown hornblende. Overall, there are excellent correlations between plagioclase and all the other primary silicate phases, consistent with crystallization along the olivine-plagioclase, olivine-plagioclase-clinopyroxene, and finally plagioclase-clinopyroxene-oxide ± olivine cotectics. There are significant kinks in the trends, reflecting the initial appearances of clinopyroxene and oxides on the liquidus during cumulus crystallization. This demonstrates that the primary control on rock composition was simple magmatic differentiation along a tholeiitic liquid line of descent. An important feature of these trends, however, is the very large scatter along most of them, with a 10 mol% or greater variation in plagioclase composition at any particular value of Mg# for olivine, clinopyroxene, and brown hornblende. This lies far outside analytical scatter, even when comparing analyses from many different laboratories. Only orthopyroxene exhibits a significantly tighter trend. This scatter could be due to the intrusion and crystallization of a range of basalt liquids representing different degrees of mantle melting (e.g., Meyer et al., 1989) or it could be due to postcumulus processes such as incomplete reequilibration of the crystal matrix with different liquids percolating through the crystal mush. Whereas the basalt glass compositions reported for the Atlantis II Fracture Zone (Dick, 1991a) have sufficiently large scatter in Ca/(Ca+Na) at constant Mg# to explain the scatter along the trends in Figure F9, this cannot explain the large scatter in TiO_2 contents seen for pyroxene (Fig. F6) or the range of nickel values seen in Figure F7. Thus, we prefer the latter hypothesis that most of the scatter is due to reaction with late-magmatic liquids and not due to a broad spectrum of primary mantle melt compositions.

F9. Plagioclase anorthite vs. olivine, cpx, brown hornblende, and opx, p. 42.

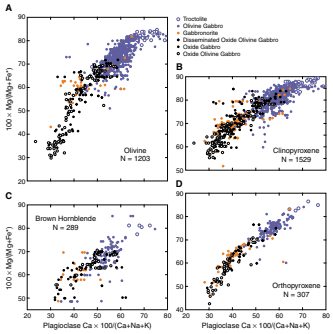

Mafic Silicate Covariations

Shown in Figure F10 are Mg# covariation diagrams for clinopyroxene, olivine, orthopyroxene, and brown hornblende. Clear curvature can be seen in the trends for olivine with clinopyroxene and orthopyroxene, showing the complex controls on Fe-Mg partitioning between these phases. These diagrams again show excellent correlations similar to those seen in the previous figure, with the worst correlations existing for brown hornblende. The latter likely reflects the inclusion of metamorphic compositions in the hornblende data set as well as the very late magmatic character of the amphibole, which likely crystallized out of equilibrium with the bulk of the matrix mineralogy. The correlation between olivine and clinopyroxene shows the largest scatter (~10 mol% for any particular value of olivine or clinopyroxene Mg#, suggesting that these minerals preserve considerable local disequilibrium produced by postcumulus processes). By contrast, the tightest correlation exists between orthopyroxene and olivine, which likely reflects the ease of olivine reequilibration and the steep slope of the orthopyroxene solvus combined with its relatively late magmatic interstitial character.

F10. Molar ratio covariation plots of Mg#, p. 43.

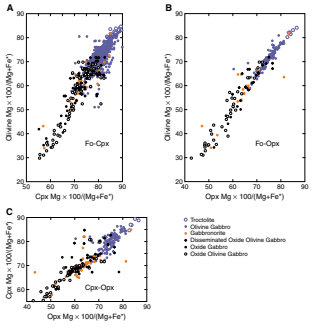

Downhole Cryptic Chemical Variations

Figure F11A and F11B are downhole plots of single-spot and average analyses of individual primary igneous mineral grains. Shown for comparison in Figure F11C is a similar plot of whole-rock Mg# reproduced from Dick et al. (2000). As can be seen, many of the characteristics of the igneous stratigraphy first identified from the whole-rock chemistry are clearly evident in the downhole mineral plots. These include the strongly bimodal chemistry of the gabbros in the upper 500 m of Hole 735B, the sparsity of ferrogabbro and gabbronorites downhole, and the disappearance of the bimodal chemical distribution at ~1000 mbsf. In addition, the strong downward iron and sodium enrichment trend from ~160 mbsf down to the major chemical discontinuity at 274 mbsf found by the Leg 118 scientists (Bloomer et al., 1991; Dick, 1991a; Natland et al., 1991; Ozawa et al., 1991) is clearly defined by the synthesis of mineral compositions. The sequence of five broad trends of upward iron and sodium enrichment in the olivine gabbros is also clearly seen. These latter features define four significant chemical discontinuities in the stratigraphy at 274, 528, 941, and 1299 mbsf, respectively. The origins of these iron enrichment trends in the olivine gabbros and the strong bimodality found in the oxide gabbros in the upper 500 m is the subject of considerable debate among the Leg 118 and Leg 176 scientists.

The extensive intercalation of extreme differentiates with the moderately primitive olivine gabbros in the upper 500 m of Hole 735B is generally considered to be the result of intrusion of late iron-titanium–rich differentiates into the olivine gabbros by percolation along shear zones and intrusion along fractures in the olivine gabbros during active deformation of the section (Bloomer et al., 1991; Dick, 1991a; Natland et al., 1991; Ozawa et al., 1991). There is, in particular, often a striking association between ferrogabbros and disseminated oxide olivine gabbro and high-temperature crystal-plastic and cataclastic deformation throughout the hole. The source of these liquids, given the strong drop in abundance of ferrogabbros in the lower kilometer of Hole 735B, would likely be the lowermost crust—either liquids produced during the crystallization of the Hole 735B olivine gabbros or from similar rocks nearby.

A simple mass balance calculation using the logged proportions of different lithologies and their average whole-rock compositions shows that whereas the bulk composition of the entire Hole 735B section is close to that of a moderately differentiated mid-ocean-ridge basalt (MORB) (Mg# = 69.2 wt% and TiO_2 = 0.87 wt%), the bulk compositions of each of the 500-m increments are inconsistent with a single upwardly differentiating sequence as identified in some layered intrusions (Dick et al., 2000). The uppermost increment, for example, has the most primitive Mg# (71.4), but has high TiO_2 of 1.41 wt%, inconsistent with a reasonable mantle melt composition. Whereas bulk Mg# does decrease upward for each 500-m sequence, bulk anorthite remains constant and bulk TiO_2 increases nearly threefold, changes inconsistent for progressive residues of fractional crystallization. Throughout the core, there are numerous small patches of undeformed oxide-rich gabbro that appear to represent local puddling and crystallization of late melt in the gabbro, showing that such liquids were formed and segregated locally. Taken by itself, however, the olivine gabbro must have lost considerable late iron-titanium–rich liquid, as it lies far from the composition of any reasonable MORB liquid with respect to incompatible element concentrations. It is thus believed that the distribution of late-

F11. Plagioclase anorthite and clinopyroxene and olivine Mg#, p. 45.

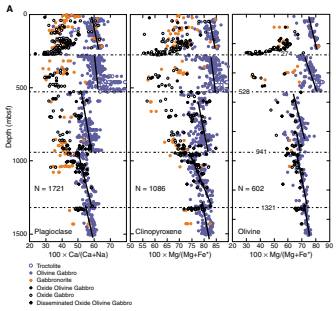

magmatic melts produced by crystallization of MORB magmas during intrusion and solidification has been strongly controlled by the ongoing deformation of the crust beneath the rift valley floor, characteristic of slow-spreading ridges (Bloomer et al., 1991; Dick, 1991a; Natland et al., 1991).

The tectonically controlled igneous differentiation of the lower ocean crust found in Hole 735B is strikingly different from the processes believed to have formed the large stratified layered intrusions and is relatively new to much of the igneous community. However, it is the initial igneous stratigraphy of the section, represented by the olivine gabbro stratigraphy, that is probably the most controversial feature of the igneous petrogenesis of Hole 735B. The five upward enrichment trends seen in the whole-rock chemistry and mineralogy of the olivine gabbros could be explained as representing a series of small upwardly differentiating intrusions or cycles of intrusions. As can be seen from inspection of Figure **F11,** many of these cycles overlap, with what appears to be the most extreme differentiates of an underlying sequence intercalated with olivine gabbros at the base of the next (e.g., the 941-mbsf discontinuity). This suggests that the discontinuities do not represent the boundaries between simple plugs that have differentiated in situ to form discrete intrusions. Rather, it would appear that there are four or five cycles of intrusion, each representing multiple injections of a related magma that are locally interspersed with screens of older rocks from a previous cycle. In detail, however, each of these discontinuities is different. Thus, we wish to consider each one separately, for as we will show, there is substantial evidence that each of the discontinuities has a different petrogenesis and they may not all represent simple breaks in the stratigraphy produced by the intrusion of new magma batches.

The 274-mbsf discontinuity lies at the base of the unique downward iron enrichment trend in lithologic Units III and IV disseminated oxide olivine gabbro and oxide gabbros. Below it is the top of an upward iron enrichment trend running through the underlying Unit V olivine gabbro. It is shown in more detail in an expanded downhole plot in Figure **F12.** The Unit III and IV ferrogabbros above the boundary contain a foliation that flattens systematically with depth, defining a simple zone of downward-increasing shear. Such shear zones are well known as "ductile faults" (Ramsay, 1976; Ramsay and Graham, 1970) and represent the progressive flattening of a foliation with increasing strain from parallel to the principal stress direction to parallel to the plane of faulting. It is common to find an abrupt discontinuity at the base of these shear zones, as is the case here, where fault displacement has juxtaposed rock from where the shear zone nucleated over undeformed rock. Recrystallized rocks, due to reduction of grain size, are normally relatively impermeable compared to coarse-grained rocks. However, where shear is active, increased permeability occurs due to the formation of microcracks and grain boundary sliding. Thus, an active ductile fault can localize fluid flow, including late-magmatic melts in a compacting gabbro massif. Such flow would be greatest where strain is largest. Thus, the downward iron enrichment trend is consistent with increasing melt-flux and melt-rock reactions between deforming olivine gabbro protoliths and late iron-rich melts along a shear zone. Significantly, it can be seen that near the top of this series of oxide gabbros and in the middle of the sequence at around 225 mbsf there are undeformed screens or shear polyhedra of olivine gabbro that lie on the upper olivine gabbro mineral composition trend. These olivine gabbros contain extension cracks filled with undeformed oxide-rich gabbro, demon-

F12. Mineral variations around the 274-mbsf discontinuity, p. 48.

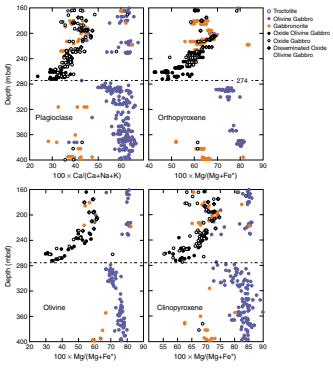

strating the presence of iron-rich melts during deformation in the shear zone. Thus, the downward iron enrichment trend is likely due to migration late iron-rich melts and melt-rock reaction along a large composite shear zone (Dick, 1991a; Dick et al., 1992).

With the synthesis of all the available data, it now appears that at least two additional downward iron-enrichment trends can be seen in the upper 500 m of Hole 735B. These are defined largely by the gabbronorites intercalated with older olivine gabbros from 0 to 136 mbsf and by ferrogabbros intercalated with older olivine gabbros from 356 to 450 mbsf (Fig. **F11**). This suggests that there was considerable imbrication of the faulting and formation of shear zones in the olivine gabbros controlling late melt distributions in this section, with a significant variation in the intruding melt compositions.

A striking feature of the olivine gabbro underlying the 274-mbsf discontinuity is a sharp swing and broad spread of plagioclase and clinopyroxene compositions right at the top of the sequence adjacent to the contact with the ferrogabbro sequence. By contrast, olivine, the most easily reequilibrated phase, shows more uniform composition below the contact and a small but steady increase in Mg# from 319 mbsf (Fig. **F12**). The rest of this lower olivine gabbro sequence can be interpreted as lying on a simple extension of the upper olivine gabbro trend. Moreover, it is striking that these two sequences are on average more magnesian and calcic than the lower three olivine gabbro sequences. This raises the possibility that these two olivine gabbro sequences actually represent a single intrusive cycle disrupted by cross-intrusion of the ferrogabbro sequence along a shear zone. Plagioclase and clinopyroxene are the two phases most resistant to rapid reequilibration with exotic magmas and thus can preserve the early magmatic record where more rapidly equilibrated phases such as olivine cannot. Thus, the broad range of plagioclase and clinopyroxene compositions for 100 m below the 274-mbsf discontinuity argues for equilibration with a large range of liquids rather than a single upwardly differentiating magma. This and the preservation of calcic-plagioclase and magnesian-clinopyroxene at the top of the lower olivine gabbro is most simply explained due to melt-rock reaction driven by percolation of a small quantity of melt from the overlying ferrogabbro intrusion into the underlying olivine gabbro. This, then, suggests that originally both the upper and lower olivine gabbros above the 528-mbsf discontinuity were part of a single olivine gabbro sequence.

The alternative hypothesis, that the upper two olivine gabbro sequences represent separate upwardly differentiated sequences, is deemed inadequate here as it fails to explain the huge spreads in plagioclase anorthite and clinopyroxene Mg# immediately below the contact and the contrasting small range in olivine forsterite content. Moreover, the large offset of forsterite at the 274-mbsf contact from the overlying olivine gabbro sequence compared to anorthite and clinopyroxene Mg# is also inconsistent with this being a simple intrusive contact, as discussed elsewhere in this paper. The apparent upward iron enrichment trend of the olivine gabbros in Unit V olivine gabbro sequence is explained then as due to reequilibration with iron-rich melts intruded along the overlying shear zone and disruption of the sequence below 400 mbsf by reaction with the primitive melts that produced the cross-intruding troctolites there.

The lowermost gabbros in the ferrogabbro sequence are mylonites representing subsolidus deformation. However, our hypothesis requires significant chemical exchange between the underlying olivine gabbro

and the overlying ferrogabbro sequence. The lower olivine gabbro shows significant iron enrichment down to ~36 m below the 274-mbsf discontinuity. As solid-state diffusion is far too slow to account for this by subsolidus reequilibration of the lower sequence with the overlying ferrogabbro, this requires significant permeability in the lower olivine gabbro at the time of intrusion of the ferrogabbro. This may have occurred because of remelting of the olivine gabbro during faulting accompanying intrusion of the ferrogabbro up the shear zone or because the underlying olivine gabbro was still partially molten at the time of faulting, or some combination of the two.

Shown in Figure F13 is an expanded view of the 528-mbsf discontinuity. We believe that this represents the most significant discontinuity in the stratigraphy of the Hole 735B olivine gabbros, with an average offset of some 13 mol% anorthite and forsterite content between the upper two olivine gabbro sequences and the lower three at this point. It should be noted that the olivine gabbro at the base of the upper olivine gabbro sequence is cross-intruded by an unrelated series of fine- to coarse-grained troctolites. Close inspection of the clinopyroxene profile in Figure F13, however, shows that a case can be made that the contact is actually gradational over some 30 m, with clinopyroxene Mg# and plagioclase anorthite content increasing sharply upward toward the boundary over this interval.

At the 941-mbsf discontinuity there are significant offsets of the trends for plagioclase anorthite as well as clinopyroxene and orthopyroxene Mg#, with generally more calcic plagioclase and magnesian pyroxene in the overlying olivine gabbro (Fig. F11). There is a somewhat smaller, more irregular offset in forsterite (as is also the case for the 1299-mbsf discontinuity). A potentially important feature of this boundary is that there is a series of gabbronorites and oxide gabbros that appear to lie on an upward extension of the lower olivine gabbro trend into the upper olivine gabbro sequence at this point. This raises the interesting question of whether or not these represent intrusion of late differentiates related to the lower olivine gabbro sequence into the overlying gabbros produced.

An expanded view of the 941-mbsf discontinuity is shown in Figure F14. There is a major high-temperature reverse-sense crystal-plastic shear zone at this horizon (Dick, Natland, Miller, et al., 1999), which extends from 930 to 960 mbsf, with a very sharp rise in intensity of deformation at 945 mbsf just below where we have drawn the 941-mbsf discontinuity. The shear zone ends abruptly at 960 mbsf, where the rock passes from mylonite into undeformed olivine gabbro over <10 cm. We analyzed gabbro on each side of this lower contact and found no change in mineral chemistry across it. The question arises as to whether there is any relationship between this 941-mbsf discontinuity and the shear zone. Despite the proximity of some brittle faults, none of the other chemical discontinuities we have identified in the hole correlate directly with the location of a fault or a major crystal-plastic shear zone. However, there is a strong association between crystal-plastic deformation and oxide gabbros through much of the hole, with abundant evidence that deformation was localized in these in the presence of melt (Dick, 1991a; Dick et al., 2000; Natland and Dick, 2001). Thus, it is possible that late-magmatic liquids concentrated at the top of the olivine gabbro, represented by the oxide gabbros and gabbronorites, may have localized deformation here by reducing the strength of rock due to liquid pore pressure. However, the zone of most intense deformation, and hence the region of the greatest strain localization, lies within the

F13. Mineral variations around the 528-mbsf discontinuity, p. 49.

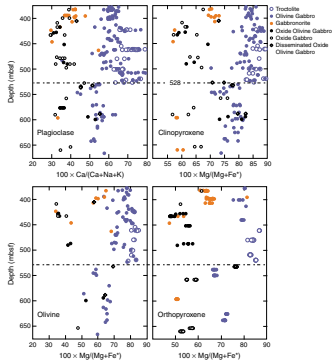

F14. Mineral variations around the 941-mbsf discontinuity, p. 50.

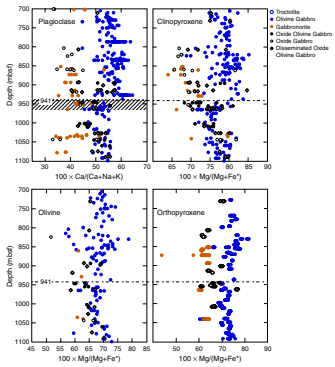

olivine gabbros, not the oxide gabbros and gabbronorites below the 941-mbsf discontinuity. Thus, whereas there is a coincidence here of strain localization and a major cryptic chemical boundary, in detail it is not convincing that this is more than coincidental.

The 1321-mbsf chemical discontinuity, shown in Figure F15, appears to be a relatively minor disruption of the overall upward trend in the olivine gabbros, with the olivine composition profile passing transparently through it. Pyroxene seems to show the greatest disruption, whereas plagioclase shows a smaller discontinuity than at the other boundaries we have discussed. However, the 1321-mbsf discontinuity does coincide with a zone of microgabbro intrusion with accompanying evidence of local melt-rock reaction with the olivine gabbro, producing a variety of oxide gabbros in the wall rock. For this reason, we have included in Figure F15 the mineral chemistry of the late microgabbro microintrusions that we have excluded elsewhere (as they show no vertical stratigraphic coherence and add unnecessary detail to a complex stratigraphy). This was one of two horizons selected for detailed study of the microgabbros and their influence on the wall-rock chemistry by Dick and co-workers. At this point this would seem to be an equally good explanation for this discontinuity as a boundary between two separate intrusive cycles in the olivine gabbros. We note that only slightly deeper in the core there is a second such reaction zone where the products of reaction are somewhat different and include oxide clinopyroxenite, websterite, and gabbronorite. Olivine gabbro on either side of this intrusion appears unaffected, and we suspect that the differences between these two zones of microintrusions reflect differences in the chemistry of the intruding melts and the degree of solidification of the wall rock at the time of intrusion.

F15. Mineral variations around the 1321-mbsf discontinuity, p. 51.

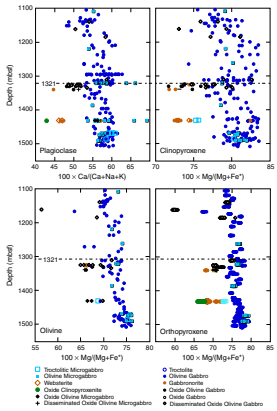

DISCUSSION AND CONCLUSIONS

Stratigraphy of Intrusion

In reviewing our results, it is first instructive to compare the chemical discontinuities we have identified to the divisions of the igneous stratigraphy made by the Leg 118 and 176 Scientific Parties and Dick et al. (1991a) (Fig. F16). Each of the chemical discontinuities, in fact, lies close to one of their boundaries, with only small differences as to where they are drawn. This is encouraging, as it suggests that neither set is arbitrary. The mineral chemistry and lithostratigraphy do suggest that a unit boundary should have been drawn between the Unit Ia massive gabbronorite and the Unit 1b olivine gabbro and gabbronorite at the subunit boundary, as this contact is essentially the same in character as the Unit III/IV boundary (though with opposite polarity). This was not originally done, however, largely because this is also a zone of intense crystal-plastic deformation and hydrothermal alteration, which made identification and separation of the two original subunits tenuous.

A small but significant difference exists between the position of our chemical discontinuity at 941 mbsf and the Unit IX/X boundary drawn by the Leg 176 petrologists. They placed their contact to coincide with a high-temperature shear zone at 960–990 mbsf. As discussed earlier, our data suggest that the latter is a structural, not an igneous, boundary and that the base of Unit X should have been drawn near 941 mbsf. It is one of the curious features of the core that whereas there are numerous high-temperature ductile shear zones and several brittle facies faults,

F16. Anorthite content of plagioclase, p. 52.

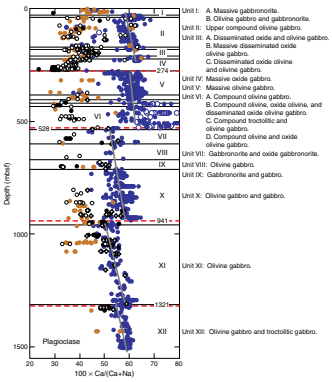

none on close inspection appears to coincide precisely with the major geochemical boundaries in the hole.

Perhaps more interesting is to look at lithostratigraphic boundaries where we did not identify a mineralogic one. In this light, we should note that the lithostratigraphy was intended as a nongenetic descriptive breakdown of a complex core into composite sections with like features. Thus, for example, the Subunit VIb/VIc boundary marks the appearance of small meter-scale troctolite and troctolitic microgabbro intrusions that cross-cut olivine gabbros otherwise continuous with those in Unit VIa, whereas the Unit VI/VII boundary marks the abrupt disappearance of these same troctolite and troctolitic microgabbro intrusions. Likewise the Subunit VIc/VId boundary marks the end of a series of ferrogabbros that cross-intrude the olivine gabbros in Subunits VIa–VIc with a shift to predominantly undeformed olivine gabbro and troctolite.

Noting the actual genetic significance of these different boundaries, then, it is worth considering those between Units VII through X. No breaks in the chemistry based on either mineralogy or bulk rock chemistry have been previously drawn here. Yet on close inspection, for example, one could well draw a chemical discontinuity based simply on an offset in anorthite between Units IX and X—suggesting that the lithostratigraphers may have correctly identified complexities in the core in Units VII–IX that are not evident in the mineralogy or chemistry because of undersampling. It is probable, then, that at least the first of the three lower olivine gabbro sequences identified on the basis of bulk rock chemistry and mineralogy could also be further subdivided.

Our preliminary examination of the database compiled here leads us to confirm many of the prior conclusions of the Leg 118 and Leg 176 Scientific Parties. In particular, the silicate mineral chemistry of the gabbros is consistent with two major cycles of intrusion. The earliest cycle consists of the upper two olivine gabbro sequences above 528 mbsf (Subunit Ib through Unit III and into IV and Units V–VI). The gabbros intruded during the early cycle are significantly more mafic than those intruded in the later cycle, which consists of the three lower olivine gabbro sequences (Units VII–X and XI–XII). Numerous small primitive troctolites cross-intrude the olivine gabbro above 528 mbsf but abruptly disappear below that discontinuity. This leads to the conclusion that the lower olivine gabbros postdate the upper olivine gabbros, crosscutting both the upper olivine gabbros and their cross-intruding troctolites. We suspect, however, that the discontinuity at 274 mbsf between the two upper olivine gabbros is due to the effects of chemical exchange during later intrusion of ferrobasalt melt and crystallization of the oxide and disseminated oxide gabbro sequences in Units III and IV, noting that other interpretations are possible (Natland and Dick, **Synthesis Chap.,** this volume). The two discontinuities separating the lower three olivine gabbro sequences are of problematic origin. Both coincide with the presence of oxide gabbro and gabbronorite, and the lower of the two represents an area of significant late microgabbro intrusion. We also suspect that whereas the upper discontinuity may represent a boundary between two phases of intrusion, the lower one owes its origin to the influence of the late microgabbro intrusions—a departure from the interpretation of the Leg 176 scientists. The latter likely occurred while the host olivine gabbro was still partially molten—allowing for extensive chemical exchange between the wall rock and the crystallizing microgabbro. These issues certainly require additional study.

Tectonic Controls on Late-Stage Melt Migration

Further inspection of the combined mineral and lithostratigraphies suggests that the shear zone identified in Units III and IV, which apparently controlled emplacement of late iron-titanium–rich melts at the top of the section (Dick et al., 1991; Natland and Dick, 2001), had several imbrications. The Unit V/VI boundary separates the massive olivine gabbros of Unit V from similar gabbros containing numerous ferrogabbro bodies. These ferrogabbros in Subunits VIa–VIc are intercalated with olivine gabbros, as in Units III and IV, and also define a similar downward iron enrichment trend. It would appear that this trend likely has a similar origin. Subunit 1a consists largely of massive gabbronorite that defines the top of yet another downward iron enrichment trend extending into Unit II, where numerous small ferrogabbro bodies cross-intrude the olivine gabbros. Thus, based on the mineralogy and lithostratigraphy, there appears to be at least three cycles of intrusion of ferrogabbros from 0 to 500 mbsf representing probable fault-controlled intrusion of late iron-titanium–rich melts. We suggest that these likely represent imbrications of the fault on which the whole Atlantis Bank plutonic massif was unroofed, which then must have extended into or originated in a crystal mush zone beneath the sheeted dikes.

The downhole mineral variations, then, are consistent with upward enrichment of the top of the gabbro section by upward density-driven compaction of melt and intrusion of iron-titanium–rich late magmatic liquids along shear zones and fractures by deformation-controlled melt migration. The particular source of these late melts, of course, could lie out of the section. We note, however, the intriguing association of oxide gabbros and crystal-plastic deformation found in the cores—with the interesting aspect that major zones of deformation correlate with oxide abundance in the upper portion of the hole but do not correlate in the lower portion of the hole (Dick, Natland, Miller, et al., 1999). In addition to this association, there is also a correlation between magmatic foliations and crystal-plastic deformation throughout the hole, with the resulting fabrics produced by both also tending to have similar alignments. The origins of magmatic foliations are controversial but include crystal settling, preferential growth in the direction of melt flow in a crystal mush, and compaction. We view it as unlikely that the foliations in Hole 735B, which also often contain a lineation and generally lie in the plane of the crystal-plastic foliation (Dick, Natland, Miller, et al., 1999), originate from crystal settling or simple compaction. We suspect that the most likely explanation is that they represent preferred crystal growth of plagioclase in the direction of late melt flow through a crystallizing compacting olivine gabbro mush. Therefore, we speculate that these associations between oxide abundance, magmatic foliation, and crystal-plastic deformation reflect the deformation-controlled flow of late iron-titanium–rich melts compacted out of the olivine gabbros at depth and intruded to higher levels in the section where they crystallize to form oxide gabbros.

Cryptic Chemical Variations in the Olivine Gabbros

With this compilation of mineral data we can carefully examine the downhole cryptic chemical mineral variations at the outcrop scale in the olivine gabbros that presumably reflect the earliest history of intrusion and crystallization. We would like to do this in hopes that it will

lead us to some insight as to what the initial scale of intrusion was and the frequency of replenishment during a cycle of intrusion. For this purpose, we screened out all other rock types and plotted the downhole variations of anorthite and forsterite in plagioclase and olivine (Fig. F17A). Although this eliminates stratigraphic complexities created by late-stage ferrogabbro intrusion, it also ignores possible contact effects and contamination of the olivine gabbros by these late melts. This screen also relies on rock names assigned by many different analysts, and thus, unavoidably, some of the variations in Figure F17A may arise from the inclusion of the odd crosscutting ferrogabbro. For most large-scale studies of cryptic variation in large intrusions, every analytical point represents an inflection point in the profile due to limitations in the number of samples that can be taken and analyzed. Even with the very large number of analyses represented by this study, we just get to where significant changes in mineral chemistry are represented by gradients in mineral composition at scales of <100 m, noting that the total number of analyzed samples (~500) is actually far fewer than the 952 discrete lithologic intervals identified in the core.

As can be seen from Figure F17A, there is a considerable amount of fine structure in the Hole 735B olivine gabbro stratigraphy at 1- to 100-m scales. The origins of this cryptic variation, defined by sometimes subtle and sometimes large swings in olivine and plagioclase composition, are unknown at present and cannot be determined on the basis of mineral chemistry alone. Instead, this requires both smaller-scale sampling of selected intervals combined with a detailed comparison of the mineral data to the cores themselves, where the compositional variations can be related to local igneous contacts, cross-cutting microgabbro and oxide gabbro intrusions, late melt flow channels, and high-temperature shear zones. Moreover, as noted above, the number of analyses is actually sufficient only to tell us that systematic cryptic variations exist but are not sufficient to really show the patterns of these variations. What we find, however, is consistent with the oft-stated hypothesis that the larger-scale gabbro units discussed to date are themselves composed of numerous related penecontemporaneous smaller intrusions derived from the same or related parental melts. Noting the rotations of the section likely during emplacement, these intrusions could be small sills, as has been suggested for the Oman section, or small inclined dikelike bodies—a lower crustal analog of a dike swarm (a microintrusion swarm).

Evidence of Large-Scale Late-Stage Permeable Melt Flow in the Olivine Gabbros

Overall, there is a fair first-order correlation between olivine and plagioclase chemistry evident in Figure F17A at wavelengths >200 m. This is impressive, as the diffusion timescales for olivine and plagioclase re-equilibration are very different, with plagioclase having very long equilibration times at magmatic temperatures. It is clear then that at this scale melt transport by permeable flow through the section has not been sufficient to disrupt the large-scale chemical stratigraphy. However, when we examine the chemistry on the finer scales shown in Figure F17A and discussed above, we find that the correlations often become quite poor. Local peaks and lows in anorthite and forsterite content are often offset from one another and frequently show opposite polarity. This is illustrated by the very large scatter found in a plot of the difference in coexisting Fo and An compositions against anorth-

F17. Olivine forsterite and plagioclase anorthite, p. 53.

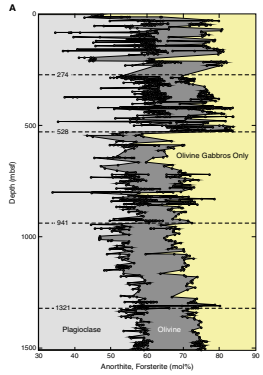

ite in Figure F17B. If anorthite and forsterite were well correlated, one would expect either that most of the data would plot near a single point or define a correlation with variable anorthite content.

In the absence of significant late-stage permeable melt flow across lithostratigraphic boundaries, original cryptic variations, reflecting progressive cotectic crystallization of a magma, would be preserved and the compositions of coexisting phases would be well correlated. The poor correlation of coexisting mineral compositions for Hole 735B olivine gabbros seen in Figure F17, then, would be expected as the result of reequilibration of the matrix of a crystal mush with melts being transported through it by permeable flow. This would result due to the very different solid-state diffusion coefficients for olivine, pyroxene, and plagioclase and differences in reaction rates for different elements within individual phases (e.g., Korenaga and Kelemen, 1997a). In such a situation, even as cryptic peaks in mineral composition profiles are subdued by reequilibration with a migrating melt, the differences in reaction rate will cause the peaks in mineral composition to shift relative to one another. Korenaga and Kelemen (1997a) recently showed in a detailed study of a 600-m layered section of the Oman Ophiolite excellent covariations of the silicate minerals that precluded large-scale melt migration through the section. In particular, they found that the nickel content of olivine correlated well with the forsterite content, with a correlation coefficient of $R^2 = 0.89$. By contrast, for Hole 735B gabbros there is no correlation at all between olivine nickel and forsterite content other than an increasing upper bound for Ni with increasing Mg# (Fig. F7). Similarly, they found a correlation coefficient for anorthite and forsterite in their gabbros of $R^2 = 0.59$, whereas the same correlation coefficient for the Hole 735B olivine gabbros is only $R^2 = 0.42$. Strong evidence for extensive late melt-rock reaction and permeable flow can also be seen in the pyroxene mineralogy, where chrome, alumina, sodium, and most particularly, titanium all show huge variations in concentration at a given Mg#.

In this light, it is interesting to compare the relative offsets of the mineral compositional trends defined by the olivine gabbro sequences at the chemical discontinuities in the upper and lower olivine gabbos. At the 528-mbsf discontinuity, the offset in forsterite content is ~18 mol%, anorthite content ~11 mol%, and clinopyroxene Mg# ~8 mol%. Comparing this to the mineral covariation plots (Figs. F9, F10), we see that this is consistent with differences predicted for cotectic crystallization of a single magma. Whereas clinopyroxene Mg# ranges from ~90 to 55 (35 mol%) along the cotectic trend, olivine Fo ranges from 84 to 30 (54 mol%) and plagioclase An ranges from 75 to 30 (45 mol%). Thus, for the relative magnitude of the offsets of the mineral trends, Fo > An > Cpx, Mg#s are about right for the intrusion of less primitive magmas, represented by the lower olivine gabbros into olivine gabbros derived from more primitive parental magmas (upper olivine gabbros). By contrast, the relative offset at the 941-mbsf discontinuity is ~7% Cpx Mg#, ~8% An, and only ~7% Fo, and at the 1321-mbsf discontinuity, ~3% Cpx Mg#, ~4% An, and only ~2% Fo! This is not consistent with simple intrusive contacts because the offset of forsterite content is smaller than those of clinopyroxene and plagioclase. Interestingly, clinopyroxene and plagioclase do preserve appropriate offsets relative to each other at the 941-mbsf discontinuity. This, combined with the coherent upward decrease in chrome in clinopyroxene from the bottom of the hole to 941 mbsf followed by a jump in chrome content (Fig. F5D), suggests

that this may have originally been a major contact between two different cycles of intrusion.

We find an explanation for this enigma by suggesting that the lower two contacts were modified by exchange with late-magmatic liquids migrating upward through the section. Because of the relatively rapid rate of diffusive exchange and reequilibration of olivine relative to plagioclase and pyroxene with a migrating liquid during permeable flow, contrasts in phase composition across layer boundaries and igneous contacts will be eliminated much faster for olivine than for plagioclase or pyroxene (Korenaga and Kelemen, 1997a). What is significant here is that whereas the 941- and 1321-mbsf discontinuities separating the three lower olivine gabbro sequences have been affected, the 528-mbsf discontinuity separating the upper and lower olivine gabbros has not. This is consistent with a significant phase of late melt flow through the three lower olivine gabbros, which did not affect the two upper olivine gabbro units. Thus, the upper gabbros were likely largely solidified and impermeable at the time of the latter intrusive cycle(s). Hence, we view the lower three and the upper two as representing two different major cycles of intrusion and suggest that the appropriate length scale for large-scale permeable melt flow in the lower crust at a slow-spreading ridge is that of the individual intrusion or cycle of intrusion. Thus, the evidence for permeable flow we find is not for transport of melts from the mantle over long distances or through the entire crustal section, but for local transport of late iron-rich melts through and out of an individual intrusion.

Contrast of Hole 735B to Gabbros from Fast-Spreading Ridges and Ophiolites

Whereas studies of the Oman Ophiolite and at Hole 735B suggest that the lower crust accretes by the intrusion of innumerable small bodies of gabbro at both fast- and slow-spreading ridges, our data suggest fairly large-scale permeable melt flow occurred locally in the Hole 735B gabbros in sharp contrast to the Oman situation documented by Korenaga and Kelemen (1997a). Given the presence of a long-lived melt lens at fast-spreading ridges (and by inference at the paleo-Oman spreading center) and its absence at slow spreading ridges, one might expect the opposite conclusion. The presence of fairly large-scale permeable melt flow in the lower crust at slow-spreading ridges, however, is likely due to the influence of coarser grain size and deformation on transport of late interstitial melt at the scale of individual intrusions. Its absence in the lower crust at fast spreading ridges, in turn, is likely due to the finer grain size and a relatively static crystallization environment. Whereas deformation may considerably enhance compaction and melt migration, this alone may not be sufficient to explain the differences. In a small sill at a fast-spreading ridge, due to the slow cooling rate, grain growth and nucleation would both be slow relative to the time for crystal settling. This would result in the isolation of mineral grains in a rapidly compacted, and therefore impermeable, fine-grained cumulate. By contrast, with more rapid cooling at a slow-spreading ridge but possibly similar scales of intrusion, crystals would grow to larger size, resulting in cumulates with much longer compaction lengths. This would in turn support larger initial porosity and permit larger-scale permeable flow and late-stage melt migration through the cumulate than would have occurred in the fine- to medium-grained

gabbros seen in Oman and drilled in old East Pacific Rise lower crust (e.g., Natland and Dick, 1996).

Comparing the mineral chemistry of the Hole 735B section to that of several well-known ophiolites and the Skaergaard Intrusion reveals several other interesting features. In Figure **F18,** we show the composition field for Hole 735B olivine together with mineral data for the CY4 drill hole from Malpas et al. (1989) on a plot of the downsection variation of plagioclase and olivine for three different sections of the Oman Ophiolite from Pallister and Hopson (1981). The latter authors noted the striking difference of the Oman section from the variations found in layered intrusions like the Skaergaard. The latter are generally believed to be the product of in situ differentiation of a single magma body. Obviously, the Oman section has to have been constructed in an entirely different manner, with no systematic vertical chemical variation from one section to the next, except for a concentration of extreme differentiates at the top of the section immediately below the sheeted dikes. This is generally believed to reflect multiple intrusions of new magma throughout its crystallization history, in contrast to the Skaergaard Intrusion. Another feature worthy of note is that both the Oman section and the Troodos section are far more forsteritic and anorthitic than Hole 735B. This is consistent with crystallization from more refractory parental liquids, the products of higher degrees of mantle melting, and a very different oceanic environment from that of the very slow spreading Southwest Indian Ridge.

It is now believed that Oman represents a composite body of gabbro composed of numerous gabbro sills, one injected into another (Boudier et al., 1996; Korenaga and Kelemen, 1997b). Similarly, there is no simple upward sequence seen in the Hole 735B gabbros; rather, it too seems to be a composite section composed of several small olivine gabbro intrusions on scales of 200 to 700 m, which themselves are each likely the compound products of a cycle of numerous even smaller penecontemporaneous intrusions. The relatively uniform subvertical chemistry profiles of the upper two and lower three olivine gabbro sequences argue that there was only minor in situ vertical differentiation on initial crystallization. Rather, they must have at first cooled fairly rapidly to form a crystal mush. We would believe that the extensive evidence for late-stage permeable flow we have found demonstrates that following this initial burst of crystallization, subsequent cooling and final solidification of these intrusions took a considerably longer time—perhaps contributing to their unusually coarse grain size. Of all the gabbro sections we have examined in ophiolites (Troodos, Leka, Karmoy, Oman, Josephine, and the Liguride ophiolites), only the Ligurian gabbros exhibit similar coarse grain size, abundant crystal-plastic shear zones, and bimodal distribution of oxide and olivine gabbros. The Ligurian gabbros crystallized in a very different environment than a mid-ocean ridge: continental breakup and intrusion into old upwelling mantle during the formation of the Ligurian Tethys (e.g., Rampone et al., 1998). It would appear, then, that the strongly bimodal chemistry observed in Hole 735B and late-stage melt removal and reintrusion to higher level is characteristic of the slow-spreading and rifting tectonic environments.

F18. Olivine and plagioclase for Oman, Troodos Ophiolite, and EPR gabbros, p. 55

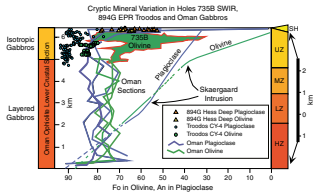

Erupted MORBs and Their Relationship to the Lower Ocean Crust

Several Leg 118 scientists (Dick et al., 1992; Natland et al., 1991) calculated the Mg# of liquids in equilibrium with the olivine gabbros and

oxide gabbros from Hole 735B and compared these to the Mg# of dredged basalt glasses from the Atlantis II Fracture Zone. These authors noted that whereas there was correspondence between the basalts and the liquids in equilibrium to the olivine gabbros, there were no erupted liquids corresponding to the majority of the ferrogabbros. This, and that the bulk composition of Hole 735B is close to a moderately differentiated MORB (Dick et al., 2000) provides compelling evidence that the Hole 735B section represents crystallization and in situ tectonic differentiation of small bodies of moderately evolved melt.

This raises an important question—what is the source of these liquids and where are the missing cumulates needed to mass balance them back to a primary MORB composition? One possibility is that they represent the products of crystallization and fractionation of primary melts intruded from the mantle directly below the hole. Gabbros, particularly primitive gabbros, are anomalously scarce compared to their supposed abundance in the ocean crust at the Atlantis II Fracture Zone and other large Indian Ocean transforms where mantle sections are exposed (Dick, 1989; Bloomer et al., 1989; Coogan et al., 2001). This led to the hypothesis that melt flow out of the mantle is highly focused toward the midpoints of ridge segments, from whence it is subsequently intruded and erupted down-axis to form the ocean crust at slow-spreading ridges (Dick, 1989; Muller et al., 1999; Smith and Cann, 1999; Whitehead et al., 1984). Abundant peridotites are found along the wall of the transform to the west of Hole 735B. At the same time, dunites marking melt-flow channels through the mantle are rare in these peridotite suites. This indicates that relatively little shallow mantle melt transport has occurred near the transform and that the missing cumulates are not likely to be in the mantle section there (Dick, 1989, Dick et al., 1991b). The magma source therefore is away from the transform, and while it could be out of the section to the east of Hole 735B (Dick et al., 2000), this depends on where the midpoint of the paleoridge segment lay. If it was centered near Hole 735B, there could be a considerable thickness of lower crust yet to be drilled there.

This still leaves the question as to why primitive melts close to equilibrium with the mantle do not erupt along most of the Southwest Indian Ridge. Where and how are primary magmas nearly universally buffered to such moderate compositions? The scarcity of gabbroic rocks and dunites with appropriate composition in the mantle sections in ophiolites suggests that this does not happen in the mantle beneath the ridge. This then leaves the lower crust beneath the ridge axis—but not in the Hole 735B section. We suspect then, seismological evidence to the contrary, that this requires some form of long-lived crystal mush zone in the lower crust near the midpoint of slow-spreading ridges.

In this light, we note that the suite of gabbros studied by Meyer et al. (1989) from the midpoint of a ridge segment at 7°16′E on the Southwest Indian Ridge is strikingly different from the Hole 735B suite, containing strongly modally layered gabbros, anorthosite, troctolite, and dunite, with olivine forsterite contents ranging up to Fo_{89} in the dunite. This suggests that the appropriate bit of the magmatic plumbing system does exist in the crust beneath the midpoints of slow-spreading ocean ridges, whereas the lack of erupted primitive MORBs suggests that they must be fairly universal. If the plumbing system in which this occurs is not long lived, then how does one explain the rather universal lack of erupted primary or even relatively primitive magmas along the length of the Southwest Indian Ridge (e.g., le Roex et al., 1983, 1989, 1985, 1992)?

ACKNOWLEDGMENTS

The authors would like to thank the officers and crew of the *JOIDES Resolution,* particularly Captain Ed Onk, who valiantly served at Site 735 through foul and fair weather for three Ocean Drilling Program legs before retiring at the end of Leg 176. His good humor and seamanship contributed enormously to our enterprise. Parker Hackett assisted in preparation and documentation of thin sections for analysis and processed a considerable amount of the data used in this paper. The authors thank S.A. Morse and R. Pedersen for perceptive and often challenging reviews that much improved the manuscript. They are otherwise blameless. Funding for this research was provided by the Woods Hole Oceanographic Institution through the Van Allen Clark Jr. Chair for Excellence in Oceanography, the U.S. Science Support Program, and a grant from the National Science Foundation (NSF-9618442). This research used samples and/or data provided by the Ocean Drilling Program (ODP). ODP is sponsored by the U.S. National Science Foundation (NSF) and participating countries under management of Joint Oceanographic Institutions (JOI), Inc.

REFERENCES

Bloomer, S.H., Meyer, P.S., Dick, H.J.B., Ozawa, K., and Natland, J.H., 1991. Textural and mineralogic variations in gabbroic rocks from Hole 735B. *In* Von Herzen, R.P., Robinson, P.T., et al., *Proc. ODP, Sci. Results,* 118: College Station, TX (Ocean Drilling Program), 21–39.

Bloomer, S.H., Natland, J.H., and Fisher, R.L., 1989. Mineral relationships in gabbroic rocks from fracture zones of Indian Ocean ridges: evidence for extensive fractionation, parental diversity, and boundary-layer recrystallization. *In* Saunders, A.D., and Norry, M.J. (Eds.), *Magmatism in the Oceanic Basins*. Spec. Publ.—Geol. Soc. London, 42:107–124.

Boudier, F., Nicolas, A., Ildefonse, B., 1996. Magma chambers in the Oman Ophiolite: fed from the top and the bottom. *Earth Planet. Sci. Lett.,* 144:239–250.

Bown, J.W., and White, R.S., 1994. Variation with spreading rate of oceanic crustal thickness and geochemistry. *Earth Planet. Sci. Lett.,* 121:435–449.

Coogan, L.A., MacLeod, C.J., Dick, H.J.B., Edwards, S.J., Kvassnes, A., Natland, J.H., Robinson, P.T., Thompson, G., and O'Hara, M.J., 2001. Whole-rock geochemistry of gabbros from the Southwest Indian Ridge: constraints on geochemical fractionations between the upper and lower oceanic crust and magma chamber processes at (very) slow-spreading ridges. *Chem. Geol.,* 178:1–22.

Dick, H.J.B., 1989. Abyssal peridotites, very slow spreading ridges and ocean ridge magmatism. *In* Saunders, A.D., and Norry, M.J. (Eds.), *Magmatism in the Ocean Basins*. Spec. Publ.—Geol. Soc. London, 42:71–105.

Dick, H.J.B., Meyer, P.S., Bloomer, S., Kirby, S., Stakes, D., and Mawer, C., 1991a. Lithostratigraphic evolution of an in-situ section of oceanic Layer 3. *In* Von Herzen, R.P., Robinson, P.T., et al., *Proc. ODP, Sci. Results,* 118: College Station, TX (Ocean Drilling Program), 439–538.

Dick, H.J.B., Natland, J.H., Alt, J.C., Bach, W., Bideau, D., Gee, J.S., Haggas, S., Hertogen, J.G.H., Hirth, G., Holm, P.M., Ildefonse, B., Iturrino, G.J., John, B.E., Kelley, D.S., Kikawa, E., Kingdon, A., LeRoux, P.J., Maeda, J., Meyer, P.S., Miller, D.J., Naslund, H.R., Niu, Y., Robinson, P.T., Snow, J., Stephen, R.A., Trimby, P.W., Worm, H.-U., and Yoshinobu, A., 2000. A long in situ section of the lower ocean crust: results of ODP Leg 176 drilling at the Southwest Indian Ridge. *Earth Planet. Sci. Lett.,* 179:31–51.

Dick, H.J.B., Natland, J.H., Miller, D.J., et al., 1999. *Proc. ODP, Init. Repts.,*176 [CD-ROM]. Available from: Ocean Drilling Program, Texas A&M University, College Station, TX 77845-9547, U.S.A.

Dick, H.J.B., Robinson, P.T., and Meyer, P.S., 1992. The plutonic foundation of a slow-spreading ridge. *In* Duncan, R., Rea, D., Kidd, R., von Rad, U., and Weissel, J. (Eds.), *Synthesis of Results from Scientific Drilling in the Indian Ocean*. Geophys. Monogr., Am. Geophys. Union, 70:1–39.

Dick, H.J.B., Schouten, H., Meyer, P.S., Gallo, D.G., Bergh, H., Tyce, R., Patriat, P., Johnson, K.T.M., Snow, J., and Fisher, A., 1991b. Tectonic evolution of the Atlantis II Fracture Zone. *In* Von Herzen, R.P., Robinson, P.T., et al., *Proc. ODP, Sci. Results,* 118: College Station, TX (Ocean Drilling Program), 359–398.

Hebert, R., Constantin, M., and Robinson, P.T., 1991. Primary mineralogy of Leg 118 gabbroic rocks and their place in the spectrum of oceanic mafic igneous rocks. *In* Von Herzen, R., Robinson, P.T., et al., *Proc. ODP, Sci. Results,* 118: College Station, TX (Ocean Drilling Program), 3–20.

Hekinian, R., Bideau, D., Francheteau, J., Cheminée, J.L., Armijo, R., Lonsdale, P., and Blum, N., 1993. Petrology of the East Pacific Rise crust and upper mantle exposed in the Hess Deep (eastern equatorial Pacific). *J. Geophys. Res.,* 98:8069–8094.

Korenaga, J., and Kelemen, P.B., 1997a. Melt migration through the oceanic lower crust: a constraint from melt percolation modeling with finite solid diffusion. *Earth Planet. Sci. Lett.,* 156:1–11.

————, 1997b. Origin of gabbros sills in the Moho transition zone of the Oman ophiolite: implications for magma transport in the oceanic lower crust. *J. Geophys. Res.,* 102:27.

Le Maitre, R.W., 1989. *A Classification of Igneous Rocks and Glossary of Terms:* Oxford (IUGS, Blackwell).

Le Roex, A.P., Dick, H.J.B., Erlank, A.J., Reid, A.M., Frey, F.A., and Hart, S.R., 1983. Geochemistry, mineralogy and petrogenesis of lavas erupted along the Southwest Indian Ridge between the Bouvet Triple Junction and 11° East. *J. Petrol.,* 24:267–318.

Le Roex, A.P., Dick, H.J.B., and Fisher, R.L., 1989. Petrology and geochemistry of MORB from 25°E to 46°E along the Southwest Indian Ridge: evidence for contrasting styles of mantle enrichment. *J. Petrol.,* 30:947–986.

Le Roex, A.P., Dick, H.J.B., Reid, A.M., Frey, F.A., Erlank, A.J., and Hart, S.R., 1985. Petrology and geochemistry of basalts from the American-Antarctic Ridge, Southern Ocean: implications for the westward influence of the Bouvet mantle plume. *Contrib. Mineral. Petrol.,* 90:367–380.

Le Roex, A.P., Dick, H.J.B., and Watkins, R.T., 1992. Petrogenesis of anomalous K-enriched MORB from the Southwest Indian Ridge: 11°53′E to 14°38′E. *Contrib. Mineral. Petrol.,* 110:253–268.

Lindsley, D.H., 1983. Pyroxene thermometry. *Am. Mineral.,* 68:477–493.

Lindsley, D.H., and Andersen, D.J., 1983. A two-pyroxene thermometer. *J. Geophys. Res.,* 88 (Suppl.):A887–A906.

Lindsley, D.H., and Dixon, S.A., 1976. Diopside-enstatite equilibria at 850°C to 1,400°C, 5 to 35 kbar. *Am. J. Sci.,* 276:1282–1301.

Malpas, J., Brace, T., and Dunsworth, S.M., 1989. Structural and petrologic relationships of the CY-4 drill hole of the Cyprus Crustal Study Project. *Pap.—Geol. Surv. Can.,* 88-9:39–68.

Meyer, P.S., Dick, H.J.B., and Thompson, G., 1989. Cumulate gabbros from the Southwest Indian Ridge, 54°S–7°16′E: implications for magmatic processes at a slow spreading ridge. *Contrib. Mineral. Petrol.,* 103:44–63.

Muller, M.R., Minshull, T.A., and White, R.S., 1999. Segmentation and melt supply at the Southwest Indian Ridge. *Geology,* 27:867–870.

Muller, M.R., Robinson, C.J., Minshull, T.A., White, R.S., and Bickle, M.J., 1997. Thin crust beneath Ocean Drilling Program Borehole 735B at the Southwest Indian Ridge? *Earth Planet. Sci. Lett.,* 148:93–107.

Nabelek, P.I., Lindsley, D.H., and Bohlen, S.R., 1987. Experimental examination of two-pyroxene graphical thermometers using natural pyroxenes with application to metaigneous pyroxenes from the Adirondack Mountains, New York. *Contrib. Mineral. Petrol.,* 97:66–71.

Natland, J.H., and Dick, H.J.B., 1996. Melt migration through high-level gabbroic cumulates of the East Pacific Rise at Hess Deep: the origin of magma lenses and the deep crustal structure of fast-spreading ridges. *In* Mével, C., Gillis, K.M., Allan, J.F., and Meyer, P.S. (Eds.), *Proc. ODP, Sci. Results,* 147: College Station, TX (Ocean Drilling Program), 21–58.

————, 2001. Formation of the lower ocean crust and the crystallization of gabbroic cumulates at a very slow spreading ridge. *J. Volcanol. Geotherm Res.,* 110:191–233.

Natland, J.H., Meyer, P.S., Dick, H.J.B., and Bloomer, S.H., 1991. Magmatic oxides and sulfides in gabbroic rocks from Hole 735B and the later development of the liquid line of descent. *In* Von Herzen, R.P., Robinson, P.T., et al., *Proc. ODP, Sci. Results,* 118: College Station, TX (Ocean Drilling Program), 75–111.

Ozawa, K., Meyer, P.S., and Bloomer, S.H., 1991. Mineralogy and textures of iron-titanium oxide gabbros and associated olivine gabbros from Hole 735B. *In* Von Herzen, R.P., Robinson, P.T., et al., *Proc. ODP, Sci. Results,* 118: College Station, TX (Ocean Drilling Program), 41–73.

Pallister, J.S., and Hopson, C.A., 1981. Samail ophiolite plutonic suite: field relations, phase variation, cryptic variation and layering, and a model of a spreading ridge magma chamber. *J. Geophys. Res.,* 86:2593–2644.

Rampone, E., Hoffman, A.W., and Raczek, I., 1998. Isotopic contrasts within the Internal Liguride ophiolite (N. Italy): the lack of a genetic mantle-crust link. *Earth Planet. Sci. Lett.,* 163:175–189.

Ramsay, J.G., 1976. Displacement and strain. *Philos. Trans. R. Soc. London, Ser. A*, 283:3–25.

Ramsay, J.G., and Graham, R.H., 1970. Strain variation in shear belt. *Can. J. Earth Sci.,* 7:786–813.

Smith, D.K., and Cann, J.R., 1999. Constructing the upper crust of the Mid-Atlantic Ridge: a reinterpretation based on the Puna Ridge, Kilauea Volcano. *J. Geophys. Res.,* 104:25379–25399.

Streckeisen, A., 1976. To each plutonic rock its proper name. *Earth Sci. Rev.,* 12:1–33.

Whitehead, J.A., Dick, H.J.B., and Shouten, H., 1984. A mechanism for magmatic accretion under spreading centers. *Nature,* 312:146–148.

Figure F1. A. Feldspar ternary showing average and single-spot analyses of plagioclase grains from Hole 735B gabbros and microgabbros. (Continued on next page.)

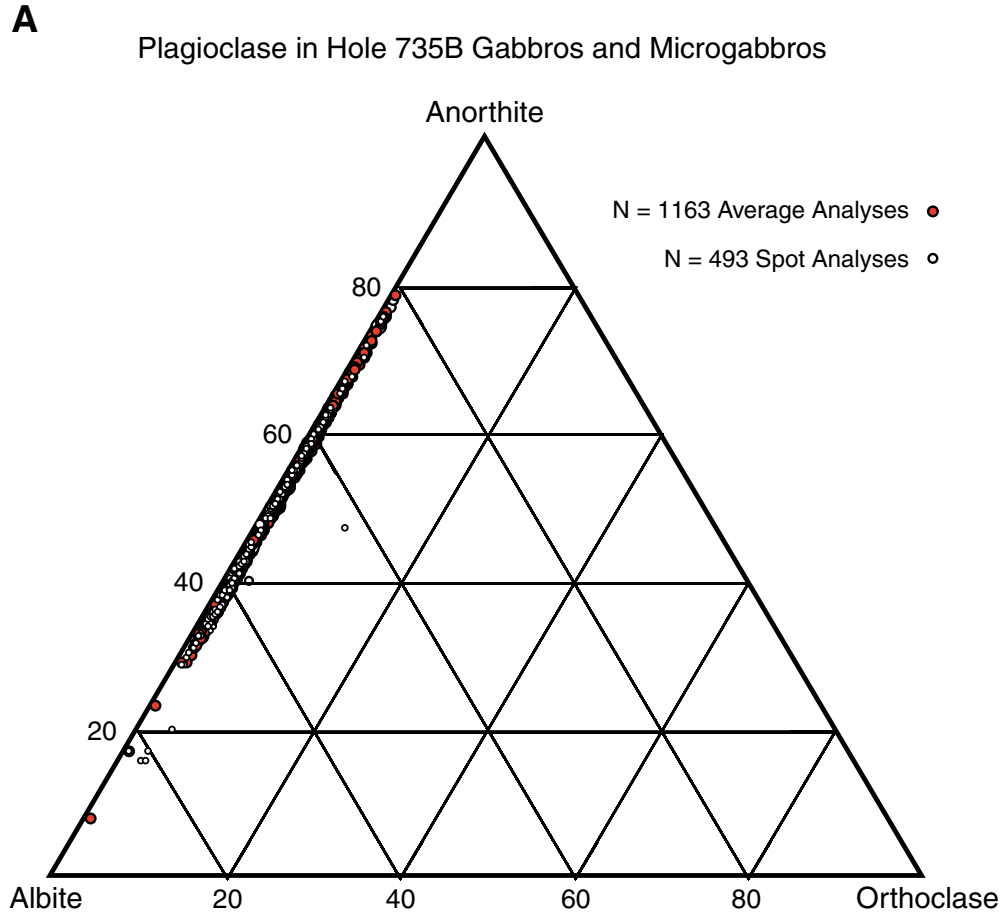

Figure F1 (continued). B. Plagioclase core and coexisting rim compositions for Hole 735B.

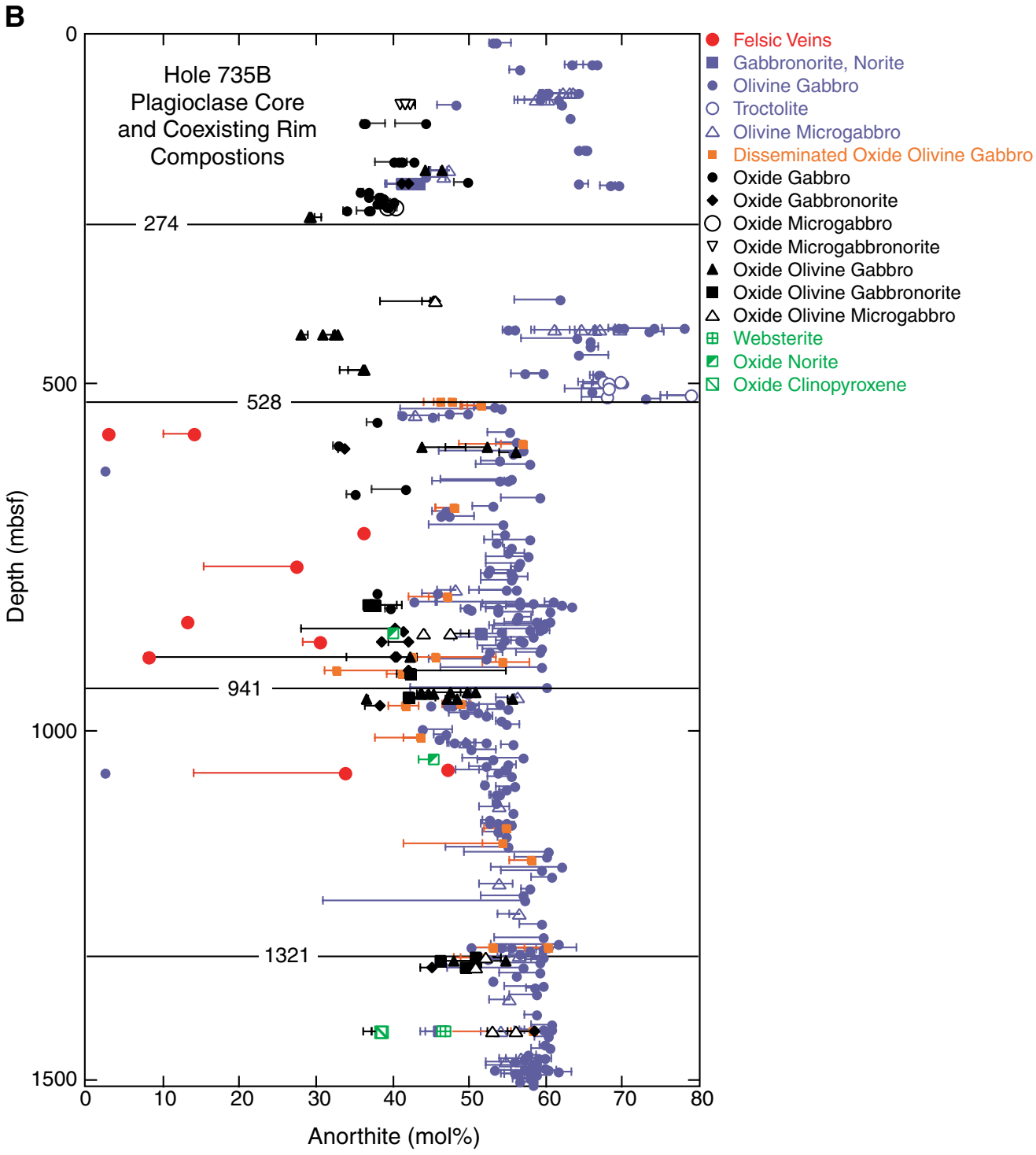

Figure F2. Stacked histograms of individual plagioclase analyses (not averages) from Table T1, p. 56, showing the overall distribution of anorthite values for the entire hole (0–1508 mbsf) and for 500-m increments.

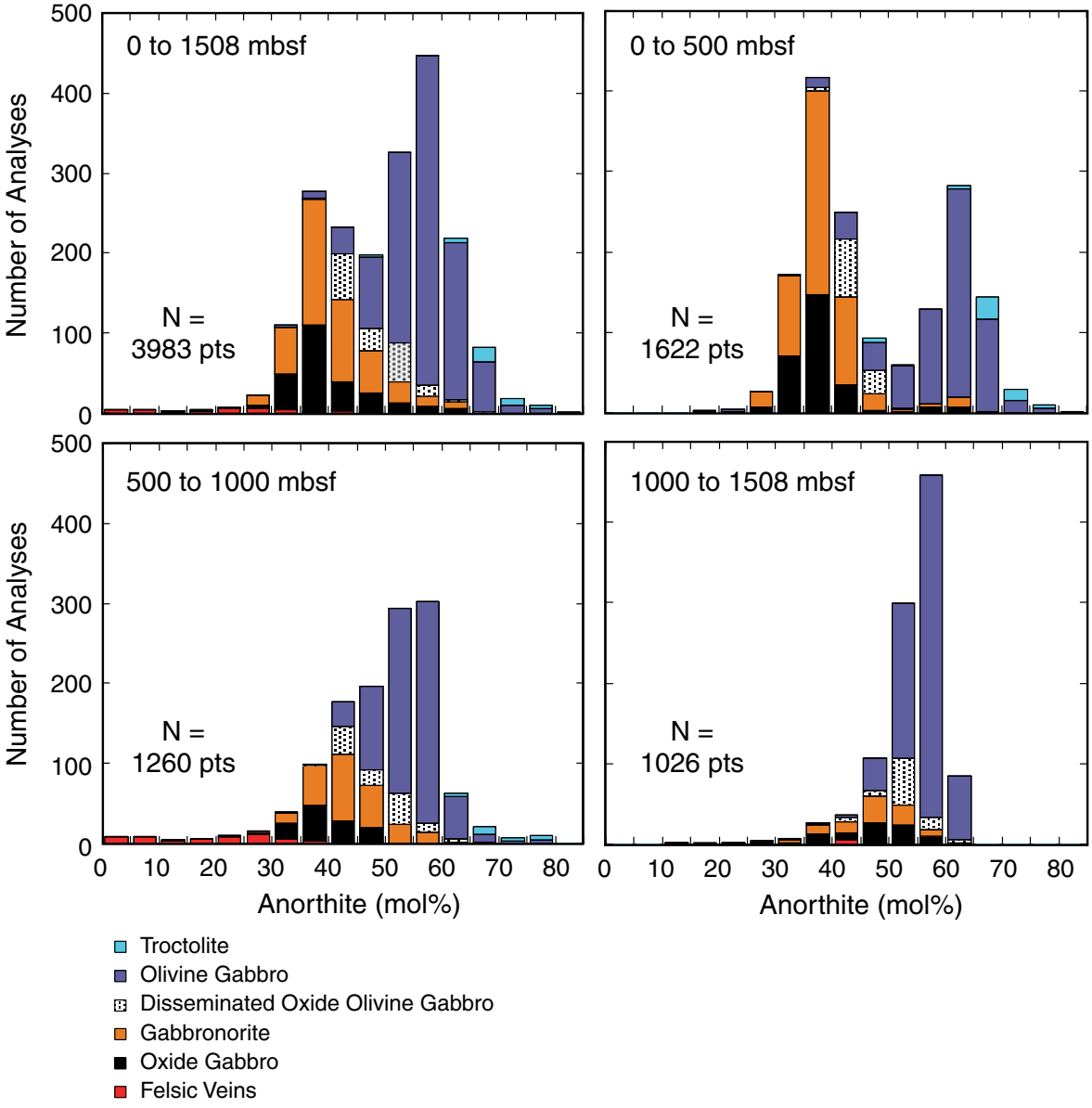

Figure F3. FeO* (all iron as FeO) vs. anorthite content for average and single-spot plagioclase analyses of Hole 735B gabbros. Arrows show a rough trend of iron enrichment in the gabbros and a separate possible trend for the felsic veins.

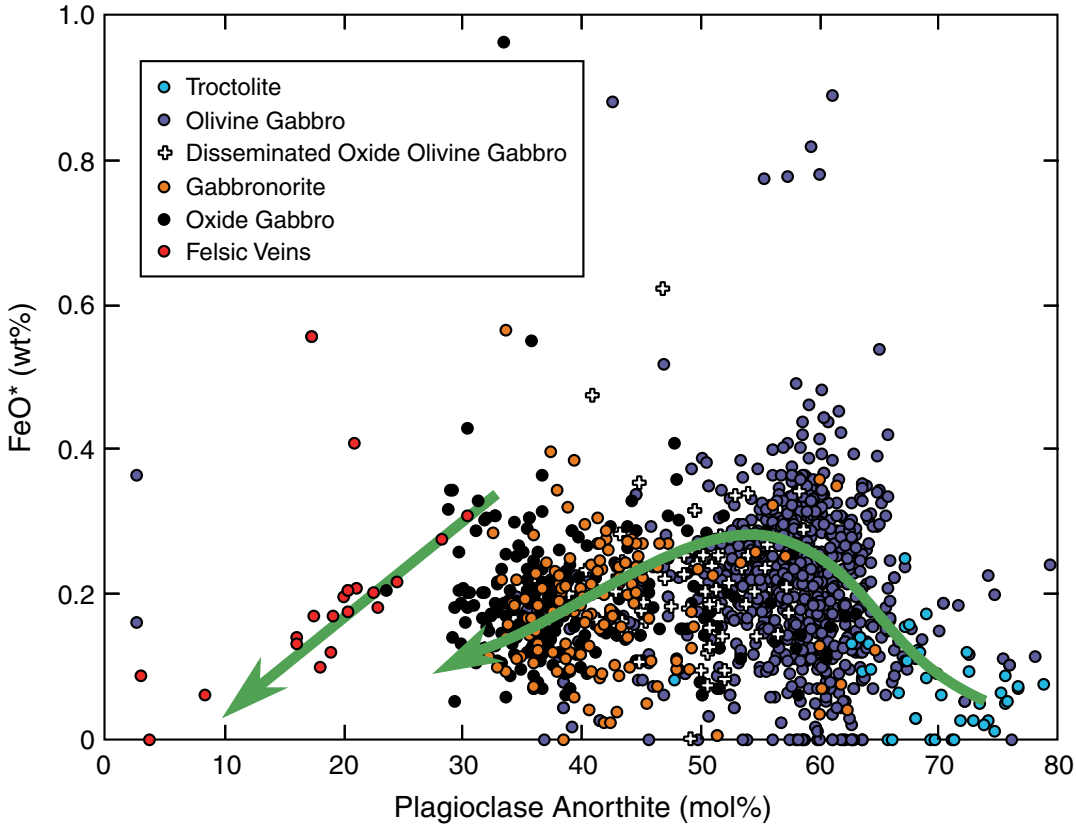

Figure F4. A. Hole 735B average and single-spot pyroxene analyses, including average core and average rim analyses from Tables T2, p. 57, and T3, p. 58. Compositions are plotted without correction for nonquadrilateral components. Shown for reference are the estimated composition trends of Wager and Brown for the Skaergaard Intrusion of Greenland and the composition of Hess Deep Hole 894G high-level gabbros (inset). F.Z. = fracture zone. Cpx = clinopyroxene, Opx = orthopyroxene. Di = diopside, Hd = hedenbergite, En = enstatite, Fs = ferrosilite. (Continued on next page.)

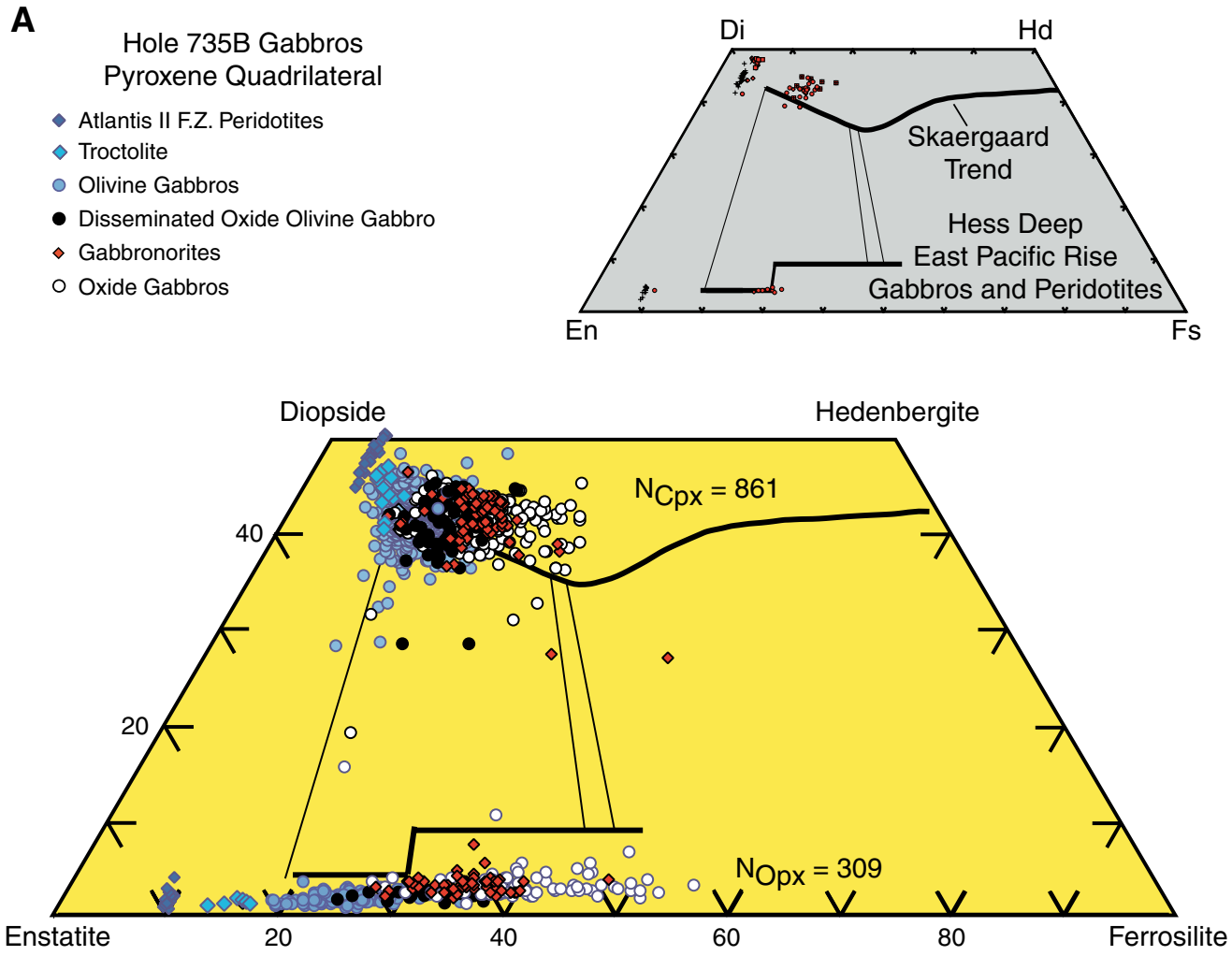

Figure F4 (continued). B. Enstatite-diopside half of the pyroxene quadrilateral contoured with the orthopyroxene-clinopyroxene solvus of Lindsley and co-workers (Lindsley, 1983; Lindsley and Andersen, 1983; Lindsley and Dixon, 1976), showing the composition field of Hess Deep Hole 894G high-level gabbros and Site 895 mantle peridotites, dunites, and gabbroic segregations from Natland and Dick (1996), with the composition fields for dredge and dive samples from Hess Deep (Hekinian et al., 1993).

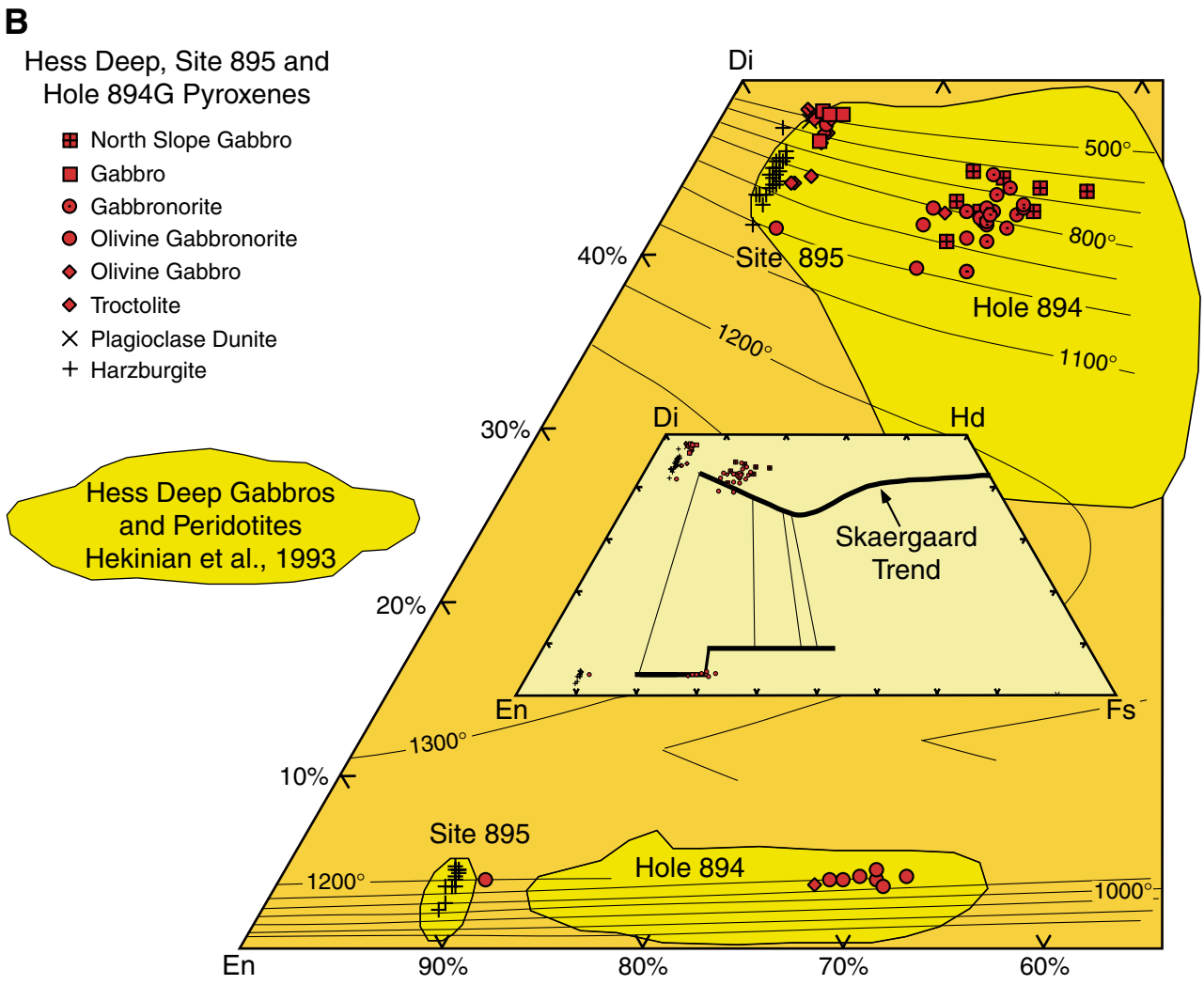

Figure F5. Compositions of clinopyroxene plotted against depth. These represent separate 10-point 10-µm spot-size contiguous traverses of the cores and rims made by H. Dick for Leg 176 samples. Similar data for the upper 500-m section do not exist. Solid symbols = core composition, short vertical bars at the ends of the tie lines = rim compositions. **A.** Molecular Mg × 100/(Mg+Fe) with all iron as FeO. **B.** Na_2O. **C.** TiO_2. **D.** Cr_2O_3.

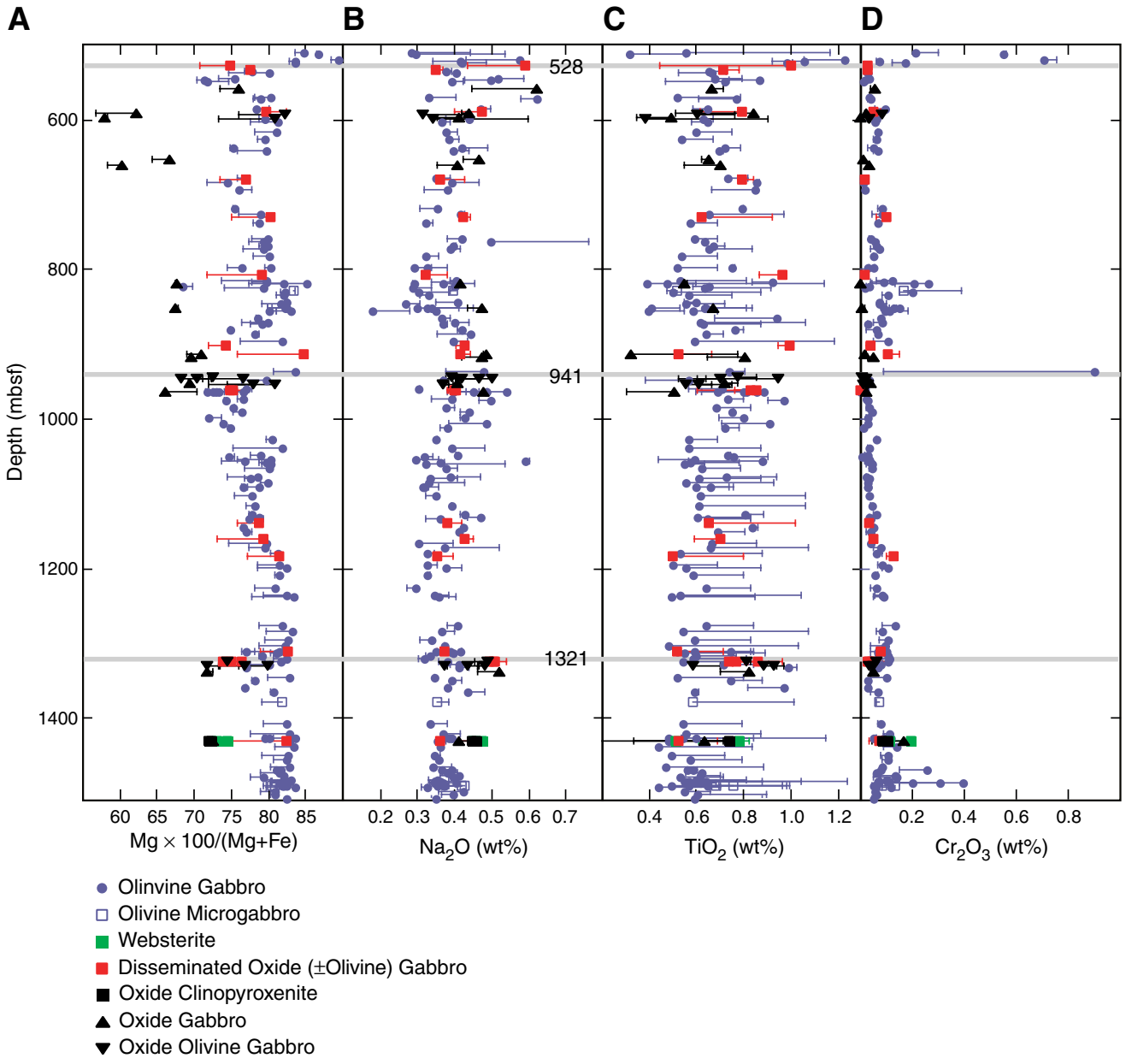

Figure F6. Minor element oxide concentrations in Hole 735B clinopyroxenes from Table T2, p. 57, plotted against the molar ratio of Mg to Mg + Fe. All iron is given as FeO. **A.** Cr_2O_3. **B.** Al_2O_3. **C.** TiO_2. **D.** Na_2O.

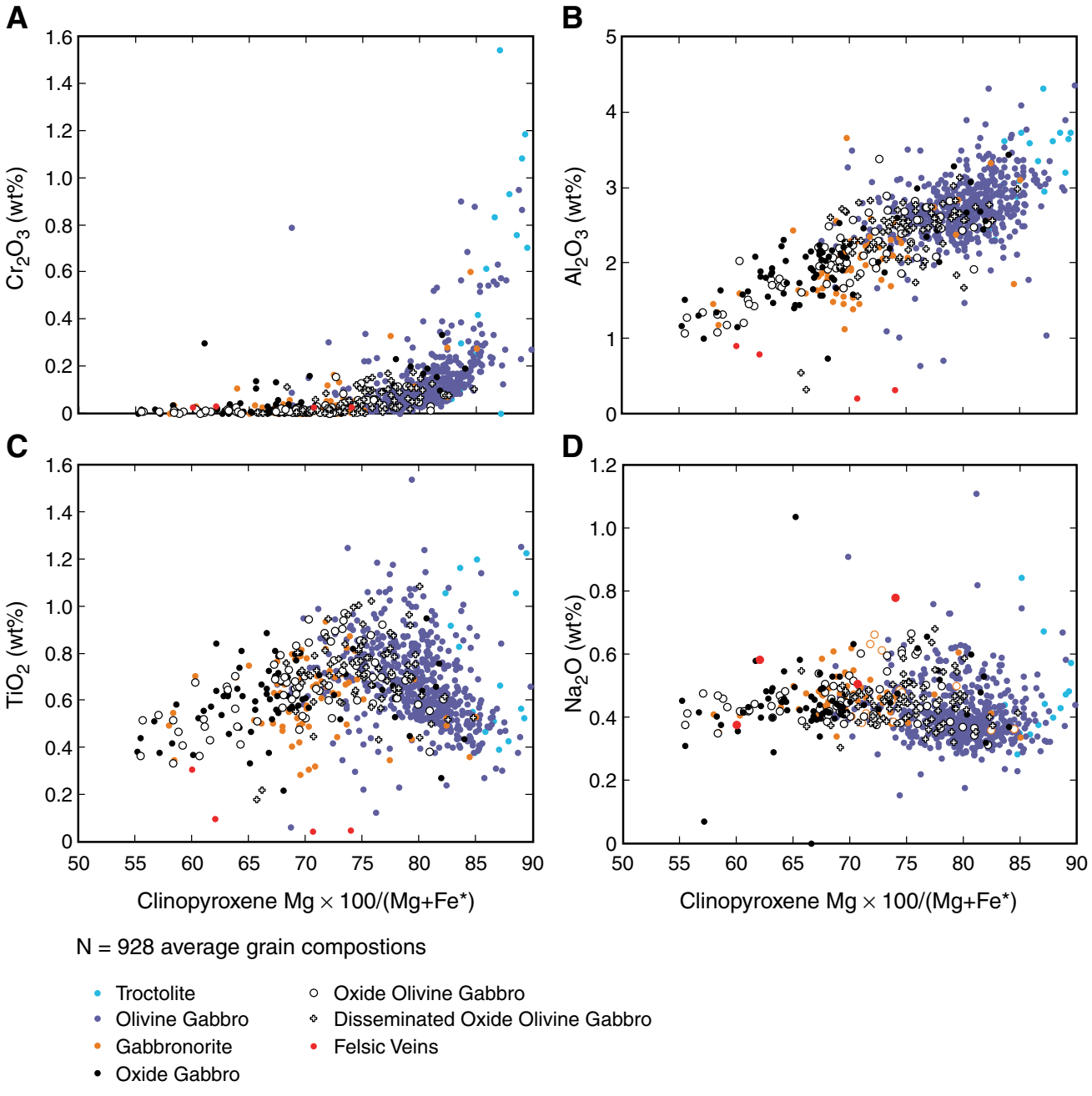

Figure F7. NiO plotted against forsterite content of average and single-spot analyses of Hole735B gabbros from Table T3, p. 58.

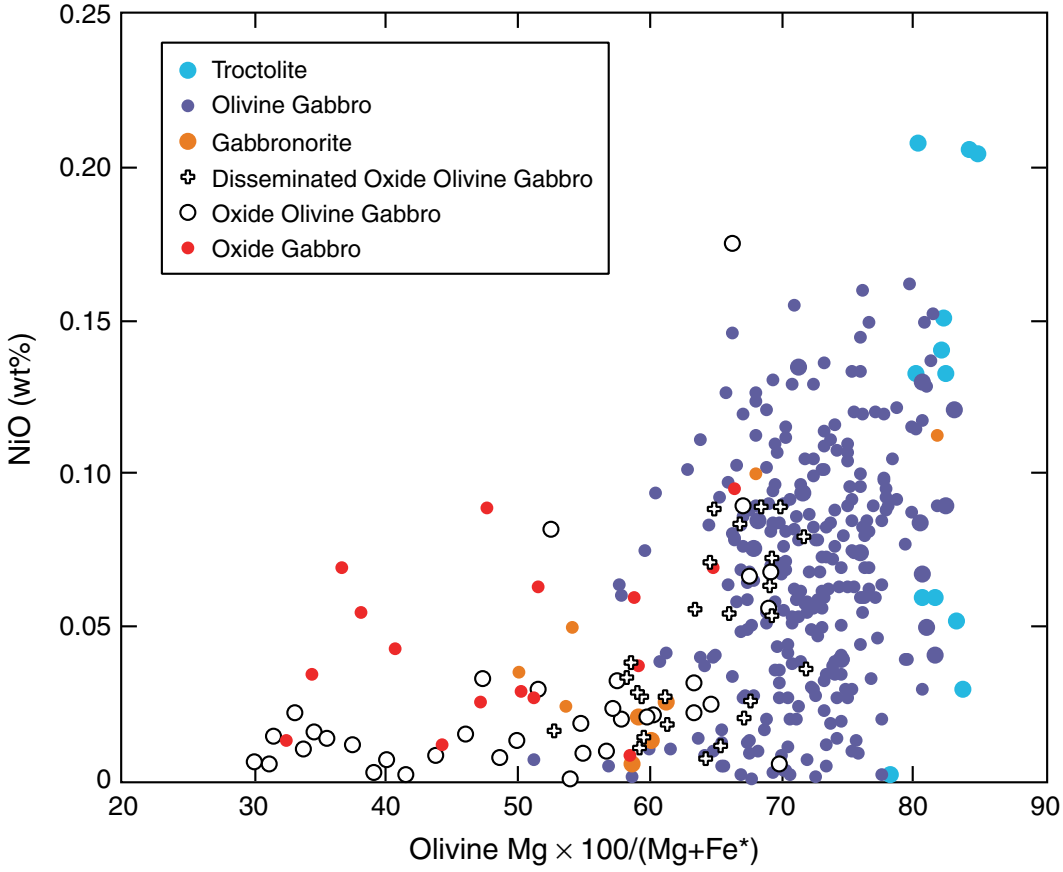

Figure F8. Oxides vs. Mg# for average and single-spot analyses of brown hornblende grains in Hole 735B gabbros. All iron is given as FeO. **A.** Al_2O_3. **B.** CaO. **C.** K_2O. **D.** TiO_2. **E.** Na_2O. **F.** Cr_2O_3.

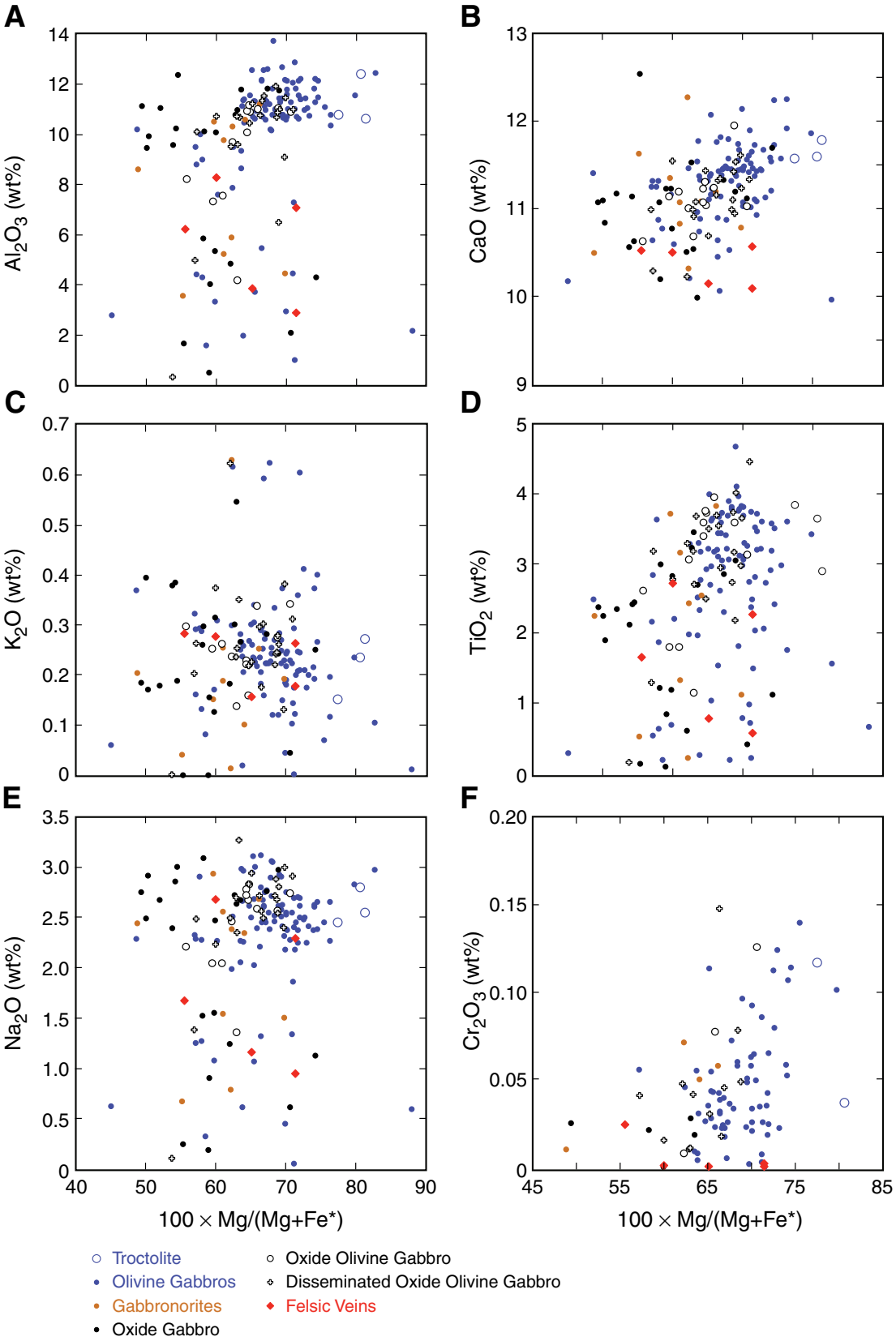

Figure F9. Plagioclase anorthite values of average and single-spot analyses plotted against coexisting (A) olivine, (B) clinopyroxene, (C) brown hornblende, and (D) orthopyroxene average and single-spot analyses for Hole 735B gabbros from Table T1, p. 56.

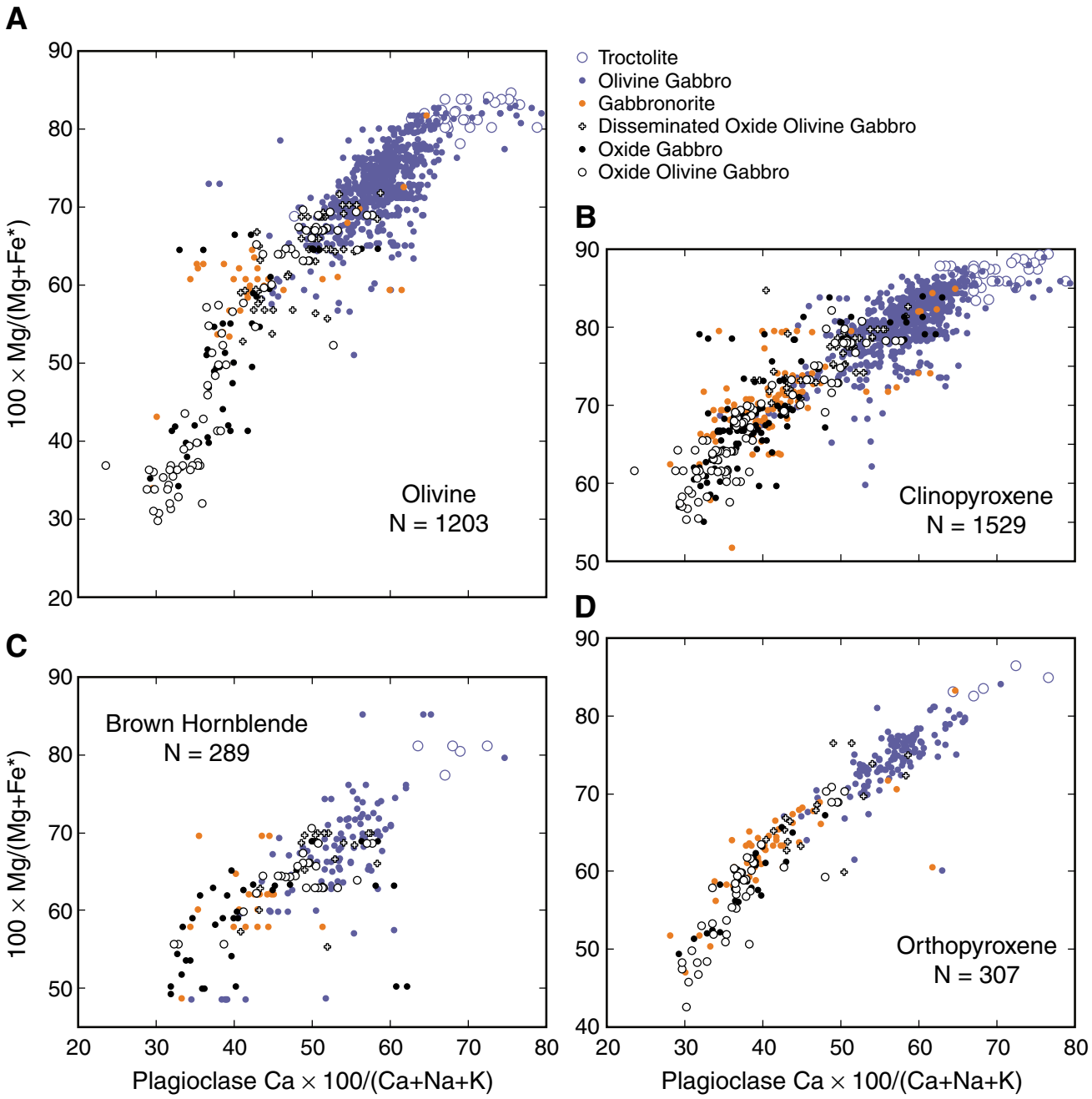

Figure F10. Molar ratio covariation plots of Mg × 100/(Mg+Fe) for mafic silicates from Hole 735B gabbros from Tables T2, p. 57, T3, p. 58, T4, p. 59, and T5, p. 60. Ratios are calculated assuming all iron as FeO. Shown are average and single-spot analyses of individual grains, including average core and rim analyses of ortho- and clinopyroxene. **A.** Olivine forsterite content vs. clinopyroxene Mg#. **B.** Olivine forsterite content vs. orthopyroxene Mg#. **C.** Clinopyroxene Mg# vs. orthopyroxene Mg#. (Continued on next page.)

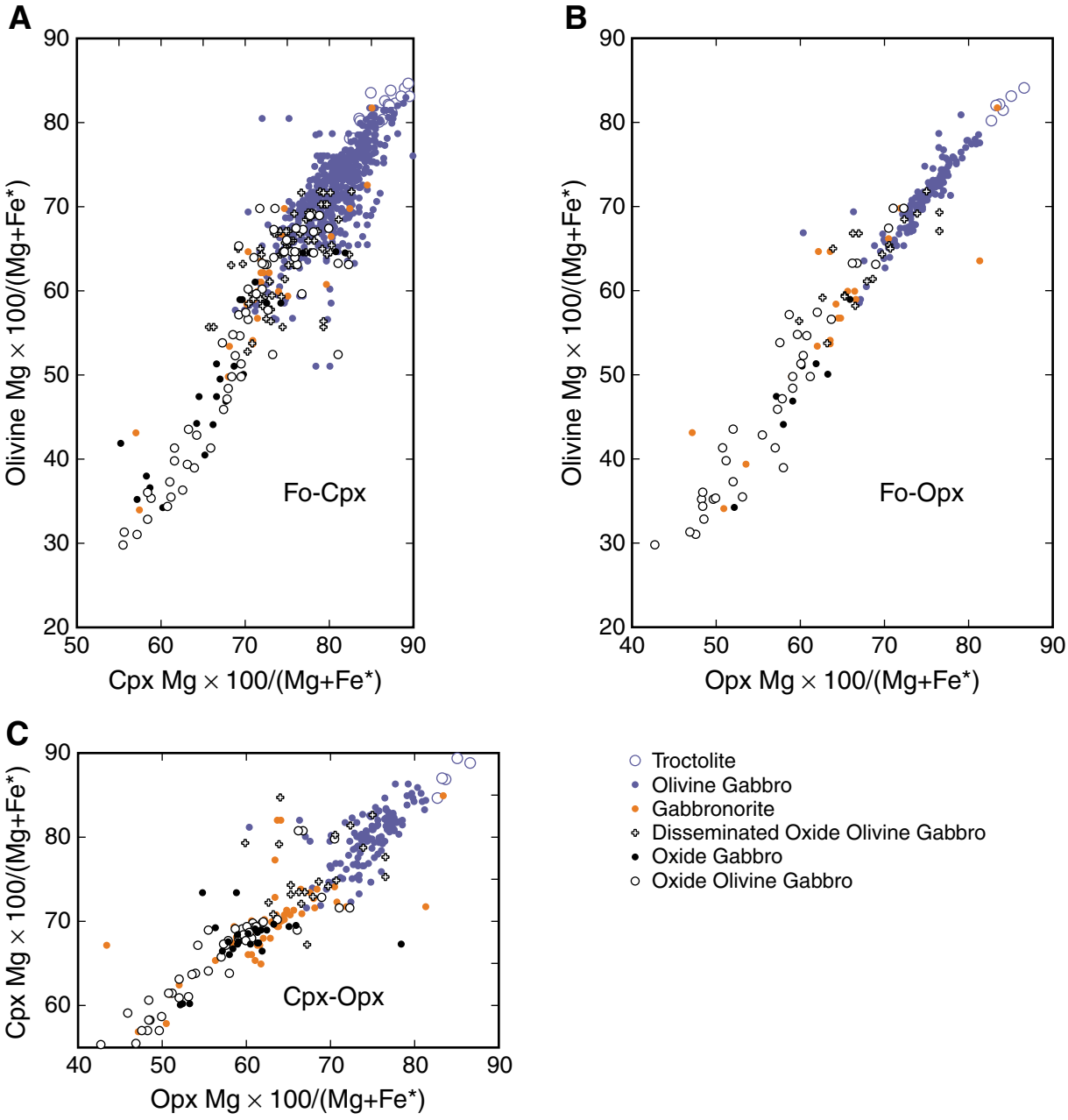

Figure F10 (continued). **D.** Clinopyroxene Mg# vs. hornblende Mg#. **E.** Olivine forsterite content vs. hornblende Mg#. **F.** Hornblende Mg# vs. orthopyroxene Mg#.

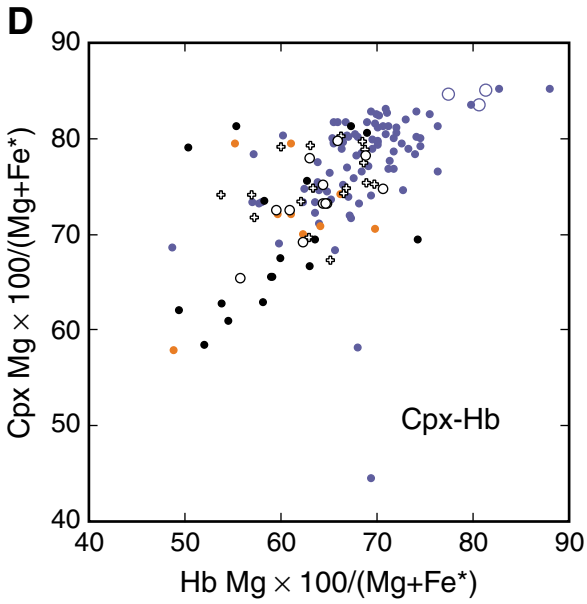

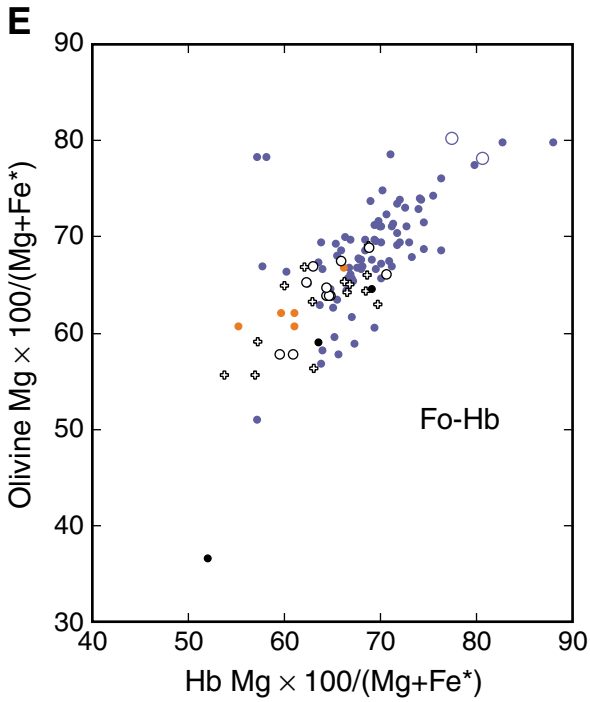

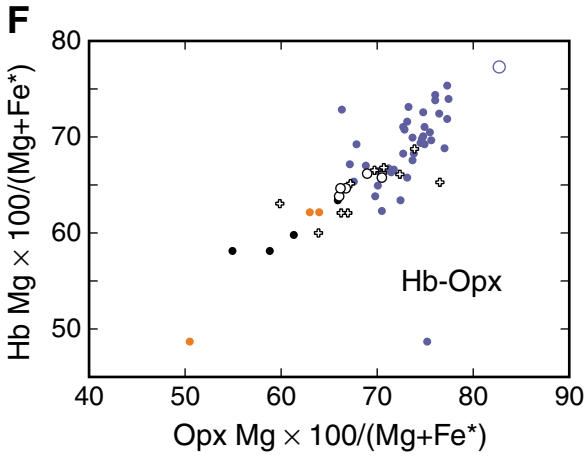

Figure F11. A. Average and single-spot analyses of plagioclase anorthite and clinopyroxene and olivine Mg# plotted vs. expanded depth. (Continued on next two pages.)

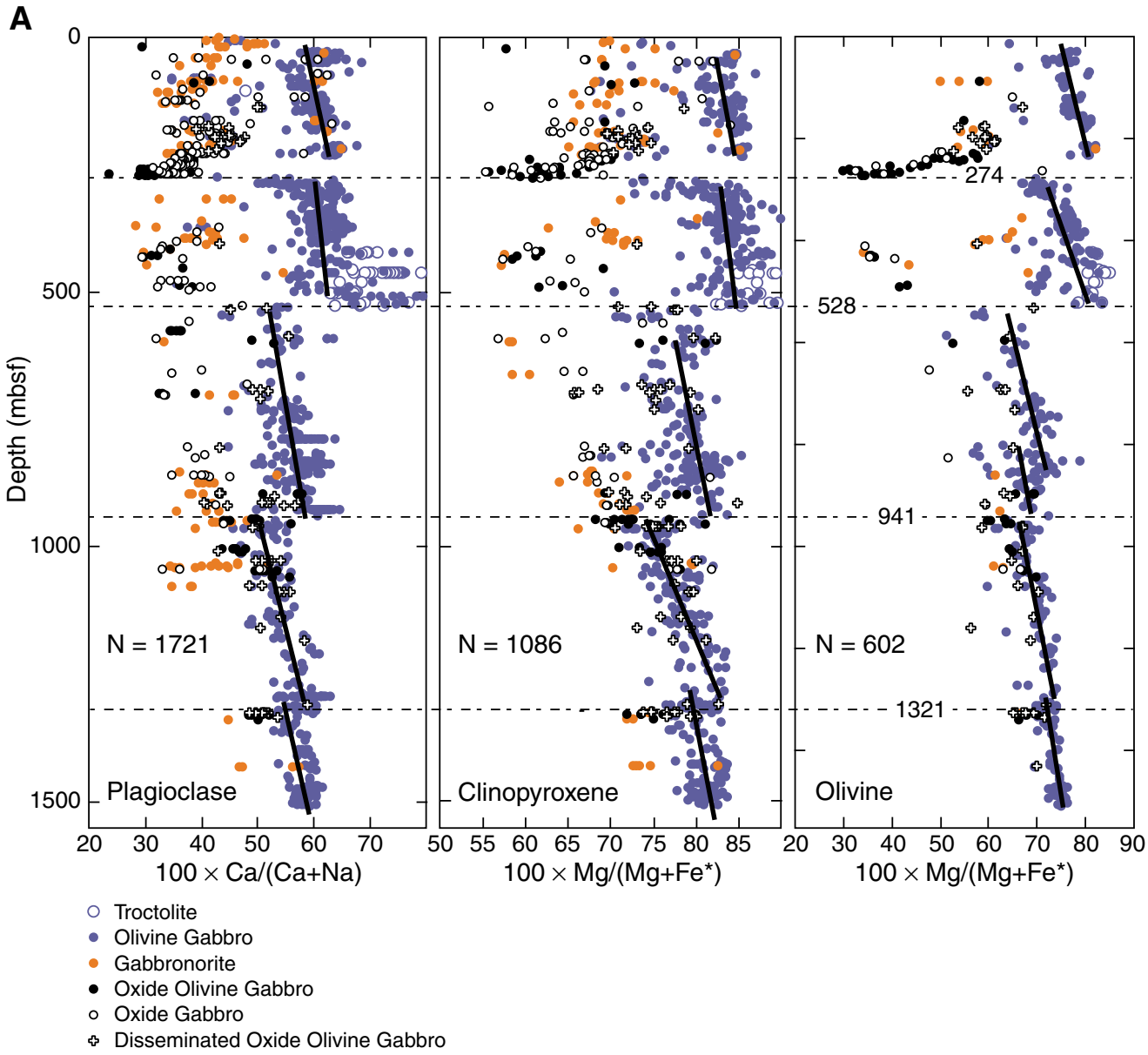

Figure F11 (continued). B. Average and single-spot analyses of orthopyroxene and brown hornblende plotted against expanded depth. (Continued on next page.)

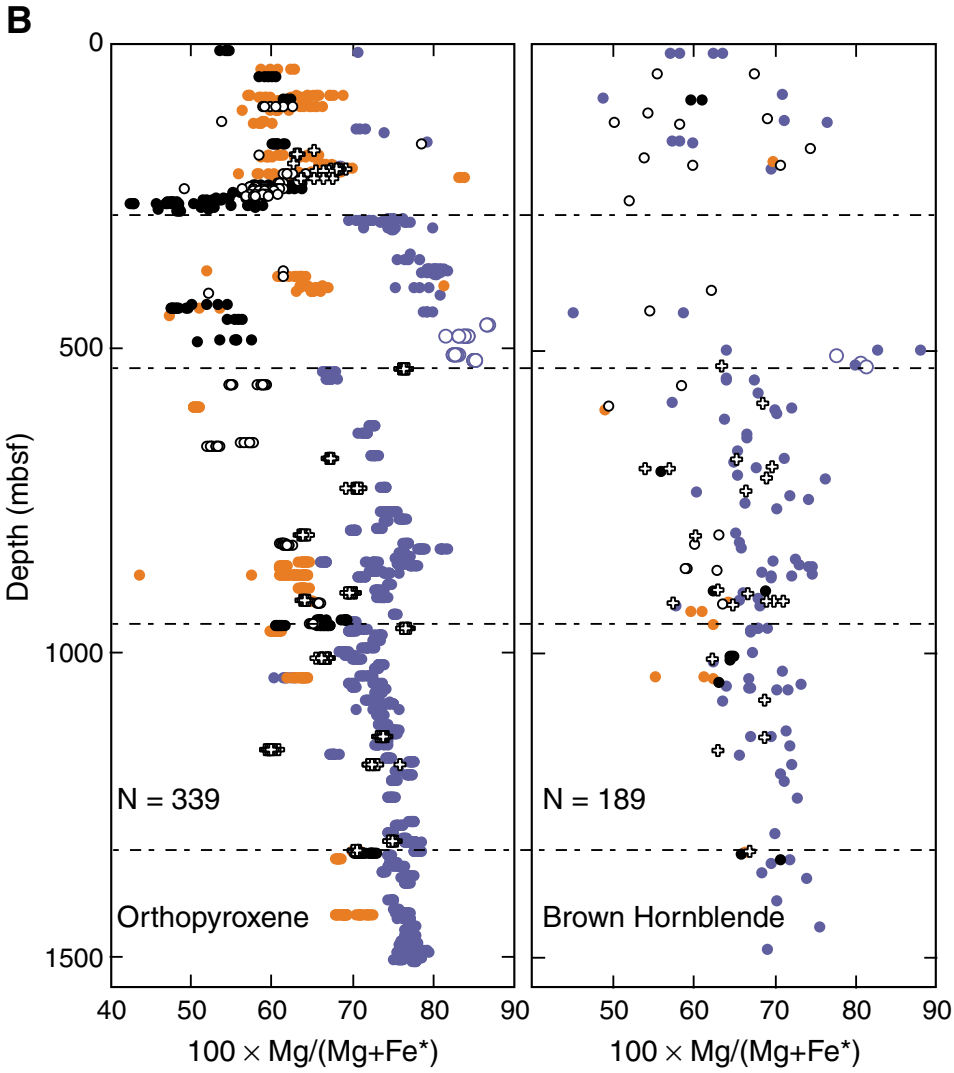

Figure F11 (continued). C. Plot of whole-rock Mg# plotted against depth for Leg 118 and Leg 176 shipboard whole-rock analyses of gabbros, microgabbros, and felsic veins taken from the Leg 176 *Initial Reports* volume (Dick, Natland, Miller, et al., 1999). Samples are subdivided mainly on the basis of TiO_2 content. Solid diamonds = troctolite, troctolitic gabbro, and olivine gabbro having <0.4 wt% TiO_2, solid blue diamonds = gabbro, gabbronorite, and disseminated oxide gabbro with between 0.4 and 1.0 wt% TiO_2, solid yellow diamonds = oxide gabbro with >1.0 wt% TiO_2, half-solid squares = felsic samples or hybrid samples with a significant felsic component. Solid gray triangle = a basaltic dike.

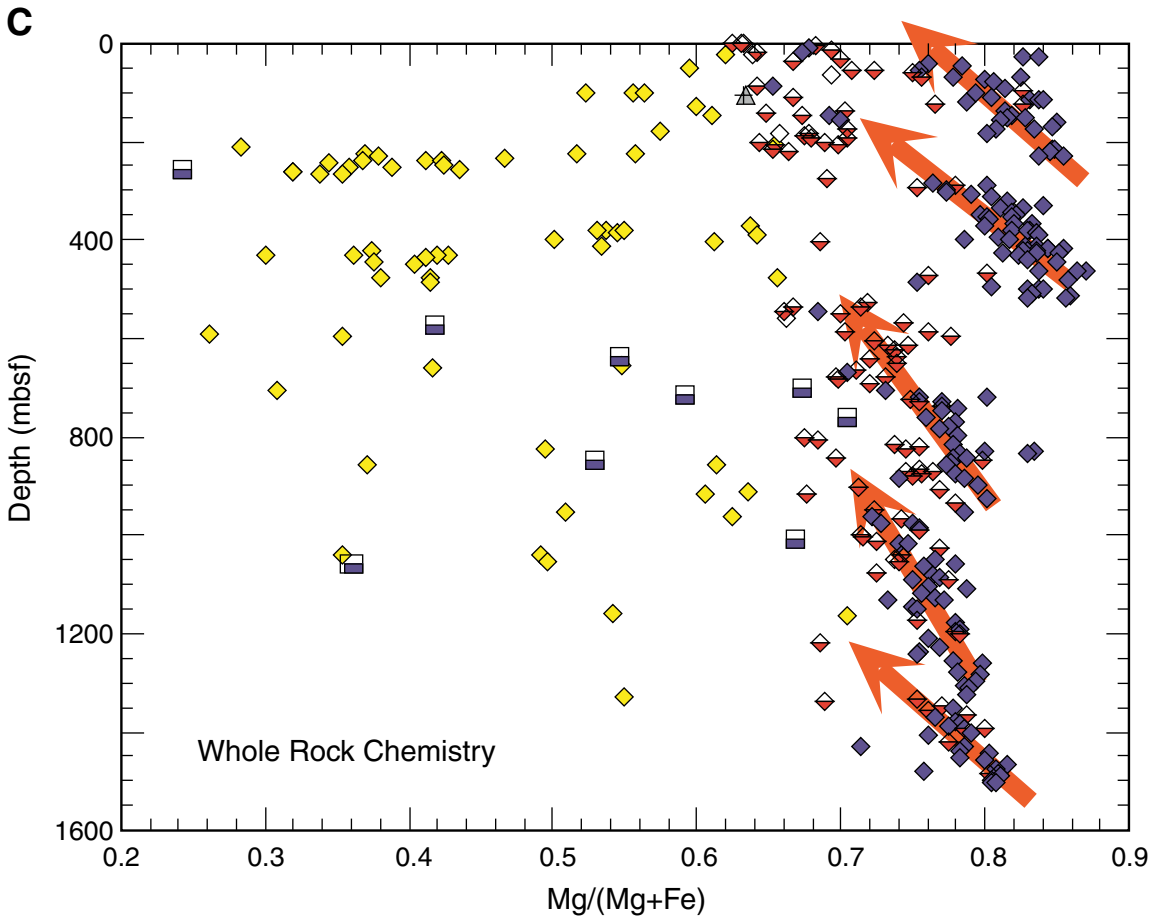

Figure F12. Expanded plots of downhole mineral variations around the 274-mbsf chemical discontinuity.

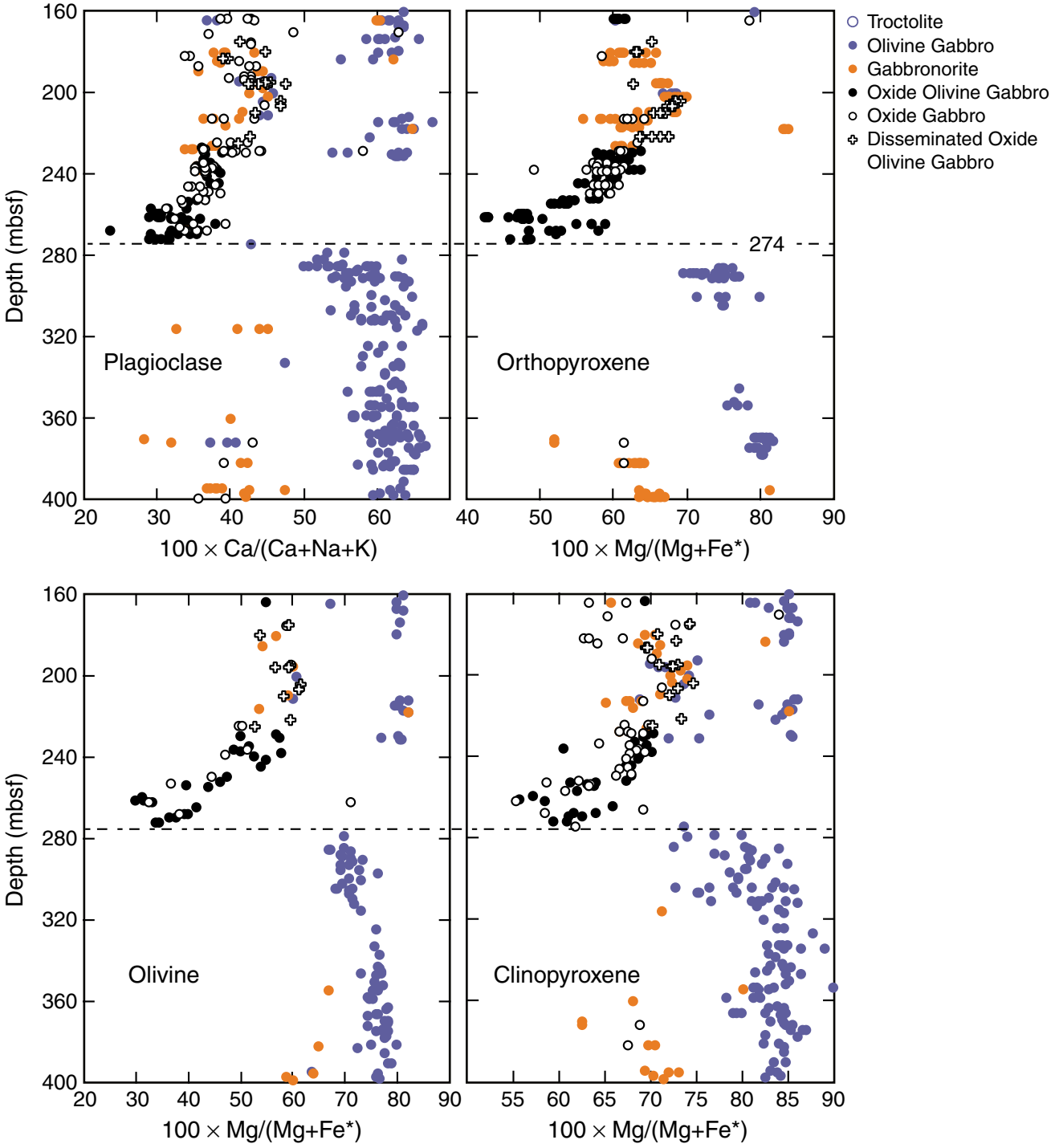

Figure F13. Expanded plots of downhole mineral variations around the 528-mbsf chemical discontinuity.

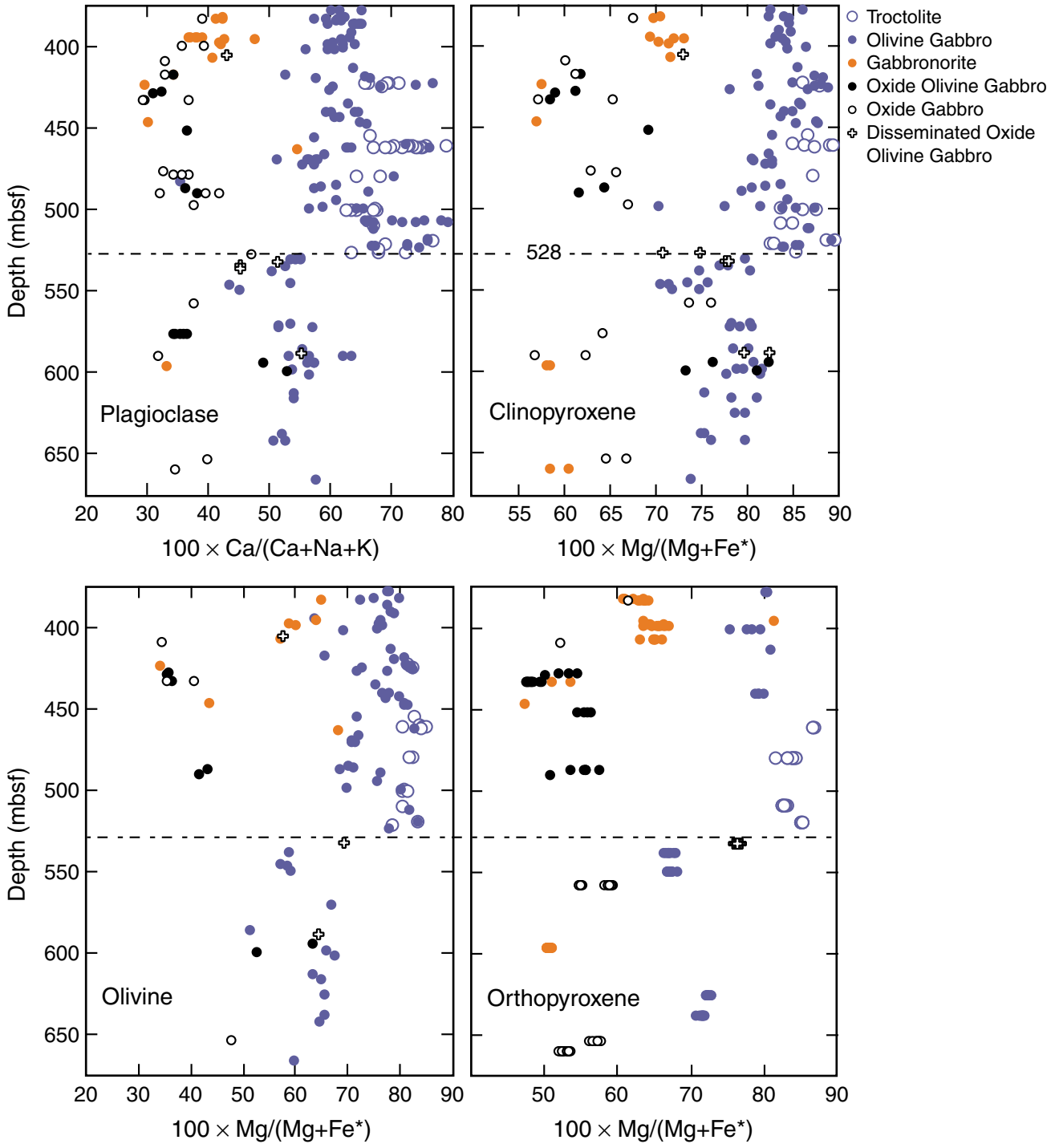

Figure F14. Expanded plots of the downhole mineral variations around the 941-mbsf chemical discontinuity. The shaded region in the plagioclase plot shows the location of the 30-m zone of crystal-plastic deformation from 930 to 960 mbsf. It is noteworthy in this context that <10% of the Hole 735B core shows such intense deformation.

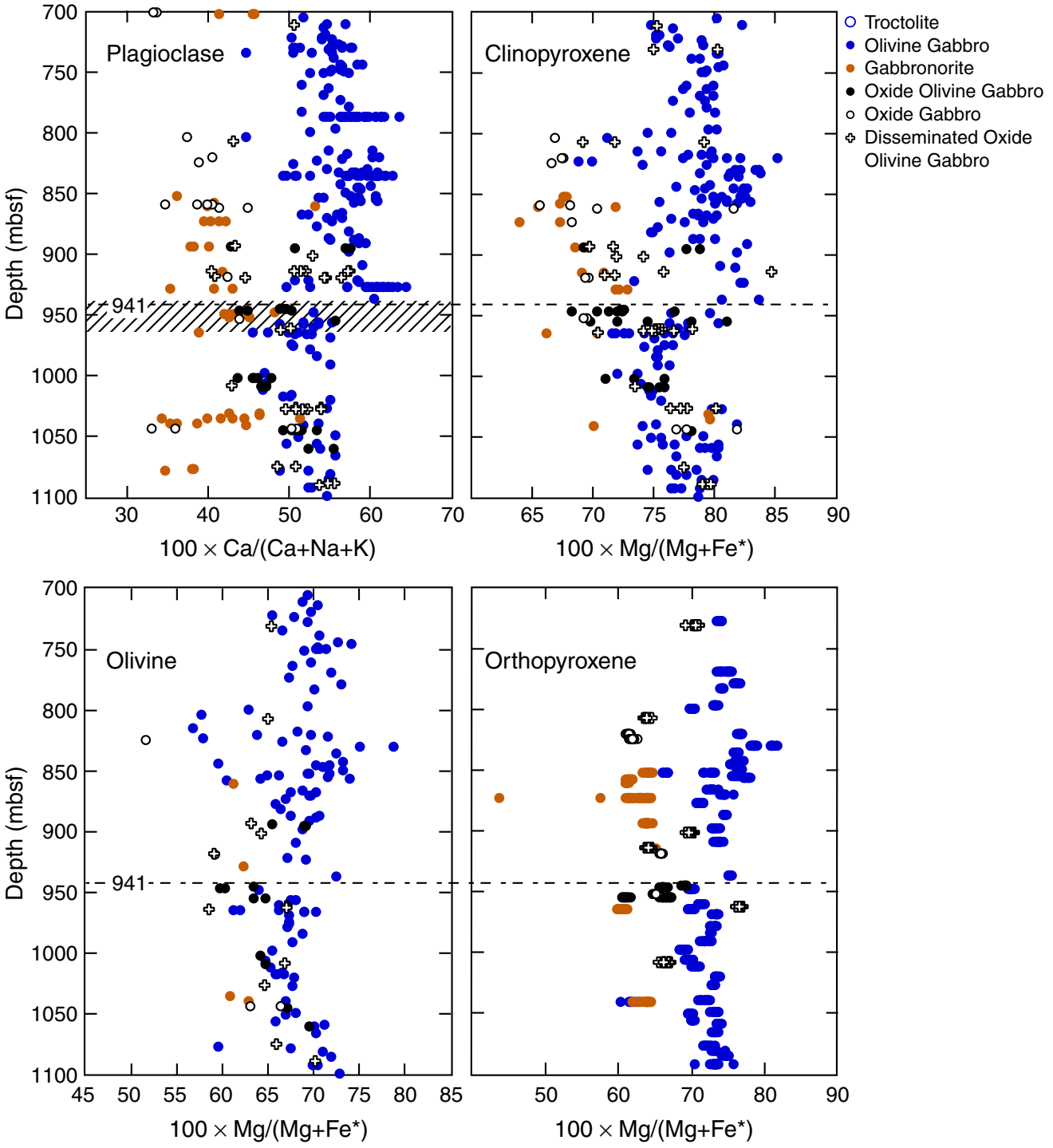

Figure F15. Expanded plots of the downhole mineral variations around the 1321-mbsf chemical discontinuity. Unlike Figures F11, p. 45, F12, p. 48, F13, p. 49, and F14, p. 50, this plot shows mineral compositions for both Hole 735B gabbros and Hole 735B microgabbro intrusions.

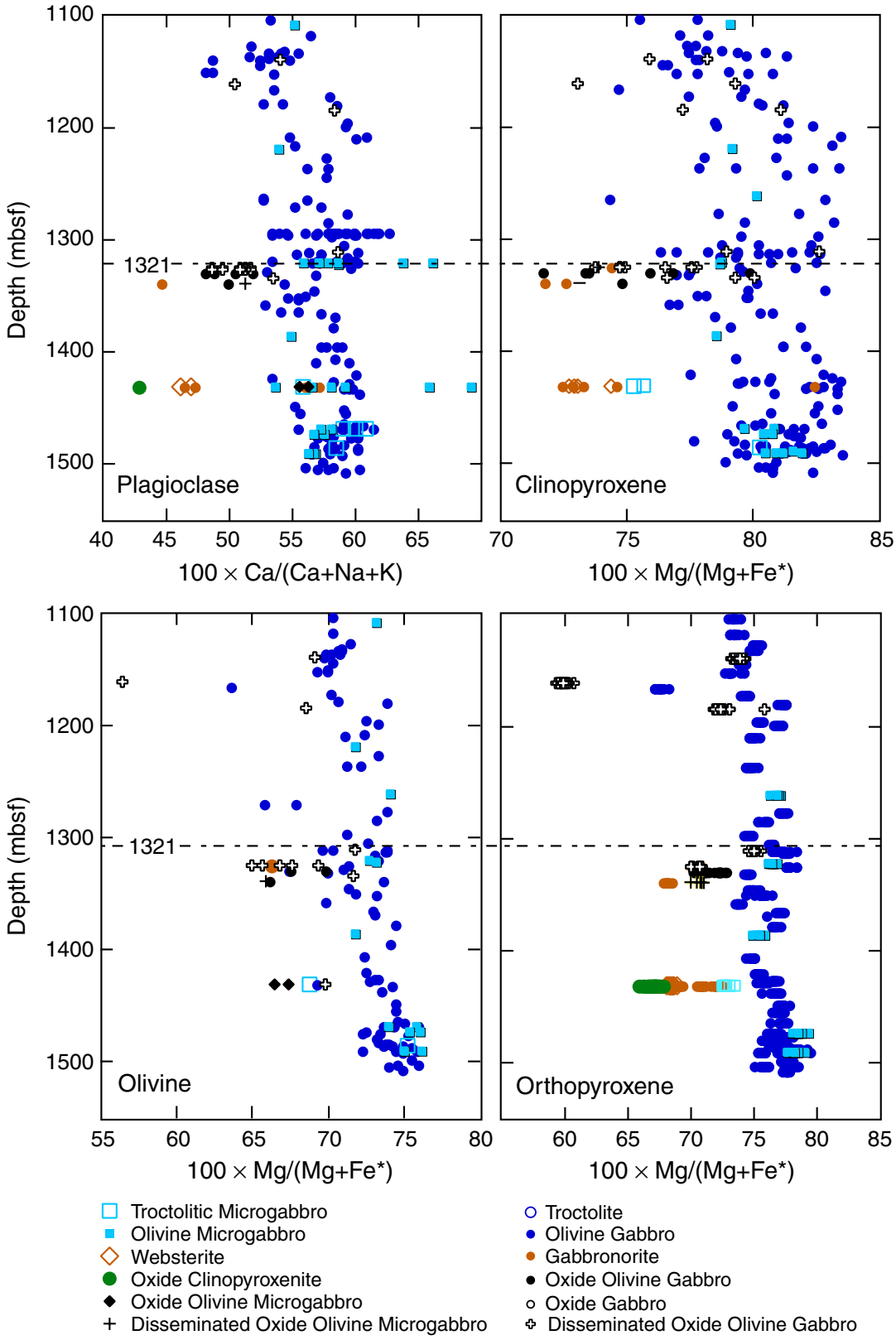

Figure F16. Downhole variation in anorthite content of plagioclase in Hole 735B gabbros showing the lithostratigraphic units defined by Dick et al. (1991a) and the Leg 118 and 176 Scientific Parties (solid lines) and the mineralogic discontinuities identified in this paper (dashed lines). Lithostratigraphic subunit boundaries are shown with lighter weight lines than unit boundaries.

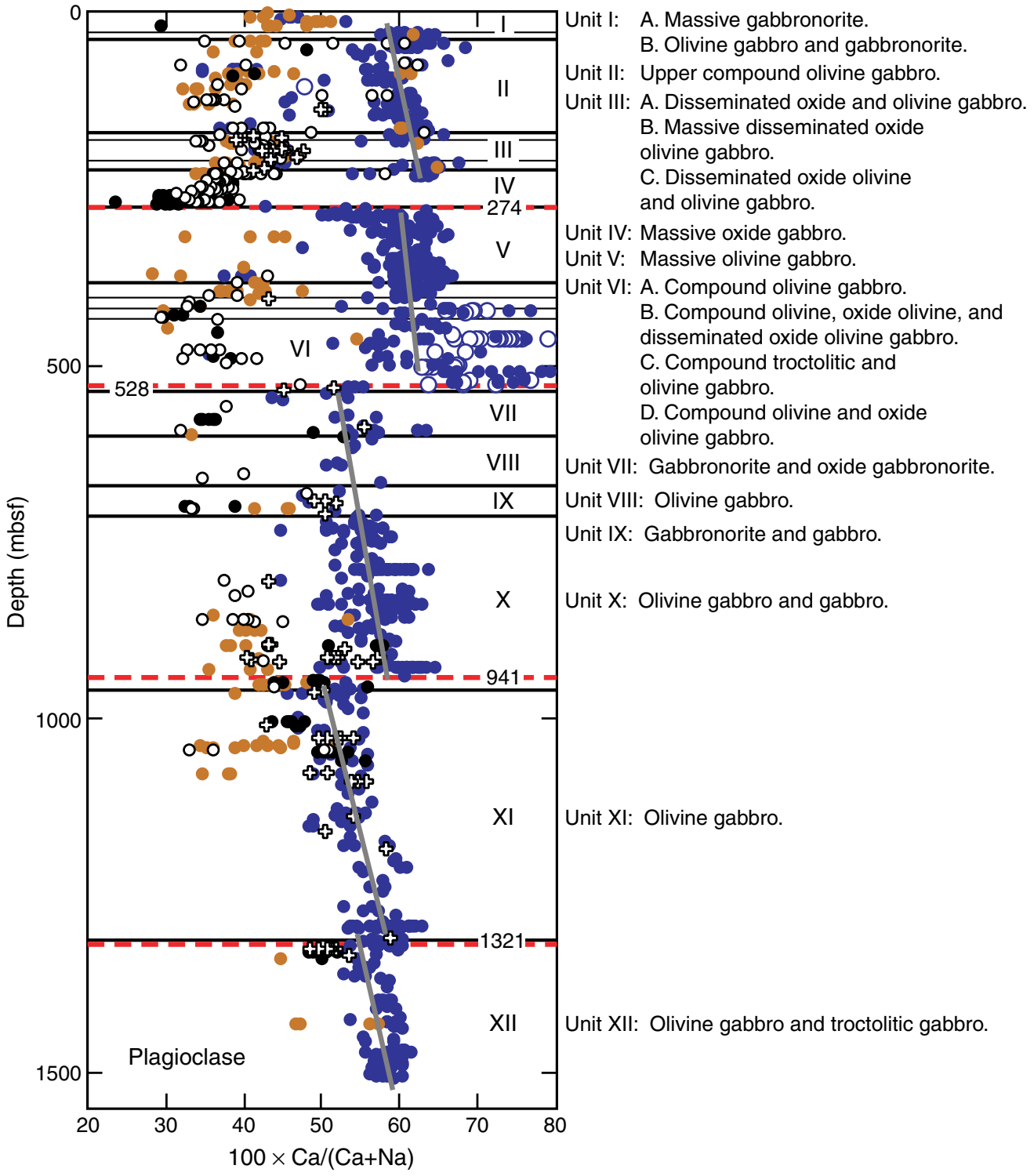

Figure F17. A. Downhole variations in olivine forsterite content and plagioclase anorthite content for average and single-spot analyses of coexisting plagioclase and olivine grains in Hole 735B olivine gabbros (gabbro, olivine gabbro, and troctolitic gabbro). Individual analyses are shown as shaded dots. Analyses of all other rock types are excluded in order to examine the vertical stratigraphy of Hole 735B independent of the influence of late-stage melt migration and intrusion of the ferrogabbros and gabbronorites. (Continued on next page.)

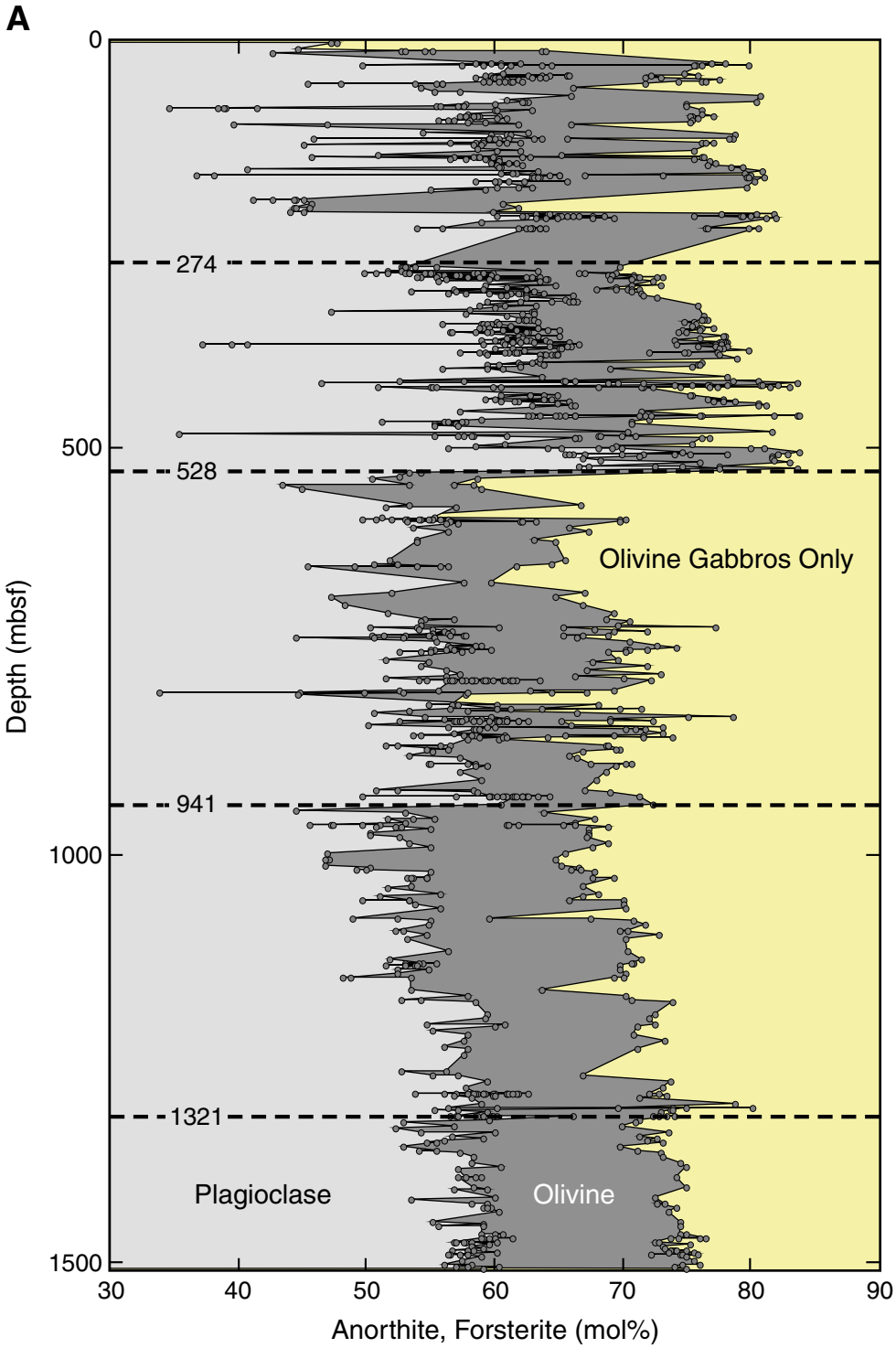

Figure F17 (continued). B. Plot of the difference between mol% An and mol% Fo for coexisting olivine and plagioclase in Hole 735B olivine gabbros against the anorthite content of the plagioclase.

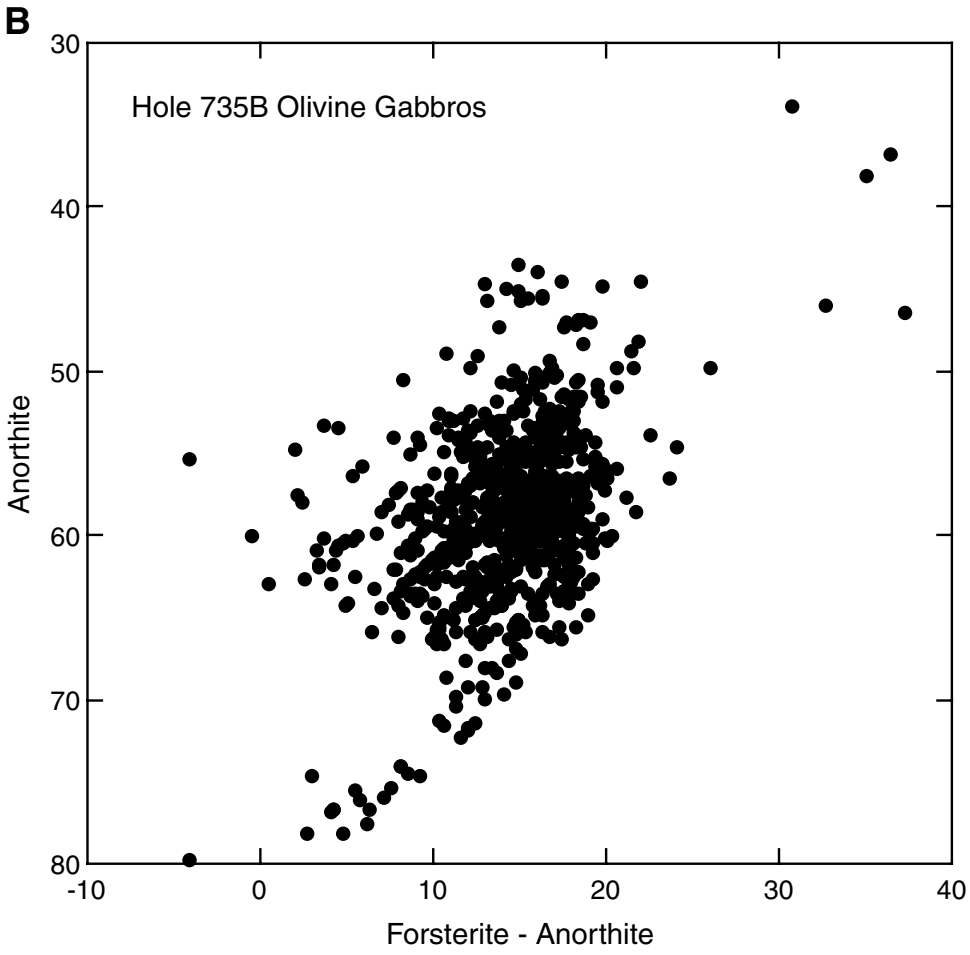

Figure F18. Plot of variations of olivine and plagioclase for three separate vertical sections through the Oman gabbro section from Pallister and Hopson (1981) modified with the addition of olivine and plagioclase compositions from the CY-4 drill hole in the Troodos Ophiolite gabbros from Malpas et al. (1989), analyses of plagioclase and olivine from Hole 894G in old East Pacific Rise high-level gabbros at Hess Deep (Natland and Dick, 1996) and the composition field for olivine for Hole 735B gabbros and microgabbros. The Skaergaard trend is shown as normalized to the height of the Oman section by Pallister and Hopson (1981). Column on far right shows the stratigraphic divisions of the Skaergaard Intrusion. SH = sandwich horizon, UZ = upper zone, MZ = middle zone, LZ = lower zone, HZ = hidden zone.

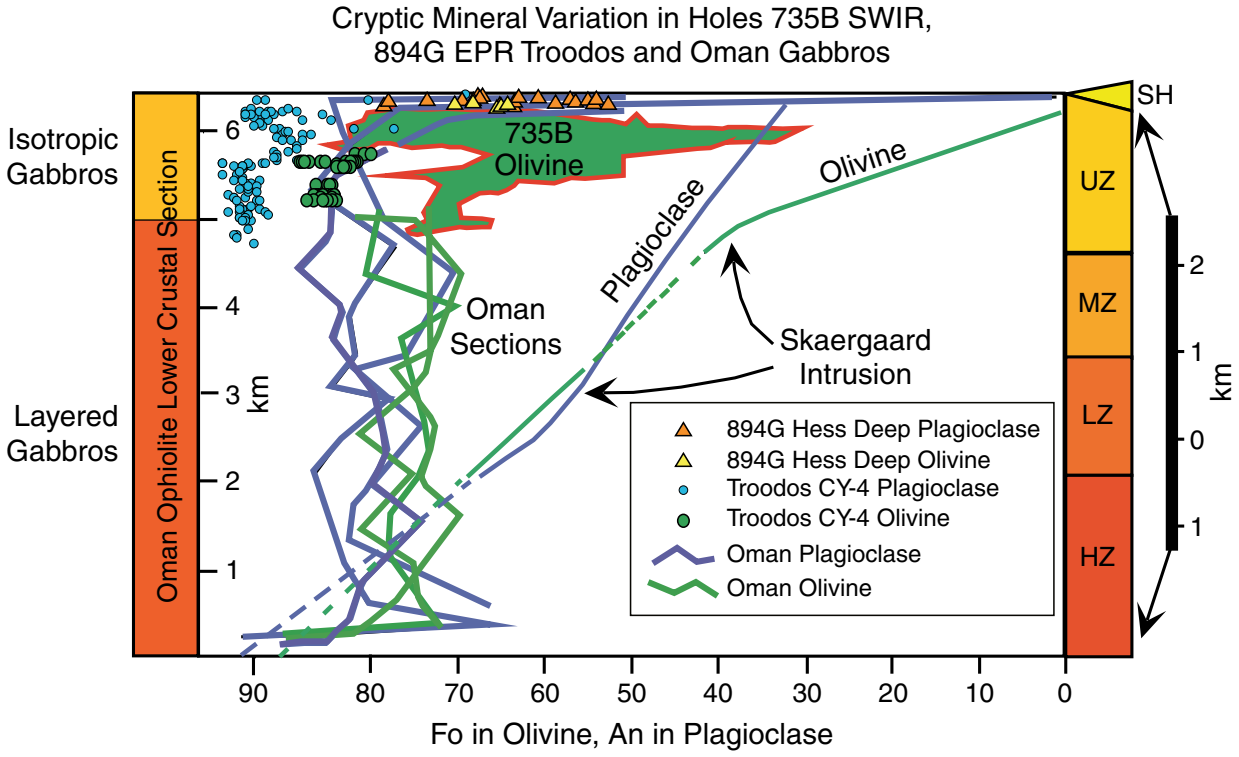

Table T1. Plagioclase analyses.

TS	Source	Leg	Hole	Core	Sect	Top (cm)	Bot. (cm)	Piece	Gr. Loc.	Depth (mbsf)	Rock type	Fo	An	Or	Mg# Cpx	Mg# Opx	Mg# Hb	Plag	Ol	Cpx	Opx	Opaq	Am	Zir	Apatite	Qtz	Other
MEY	MEY	118	735B	1	1	19.0	21.0			0.49	Gabbronorite		42.8	0.1	74.1												
HEB	CON/HER	118	735B	1	1	90.0	92.0	14		2.34	Gabbro		44.2	0.2	69.9			45	0	0	0						55
HEB	CON/HER	118	735B	1	1	90.0	92.0	14		2.34	Gabbro		47.2	0.4	69.9			45	0	0	0						55
HEB	CON/HER	118	735B	1	1	90.0	92.0	14		2.34	Gabbro		47.7	0.2	69.9			45	0	0	0						55
HEB	CON/HER	118	735B	1	1	90.0	92.0	14		2.34	Gabbro		41.9	0.5	69.9			45	0	0	0						55
	HEB	118	735B	1	1	90.0	92.0	14		2.34	Gabbronorite		44.2	0.2	69.8												
	HEB	118	735B	1	1	90.0	92.0	14		2.34	Gabbronorite		47.2	0.4	69.8												
	HEB	118	735B	1	1	90.0	92.0	14		2.34	Gabbronorite		45.7	0.3	69.8												
	HEB	118	735B	1	1	90.0	92.0	14		2.34	Gabbronorite		2.2	0.2	69.8												
133	OZA	118	735B	1	2	59.0	61.0			5.43	Metagabbro		44.9	0.4	73.6												

Table T1 (continued).

TS	Source	Leg	Hole	Core	Sect.	Top (cm)	Bot. (cm)	Piece	Gr. Loc.	Depth (mbsf)	CP	Pt	Gr	Loc	Grain size (mm)		SiO_2	TiO_2	Al_2O_3	FeO	MnO	MgO	CaO	Na_2O	K_2O	BaO
MEY	MEY	118	735B	1	1	19.0	21.0			0.49		1	Pl 1	PtC			56.81		26.39	0.04		0.00	8.63	6.36	0.01	
HEB	CON/HER	118	735B	1	1	90.0	92.0	14		2.34	4	13	Pl 13	Neo	M	F	56.96	0.00	27.05	0.09	0.00	0.04	9.19	6.40	0.03	
HEB	CON/HER	118	735B	1	1	90.0	92.0	14		2.34	4	4	Pl 4	Pt	M	M	56.02	0.00	27.78	0.15	0.00	0.04	9.83	6.02	0.07	
HEB	CON/HER	118	735B	1	1	90.0	92.0	14		2.34	4	6	Pl 6	Pt	M	F	56.84	0.00	27.57	0.09	0.00	0.03	9.66	5.83	0.03	
HEB	CON/HER	118	735B	1	1	90.0	92.0	14		2.34	4	8	Pl 8	Neo	M	F	57.98	0.00	26.55	0.31	0.00	0.04	8.55	6.50	0.09	
	HEB	118	735B	1	1	90.0	92.0	14		2.34		1	Pl	B			56.96		27.05	0.09		0.04	9.19	6.40	0.03	
	HEB	118	735B	1	1	90.0	92.0	14		2.34		2	Pl	B			56.02		27.78	0.15		0.04	9.83	6.02	0.07	
	HEB	118	735B	1	1	90.0	92.0	14		2.34		2	Pl	Ave			56.49		27.42	0.11		0.04	9.51	6.21	0.05	
	HEB	118	735B	1	1	90.0	92.0	14		2.34		2	Pl	Sd			0.66		0.52	0.04		0.00	0.45	0.27	0.03	
133	OZA	118	735B	1	2	59.0	61.0			5.43		101	Pl	B			57.40	0.04	26.70	1.09			8.85	5.94	0.07	

Table T1 (continued).

TS	Source	Leg	Hole	Core	Sect.	Top (cm)	Bot. (cm)	Piece	Gr. Loc.	Depth (mbsf)	P_2O_5	NiO	Cr_2O_3	Total	An	Ab	Or
MEY	MEY	118	735B	1	1	19.0	21.0			0.49				98.24	42.8	57.1	0.1
HEB	CON/HER	118	735B	1	1	90.0	92.0	14		2.34				99.76	44.2	55.7	0.2
HEB	CON/HER	118	735B	1	1	90.0	92.0	14		2.34				99.91	47.2	52.4	0.4
HEB	CON/HER	118	735B	1	1	90.0	92.0	14		2.34				100.05	47.7	52.1	0.2
HEB	CON/HER	118	735B	1	1	90.0	92.0	14		2.34				100.02	41.9	57.6	0.5
	HEB	118	735B	1	1	90.0	92.0	14		2.34				99.76	44.2	55.7	0.2
	HEB	118	735B	1	1	90.0	92.0	14		2.34				99.91	47.2	52.4	0.4
	HEB	118	735B	1	1	90.0	92.0	14		2.34				99.82	45.7	54.0	0.3
	HEB	118	735B	1	1	90.0	92.0	14		2.34				0.10	2.2	2.3	0.2
133	OZA	118	735B	1	2	59.0	61.0			5.43				100.09	44.9	54.7	0.4

Notes: Fo = forsterite, An = anorthite, Or = orthoclase, Cpx = clinopyroxene, Opx = orthopyroxene, Opaq = opaques, Hb = hornblende, Plag = plagioclase, Ol = olivine, Am = amphibole, Qtz = quartz. CP = crystal-plastic or brittle deformation intensity, Pt = point number, Gr = grain number prefixed by mineral abbreviation. Loc = location in grain: PtC = point in core, neo = neoblast, B = random point in grain interior. Sd = standard deviation (1 σ). Only a portion of this table appears here. The complete table is available in **ASCII.**

Table T2. Clinopyroxene analyses.

TS	Source	Leg	Hole	Core	Sect.	Top (cm)	Bot. (cm)	Piece	Grain Loc.	Depth (mbsf)	Rock type	Fo	An	Or	Mg# Cpx	Mg# Opx	Mg# Hb	Plag	Ol	Cpx	Opx	Opaq	Am	Zir	Apatite	Qtz
HEB	CON/HEB	118	735B	1	1	90.0	92.0	14		2.34	Gabbro		45.2	0.3	70.2			45.0	0.0	0.0	0.0					
HEB	CON/HEB	118	735B	1	1	90.0	92.0	14		2.34	Gabbro		45.2	0.3	69.3			45.0	0.0	0.0	0.0					
HEB	CON/HEB	118	735B	1	1	90.0	92.0	14		2.34	Gabbro		45.2	0.3	70.2			45.0	0.0	0.0	0.0					
133	OZA	118	735B	1	2	59	61			5.43	Unknown		45.9	0.3	73.2											
133	OZA	118	735B	1	2	59	61			5.43	Unknown		45.9	0.3	72.9											
133	OZA	118	735B	1	2	59	61			5.43	Unknown		45.9	0.3	74.4											
133	OZA	118	735B	1	2	59	61			5.43	Unknown		45.9	0.3	74.0											
133	OZA	118	735B	1	2	59	61			5.43	Unknown		45.9	0.3	73.6											
133	OZA	118	735B	1	2	59	61			5.43	Unknown		45.9	0.3	0.7											

Table T2 (continued).

TS	Source	Leg	Hole	Core	Sect.	Top (cm)	Bot. (cm)	Piece	Grain Loc.	Depth (mbsf)	Other	CP	Pt	Gr	Loc	Grain size (mm)		SiO_2	TiO_2	Al_2O_3	Cr_2O_3	FeO	MnO	MgO	CaO	Na_2O
HEB	CON/HEB	118	735B	1	1	90.0	92.0	14		2.34	55.0	4.0	14	Cpx 14	Pt	M	F	51.35	0.10	0.78	0.00	10.02	0.49	13.22	22.73	0.24
HEB	CON/HEB	118	735B	1	1	90.0	92.0	14		2.34	55.0	4.0	17	Cpx 17	Pt	M	C	47.40	0.69	5.52	0.00	10.57	0.45	13.39	20.12	0.69
HEB	CON/HEB	118	735B	1	1	90.0	92.0	14		2.34	55.0	4.0	3	Cpx 3	Pt	M	C	51.52	0.32	1.81	0.00	10.03	0.52	13.28	21.41	0.31
133	OZA	118	735B	1	2	59	61			5.43			108	Cpx	B			51.84	0.70	2.70	0.04	9.28	0.23	14.23	20.19	0.39
133	OZA	118	735B	1	2	59	61			5.43			109	Cpx	B			52.00	0.74	2.69	0.01	9.27	0.26	14.00	20.81	0.44
133	OZA	118	735B	1	2	59	61			5.43			110	Cpx	B			51.93	0.80	2.35	0.00	8.64	0.20	14.06	20.14	0.50
133	OZA	118	735B	1	2	59	61			5.43			111	Cpx	B			52.84	0.09	0.66	0.00	8.66	0.30	13.81	22.42	0.23
133	OZA	118	735B	1	2	59	61			5.43			4	Cpx	Ave			52.15	0.58	2.10	0.01	8.96	0.25	14.03	20.89	0.39
133	OZA	118	735B	1	2	59	61			5.43			4	Cpx	Sd			0.46	0.33	0.97	0.02	0.36	0.04	0.18	1.06	0.12

Table T2 (continued).

TS	Source	Leg	Hole	Core	Sect.	Top (cm)	Bot. (cm)	Piece	Grain Loc.	Depth (mbsf)	K_2O	P_2O_5	NiO	Total	Wo	En	Fs
HEB	CON/HEB	118	735B	1	1	90.0	92.0	14		2.34	0.01		0.00	98.94	37.6	16.0	693
HEB	CON/HEB	118	735B	1	1	90.0	92.0	14		2.34	0.02		0.00	98.85	39.7	17.6	932
HEB	CON/HEB	118	735B	1	1	90.0	92.0	14		2.34	0.02		0.00	99.22	38.7	16.4	803
133	OZA	118	735B	1	2	59	61			5.43				99.59	42.7	41.9	15.3
133	OZA	118	735B	1	2	59	61			5.43				100.22	43.8	41.0	15.2
133	OZA	118	735B	1	2	59	61			5.43				98.62	43.4	42.1	14.5
133	OZA	118	735B	1	2	59	61			5.43				99.00	46.3	39.7	14.0
133	OZA	118	735B	1	2	59	61			5.43				99.36	44.1	41.2	14.8
133	OZA	118	735B	1	2	59	61			5.43				0.70	0.0	0.0	0.0

Notes: Fo = forsterite, An = anorthite, Or = orthoclase, Cpx = clinopyroxene, Opx = orthopyroxene, Opaq = opaques, Hb = hornblende, Plag = plagioclase, Ol = olivine, Am = amphibole, Qtz = quartz. CP = crystal-plastic or brittle deformation intensity, Pt = point number, Gr = grain number prefixed by mineral abbreviation. Loc = location in grain: PtC = point in core, neo = neoblast, B = random point in grain interior. Sd = standard deviation (1 σ). Only a portion of this table appears here. The complete table is available in **ASCII.**

Table T3. Olivine analyses.

TS	Source	Leg	Hole	Core	Sect.	Top (cm)	Bot. (cm)	Piece	Grain Loc.	Depth (mbsf)	Rock type	Fo	An	Or	Mg# Cpx	Mg# Opx	Mg# Hb	Plag	Ol	Cpx	Opx	Opaq	Am	Zir
63	OZA	118	735B	2	2	118.0	123.0			12.41	Olivine orthopyroxene gabbro	62.0	52.9	0.3	77.0	70.6								
63	OZA	118	735B	2	2	118.0	123.0			12.41	Olivine orthopyroxene gabbro	65.4	52.9	0.3	77.0	70.6								
63	OZA	118	735B	2	2	118.0	123.0			12.41	Olivine orthopyroxene gabbro	63.8	52.9	0.3	77.0	70.6								
63	OZA	118	735B	2	2	118.0	123.0			12.41	Olivine orthopyroxene gabbro	64.9	52.9	0.3	77.0	70.6								
63	OZA	118	735B	2	2	118.0	123.0			12.41	Olivine orthopyroxene gabbro	64.0	52.9	0.3	77.0	70.6								
63	OZA	118	735B	2	2	118.0	123.0			12.41	Olivine orthopyroxene gabbro	1.5	52.9	0.3	77.0	70.6								
MEY	MEY	118	735B	7	1	134.0	136.0			28.41	Olivine gabbro	78.0	60.5		84.7									
MEY	MEY	118	735B	7	2	1.0	8.0			28.61	Olivine gabbro	76.9	60.1		84.4									
135	OZA	118	735B	8	1	22.0	24.0			30.18	Unknown	71.4	61.6	0.2	84.5	60.6								

Table T3 (continued).

TS	Source	Leg	Hole	Core	Sect.	Top (cm)	Bot. (cm)	Piece	Grain Loc.	Depth (mbsf)	Apatite	Qtz	Other	CP	Pt	Gr	loc	Grain size (mm)	SiO_2	TiO_2	Al_2O_3	Cr_2O_3	FeO	MnO	MgO	CaO
63	OZA	118	735B	2	2	118.0	123.0			12.41					105	OL	B		37.23				33.92	0.50	31.06	0.03
63	OZA	118	735B	2	2	118.0	123.0			12.41					113	OL	B		37.13				30.05	0.52	31.87	0.01
63	OZA	118	735B	2	2	118.0	123.0			12.41					114	OL	B		37.58				32.65	0.49	32.30	0.04
63	OZA	118	735B	2	2	118.0	123.0			12.41					115	OL	B		37.53				31.07	0.44	32.18	0.02
63	OZA	118	735B	2	2	118.0	123.0			12.41					4	OL	Ave		37.37				31.92	0.49	31.85	0.03
63	OZA	118	735B	2	2	118.0	123.0			12.41					4	OL	Sd		0.22				1.71	0.04	0.56	0.01
MEY	MEY	118	735B	7	1	134.0	136.0			28.41						OL	Ave									
MEY	MEY	118	735B	7	2	1.0	8.0			28.61						OL	Ave									
135	OZA	118	735B	8	1	22.0	24.0			30.18					1	OL	B		38.45				26.15	0.33	36.56	0.05

Table T3 (continued).

TS	Source	Leg	Hole	Core	Sect.	Top (cm)	Bot. (cm)	Piece	Grain Loc.	Depth (mbsf)	Na_2O	K_2O	P_2O_5	NiO	Total
63	OZA	118	735B	2	2	118.0	123.0			12.41					102.74
63	OZA	118	735B	2	2	118.0	123.0			12.41					99.59
63	OZA	118	735B	2	2	118.0	123.0			12.41				0.10	103.15
63	OZA	118	735B	2	2	118.0	123.0			12.41				0.05	101.29
63	OZA	118	735B	2	2	118.0	123.0			12.41				0.04	101.69
63	OZA	118	735B	2	2	118.0	123.0			12.41				0.05	1.61
MEY	MEY	118	735B	7	1	134.0	136.0			28.41					
MEY	MEY	118	735B	7	2	1.0	8.0			28.61					
135	OZA	118	735B	8	1	22.0	24.0			30.18				0.07	101.61

Notes: Fo = forsterite, An = anorthite, Or = orthoclase, Cpx = clinopyroxene, Opx = orthopyroxene, Opaq = opaques, Hb = hornblende, Plag = plagioclase, Ol = olivine, Am = amphibole, Qtz = quartz. CP = crystal-plastic or brittle deformation intensity, Pt = point number, Gr = grain number prefixed by mineral abbreviation. Loc = location in grain: PtC = point in core, neo = neoblast, B = random point in grain interior. Sd = standard deviation (1 σ). Only a portion of this table appears here. The complete table is available in **ASCII.**

Table T4. Orthopyroxene analyses.

1	TS	Source	Leg	Hole	Core	Sect.	Top (cm)	Bot. (cm)	Piece	Grain Loc.	Depth (mbsf)	Rock Type	Fo	An	Or	Mg# Cpx	Mg#	Mg# Hb	Plag	Ol	Cpx	Opx	Opaq	Am	Zir	Apatite	Qtz
142	1	OZA	118	735B	31	1	16.0	19.0			143.64	Unknown	58.6	45.6	0.7	71.0	64.1										
580	1	OZA	118	735B	73	3	73.0	75.0			369.03	Olivine gabbro	77.9	65.9	0.3	84.3	79.9										
138	1	OZA	118	735B	31	1	16.0	19.0			143.64	Unknown	58.6	45.6	0.7	71.0	62.8										
139	1	OZA	118	735B	31	1	16.0	19.0			143.64	Unknown	58.6	45.6	0.7	71.0	63.3										
140	1	OZA	118	735B	31	1	16.0	19.0			143.64	Unknown	58.6	45.6	0.7	71.0	65.2										
141	1	OZA	118	735B	31	1	16.0	19.0			143.64	Unknown	58.6	45.6	0.7	71.0	65.1										
573	1	OZA	118	735B	73	3	73.0	75.0			369.03	Olivine gabbro	77.9	65.9	0.3	84.3	79.2										
574	1	OZA	118	735B	73	3	73.0	75.0			369.03	Olivine gabbro	77.9	65.9	0.3	84.3	80.1										
575	1	OZA	118	735B	73	3	73.0	75.0			369.03	Olivine gabbro	77.9	65.9	0.3	84.3	80.4										

Table T4 (continued).

1	TS	Source	Leg	Hole	Core	Sect.	Top (cm)	Bot. (cm)	Piece	Grain Loc.	Depth (mbsf)	Other	CP	Pt	Gr.	Loc	Grain Size (mm)	SiO_2	TiO_2	Al_2O_3	Cr_2O_3	FeO	MnO	MgO	CaO	Na_2O
142	1	OZA	118	735B	31	1	16.0	19.0			143.64			4	Opx	Ave		53.18	0.16	0.63	0.02	22.09	0.58	22.17	0.75	0.03
580	1	OZA	118	735B	73	3	73.0	75.0			369.03			7	Opx	Ave		55.40	0.24	1.75	0.09	12.94	0.26	28.81	0.88	
138	1	OZA	118	735B	31	1	16.0	19.0			143.64			20	Opx	B		52.52	0.36	1.03	0.05	22.08	0.55	20.92	1.30	0.00
139	1	OZA	118	735B	31	1	16.0	19.0			143.64			21	Opx	B		52.50	0.26	1.08	0.02	22.53	0.61	21.84	0.83	0.07
140	1	OZA	118	735B	31	1	16.0	19.0			143.64			32	Opx	B		54.17	0.01	0.25	0.01	21.92	0.62	23.09	0.41	0.02
141	1	OZA	118	735B	31	1	16.0	19.0			143.64			33	Opx	B		53.54	0.04	0.17	0.02	21.82	0.56	22.85	0.46	0.03
573	1	OZA	118	735B	73	3	73.0	75.0			369.03			13	Opx	B		55.46	0.19	1.66	0.11	13.21	0.24	28.24	0.86	
574	1	OZA	118	735B	73	3	73.0	75.0			369.03			17	Opx	B		55.58	0.34	1.41	0.04	13.00	0.32	29.43	0.96	
575	1	OZA	118	735B	73	3	73.0	75.0			369.03			32	Opx	B		55.93	0.26	1.19	0.12	12.81	0.27	29.44	0.86	

Table T4 (continued).

1	TS	Source	Leg	Hole	Core	Sect.	Top (cm)	Bot. (cm)	Piece	Grain Loc.	Depth (mbsf)	K_2O	P_2O_5	NiO	Total
142	1	OZA	118	735B	31	1	16.0	19.0			143.64				99.60
580	1	OZA	118	735B	73	3	73.0	75.0			369.03				100.38
138	1	OZA	118	735B	31	1	16.0	19.0			143.64				98.80
139	1	OZA	118	735B	31	1	16.0	19.0			143.64				99.67
140	1	OZA	118	735B	31	1	16.0	19.0			143.64				100.48
141	1	OZA	118	735B	31	1	16.0	19.0			143.64				99.44
573	1	OZA	118	735B	73	3	73.0	75.0			369.03				99.96
574	1	OZA	118	735B	73	3	73.0	75.0			369.03				101.07
575	1	OZA	118	735B	73	3	73.0	75.0			369.03				100.88

Notes: Fo = forsterite, An = anorthite, Or = orthoclase, Cpx = clinopyroxene, Opx = orthopyroxene, Opaq = opaques, Hb = hornblende, Plag = plagioclase, Ol = olivine, Am = amphibole, Qtz = quartz. CP = crystal-plastic or brittle deformation intensity, Pt = point number, Gr = grain number prefixed by mineral abbreviation. Loc = location in grain: PtC = point in core, neo = neoblast, B = random point in grain interior. Sd = standard deviation (1 σ). Only a portion of this table appears here. The complete table is available in **ASCII.**

Table T5. Brown hornblende analyses.

TS	Source	Leg	Hole	Core	Sect.	Top (cm)	Bot. (cm)	Piece	Grain Loc.	Depth (mbsf)	Rock Type	Fo	An	Or	Mg# Cpx	Mg# Opx	Mg#	Plag	Ol	Cpx	Opx	Opaq	Amph	Zir	Apatite	Qtz	Other
ROB	ROB	176	735B	2	1	123.0	127.0			7.70	Gabbro		45.2	0.4	73.4		57.4										
ROB	ROB	176	735B	2	1	123.0	127.0			7.70	Gabbro		45.2	0.4	73.4		56.5										
ROB	ROB	176	735B	2	1	123.0	127.0			7.70	Gabbro		45.2	0.4	73.4		56.9										
ROB	ROB	176	735B	2	1	123.0	127.0			7.70	Gabbro		45.2	0.4	73.4		0.7										
ROB	ROB	176	735B	2	1	123.0	127.0			7.70	Gabbro		45.2	0.4	73.4		58.8										
ROB	ROB	176	735B	2	1	123.0	127.0			7.70	Gabbro		45.2	0.4	73.4		57.2										
ROB	ROB	176	735B	2	1	123.0	127.0			7.70	Gabbro		45.2	0.4	73.4		58.0										
ROB	ROB	176	735B	2	1	123.0	127.0			7.70	Gabbro		45.2	0.4	73.4		1.1										
ROB	ROB	176	735B	2	1	123.0	127.0			7.70	Gabbro		45.2	0.4	73.4		62.0										

Table T5 (continued).

TS	Source	Leg	Hole	Core	Sect.	Top (cm)	Bot. (cm)	Piece	Grain Loc.	Depth (mbsf)	CP	Pt	Gr	Loc	Grain Size (mm)	SiO_2	TiO_2	Al_2O_3	Cr_2O_3	FeO	MnO	MgO	CaO	Na_2O
ROB	ROB	176	735B	2	1	123.0	127.0			7.70	4	1	Am1	B	C	45.17	1.89	9.30		16.00	0.22	12.09	11.14	2.36
ROB	ROB	176	735B	2	1	123.0	127.0			7.70	4	2	Am1	B	C	44.33	2.44	9.73		16.02	0.19	11.65	11.37	2.30
ROB	ROB	176	735B	2	1	123.0	127.0			7.70	4	2	Am1	Ave	C	44.75	2.17	9.52		16.01	0.21	11.87	11.25	2.33
ROB	ROB	176	735B	2	1	123.0	127.0			7.70	4	2	Am1	Sd	C	0.59	0.39	0.31		0.01	0.02	0.31	0.17	0.04
ROB	ROB	176	735B	2	1	123.0	127.0			7.70	4	2	Am3	B	C	44.84	1.85	9.00		15.43	0.21	12.33	10.82	2.26
ROB	ROB	176	735B	2	1	123.0	127.0			7.70	4	1	Am3	B	C	44.23	1.90	9.07		16.14	0.20	12.11	10.94	2.32
ROB	ROB	176	735B	2	1	123.0	127.0			7.70	4	2	Am3	Ave	C	44.54	1.87	9.03		15.79	0.20	12.22	10.88	2.29
ROB	ROB	176	735B	2	1	123.0	127.0			7.70	4	2	Am3	Sd	C	0.43	0.04	0.05		0.50	0.00	0.16	0.08	0.04
ROB	ROB	176	735B	2	1	123.0	127.0			7.70	4	1	Am5	B	C	45.70	1.88	8.81		14.17	0.27	12.98	11.66	2.03

Table T5 (continued).

TS	Source	Leg	Hole	Core	Sect.	Top (cm)	Bot. (cm)	Piece	Grain Loc.	Depth (mbsf)	K_2O	P_2O_5	NiO	Total
ROB	ROB	176	735B	2	1	123.0	127.0			7.70	0.30			98.46
ROB	ROB	176	735B	2	1	123.0	127.0			7.70	0.35			98.40
ROB	ROB	176	735B	2	1	123.0	127.0			7.70	0.32			98.43
ROB	ROB	176	735B	2	1	123.0	127.0			7.70	0.04			0.04
ROB	ROB	176	735B	2	1	123.0	127.0			7.70	0.29			97.02
ROB	ROB	176	735B	2	1	123.0	127.0			7.70	0.29			97.19
ROB	ROB	176	735B	2	1	123.0	127.0			7.70	0.29			97.11
ROB	ROB	176	735B	2	1	123.0	127.0			7.70	0.00			0.12
ROB	ROB	176	735B	2	1	123.0	127.0			7.70	0.31			97.81

Notes: Fo = forsterite, An = anorthite, Or = orthoclase, Cpx = clinopyroxene, Opx = orthopyroxene, Opaq = opaques, Hb = hornblende, Plag = plagioclase, Ol = olivine, Am = amphibole, Qtz = quartz. CP = crystal-plastic or brittle deformation intensity, Pt = point number, Gr = grain number prefixed by mineral abbreviation. Loc = location in grain: PtC = point in core, neo = neoblast, B = random point in grain interior. Sd = standard deviation (1 σ). Only a portion of this table appears here. The complete table is available in **ASCII.**

CHAPTER NOTE*

N1. 6 January 2003—After this chapter was published, it was found that Jinichiro Maeda's name was inadvertently omitted from the authorship. The correct authorship appears in this version.

*Dates reflect file corrections or revisions.